# Emission of high-energy gamma rays in heavy-ion reactions at nonrelativistic energies

V. V. Kamanin, A. Kugler, and Yu. É. Penionzhkevich

*Joint Institute for Nuclear Research, Dubna*

I. S. Batkin and I. V. Kopytin

*Lenin Komsomol State University, Voronezh*

Fiz. Elem. Chastits At. Yadra **20**, 741–829 (July–August 1989)

A review is given of the results of experimental and theoretical study of the emission of high-energy $\gamma$ rays with $E_\gamma$ above the energy per nucleon ($E/A$) of the bombarding particle in heavy-ion collisions with energies from 8 to more than 100 MeV/nucleon. Methods of detecting the $\gamma$ rays and also neutrons and charged particles are considered. Particular attention is devoted to the region of $\gamma$-ray energies corresponding to decay of giant dipole resonances. The data on such resonances obtained by different methods of separating the heavy-ion reaction channel are compared. The experimental data are analyzed by means of standard theoretical approaches (for example, in the framework of the statistical theory) and also by means of models proposed by the authors of the review.

## INTRODUCTION

In this review we consider the results of experimental and theoretical study of the emission of high-energy $\gamma$ rays in heavy-ion collisions in which the bombarding ions have energies from 8 to 100 MeV/nucleon. In this energy range, the kinetic energy of the incident nucleus is greater than the height of the Coulomb barrier but significantly less than the rest energy of each of the interacting nuclei. The first circumstance means that many reaction channels, including the complete-fusion channel, are open, while the second circumstance permits use of the nonrelativistic approximation in a theoretical analysis.

By a high-energy $\gamma$ ray we shall in what follows mean a $\gamma$ ray whose energy $E_\gamma$ is greater than $E/A_1$, where $E$ is the kinetic energy of the relative motion of the ions, and $A_1$ is the mass number of the incident ion. Defined in this way, a "high-energy $\gamma$ ray" is obviously a relative concept, since, depending on the value of $E/A_1$, it can be a $\gamma$ ray with energy 10–20 MeV or 100–200 MeV. Nevertheless, whatever the value of $E_\gamma$, one can pose this question: What is the mechanism (or mechanisms) of the reaction that leads to the emission of $\gamma$ rays with an energy kinematically forbidden for single nucleon processes?

Heavy-ion collisions result in the emission of not only $\gamma$ rays but also other particles (nucleons, light nuclei, pions, etc.) with energies that are not possible for single-nucleon processes. However, to elucidate the mechanism of heavy-ion reactions study of the $\gamma$ rays, rather than of the other particles, has a number of distinct advantages.

First, the relative weakness of the electromagnetic interaction permits the use of the lowest orders of perturbation theory.

Second, the structure of the electromagnetic currents is well known, and this eliminates uncertainty in the construction of the Matrix elements of the radiation process.

Third, the problem of the effect of the nuclear field on the emitted particle is removed because the particle is a $\gamma$ ray.

Fourth, the relative smallness of the $\gamma$-ray momentum permits the use of a multipole expansion of the amplitude of the electromagnetic interaction in a number of cases.

Naturally, all these factors significantly raise the accuracy of the information obtained about the physics of the phenomenon and attract the interest of investigators.

This problem has been the subject of many recent experimental and theoretical studies. The experimental studies can be divided into two main groups. In one, the yield of $\gamma$ rays was studied in collisions of ions with energies 5–12 MeV/nucleon, and in the other the energy of the incident ions exceeded 20 MeV/nucleon. Naturally, the range of energies of the photons emitted in these groups also differed. In the first case the $\gamma$-ray energy was mainly in the interval 8–25 MeV, whereas in the second group the spectral properties of $\gamma$ rays with energy above 25 MeV were investigated. The ranges of the photon energies also largely determined the characteristic shapes of the spectra. In the low-energy range ($E_\gamma \sim 8$–25 MeV) the spectra were observed to have irregularities at energies characteristic of giant nuclear resonances superimposed on the background of the general exponential decrease with increasing $\gamma$-ray energy.

As a rule, the high-energy spectra ($E_\gamma \sim 25$–200 MeV) were found to be smooth and could be fairly well described by simply an exponential dependence on the $\gamma$-ray energy. If the reaction mechanisms are to be elucidated by these characteristically different experimental $\gamma$-ray spectra, we must also expect to use different theoretical models. However, as we have already noted, the main aim is to determine the mechanism of production of hard photons with energy above the kinematic limit for single-nucleon processes.

In Sec. 1, the methods of detecting high-energy $\gamma$ rays are analyzed, and a comparative estimation of the properties of the scintillation materials used in these methods is made.

In Sec. 2, the experimental situation in the study of the spectra of $\gamma$ rays with energies up to 30 MeV is analyzed. The results of experimental investigations at $\gamma$-ray energies above 30 MeV are also briefly presented.

Section 3 presents a review of the theoretical approaches to the elucidation of the mechanism of heavy-ion

 0090-4759/89/040311-40$04.40  

reactions that leads to the production of high-energy photons. A microscopic model that, without using free parameters, permits the calculation of the differential cross sections of $\gamma$-ray production with comparative ease is presented.

Section 4 is devoted to a discussion of the results obtained in the framework of the proposed theory.

## 1. METHODS OF DETECTION OF HIGH-ENERGY $\gamma$ RAYS

In experiments on the emission of high-energy $\gamma$ rays in heavy-ion reactions, different forms of scintillation detectors based on the well-known scintillators NaI(Tl) (for $E_\gamma < 30$ MeV) and lead glass (for $E_\gamma > 20$ MeV) were initially used. Both materials are widely available and comparatively cheap. The low value of the photoyield and, accordingly, the high threshold of $\gamma$-ray detection ($\sim 8$ MeV) of the lead glass was seen as an advantage of that material.[1] Later, new scintillators were found. They possessed either a better $\gamma$-ray detection efficiency (for example, BGO, bismuth germanate[2,3]) or a better time resolution and ability to distinguish the detection of charged particles from $\gamma$ rays by means of the ratio of the two components of the light burst [for example, barium fluoride $BaF_2$ (Refs. 4 and 5)]. In plans for new facilities, cesium iodide CsI(Tl) has also been proposed,[6,7] because the ratio of the two components of the light burst has been found to depend on the form of the detected radiation in the case of this material.[8,9] The main parameters of the scintillators are given in Table I.

The interaction of $\gamma$ rays with $E_\gamma > 8$ MeV with the material of the scintillator leads in the majority of cases to the production of a pair of particles—an electron and a positron. On the average, each particle of the pair carries away half of the energy of the original $\gamma$ ray. In turn, the interaction of the electron and the positron with the matter leads to the emission of secondary $\gamma$ rays, mainly through bremsstrahlung. Thus, there develops in the scintillator a shower of secondary electrons, positrons, and $\gamma$ rays, which occupy a region in the form of a cone. It is convenient to characterize its linear dimensions by the radiation length, i.e., the distance over which the radiation losses of a high-energy electron through bremsstrahlung leads to a decrease of its energy by a factor $e$ ($e = 2.7...$). For example, for a detector made of the scintillator $BaF_2$ in the form of a cylinder of height 30 cm and diameter 5 cm, 25% of the initial energy $E_\gamma = 300$ MeV of a $\gamma$ ray that enters the detector along its symmetry axis escapes through the side surface.

An increase of the diameter of the cylinder to 15 cm leads to a decrease of this value of 5% (see Fig. 1a). We recall that the radiation length in the scintillator $BaF_2$ is about 2 cm. It follows from this that a $\gamma$-ray detector must have a length and diameter of the order of a few radiation lengths in order to increase the probability that the complete cascade remains in the detector. It is found that the "loss" of energy of the initial $\gamma$ ray, i.e., the escape of secondary particles from the detector, is the main reason for the broadening of the peak corresponding to detection of a monoenergetic high-energy $\gamma$ ray (see Fig. 1b). As an example, we can give the results of investigations of an assembly of detectors made from seven hexgonal $BaF_2$ modules, each of diameter 26 mm and length 200 mm, in a beam of monoenergetic $\gamma$ rays from the facility MAMI A (see Ref. 7). The results of measurement for the case of 50-MeV $\gamma$ rays incident on the central detector are shown in Fig. 2.[7] In more than 90% of the cases detection of the $\gamma$ ray in the central detector was accompanied by the detection of a pulse corresponding to an energy above 100 keV in one of the detectors surrounding the central detector. Therefore, the important thing for the detection of high-energy $\gamma$ rays is not so much the "photoyield" parameter (Table I), which determines the energy resolution for low $\gamma$-ray energies, as the amount of "loss" of energy of the initial $\gamma$ ray from the volume of the detector. For example, in the assembly of seven hexagonal $BaF_2$ modules the width of the peak of the amplitude spectrum of the central detector corresponding to detection of a 20-MeV $\gamma$ ray was 12% of $E_\gamma$. By adding the amplitude of the central detector to the amplitudes of the signals observed simultaneously in

TABLE I. Properties of scintillation materials.

| Parameter | Scintillator | | | | |
|---|---|---|---|---|---|
| | BGO | $BaF_2$ | CsI(Tl) | NaI(Tl) | SF5 |
| Density, g/cm$^3$ | 7.1 | 4.8 | 4.5 | 3.7 | 4.1 |
| Radiation length, cm | 1.12 | 2.05 | 1.87 | 2.59 | 2.47 |
| Photoyield, $\gamma$ ray/MeV | 800 | 1400 | 4200 | 10000 | 1—8 |
| Decay time of light flash, nsec | 300 | 1/630 | 1000/300 | 250 | 1 |
| Resolution time, nsec | 4 | 0.7 | 4 | 2 | 0.5 |
| Cross section for radiative capture of thermal neutrons ($10^{-24}$ cm$^2$) by a molecule of the scintillator material | 7.1 | 1.2 | 35 | 6.7 | 0.3 |
| Energy resolution for $E_\gamma = 661$ keV, % | 12 | 9 | 7 | 6 | — |

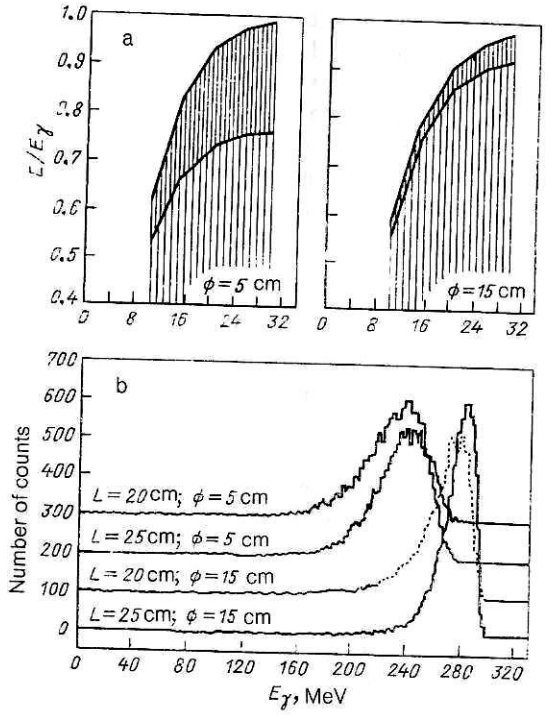


FIG. 1. Results of modeling of the process of detection of 300-MeV $\gamma$ rays incident in a cylindrical $BaF_2$ detector along its symmetry axis[7]: a) losses of primary energy of the $\gamma$ rays in the volume of the detector (lower curve) and the sum of these losses with the energy escape through the side surface as functions of the height and diameter of the cylinder; b) calculated response functions for detectors of different sizes.

the six outer modules it was possible to reduce the width of the peak to 6% of the energy of the initial $\gamma$ ray. This $\gamma$-ray detector was used to study the reactions $^{40}$Ar(44 MeV/nucleon) + $^{158}$Gd (Ref. 4) and $^{92}$Mo(19.5 MeV/nucleon) + $^{92}$Mo (Ref. 10).

In other experiments, mainly for detection of $\gamma$ rays with energy above 20 MeV, a condition of observation was again coincidence of pulses from detection of a high-energy $\gamma$ ray in a central detector and in a shielding layer surrounding it with subsequent addition of the two pulses. As an example, we can mention the facility HERMES.[11] It consists of a central NaI(Tl) crystal in the form of a cylinder of diameter 15 cm and height 25 cm surrounded by a NaI(Tl) crystal with external diameter 28 cm. A resolution of order 2.8% was achieved for a $\gamma$ ray with energy 22.5 MeV. Qualitatively the same results could also be obtained using large detectors and collimation of the high-energy $\gamma$ rays to ensure that they entered the central region of a large detector. Examples are the BNL-MKII and BNL-MKIII facilities,[12] which were based on NaI(Tl) detectors in the form of cylinders of diameter 24 cm and heights 25 and 36 cm, respectively.[12] The complete detector was, moreover, situated in an active plastic shield, and detection was made only in the absence of a signal in the shield. An energy resolution of about 2.2% at $E_\gamma = 22$ MeV was achieved.

However, to extract the true shape of the $\gamma$-ray spectra, the important thing is not so much the energy resolution as the shape of the entire instrumental spectrum of the detector for monoenergetic $\gamma$ rays, i.e., the response function of the detector. Strong differences in the shape of the high-energy "tail" of the response function lead to different instrumental spectra. An example is the difference between the instrumental spectra obtained from measurement of high-energy $\gamma$ rays by lead-glass and $BaF_2$ detectors ($\gamma$-ray spectra for both detector types, measured in the $^{58}$Fe + $^{116}$Sn reaction, are shown in Fig. 3). The difference in the slopes is explained by the presence of the high-energy tail in the instrumental spectra for detection of monoenergetic $\gamma$ rays (Fig. 4). Such a shape of the response function for the lead-glass detectors casts doubt on the results of temperature determination from the instrumental spectra of high-energy $\gamma$ rays that

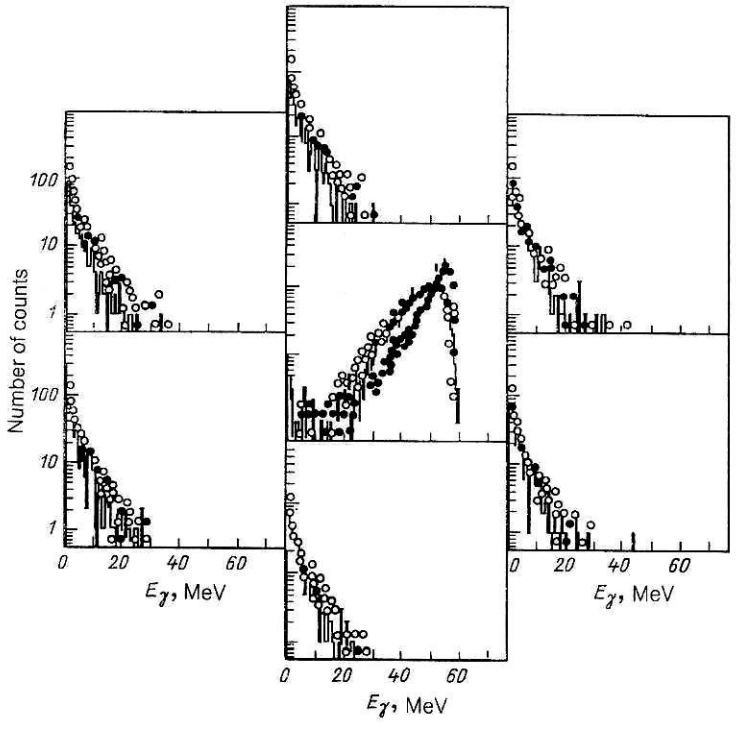


FIG. 2. Instrumental spectra (open circles) observed in each of seven hexagonal $BaF_2$ modules (each of diameter 26 mm and length 200 mm) for cases of incidence of $\gamma$ rays with $E_\gamma = 50$ MeV in the central detector surrounded by the remaining six detectors. Also shown in the center is the spectrum of the total energy (black circles) measured in the complete assembly of seven modules for cases of incidence of $\gamma$ rays with $E_\gamma = 50$ MeV in the central detector.[7] The histogram represents calculations by the Monte Carlo method.

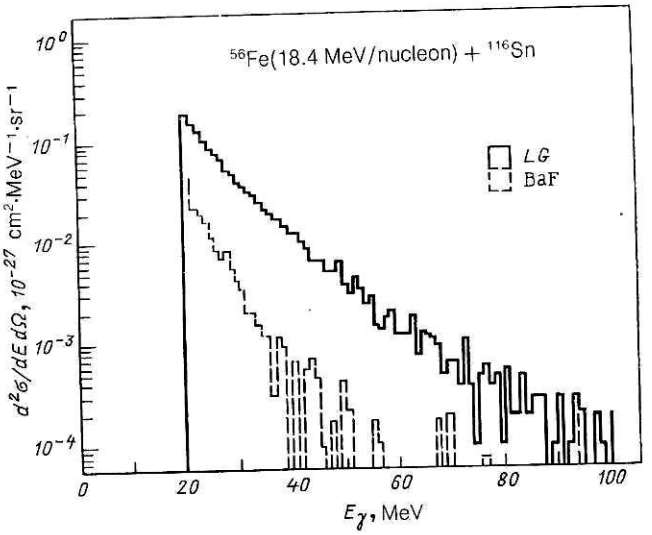


FIG. 3. Instrumental spectra obtained in measurements of high-energy $\gamma$ rays by lead glass (LG) and $BaF_2$ (BaF) detectors for the reaction indicated in the figure at angle 90° (Ref. 7).

were obtained earlier using lead glass as the material of detectors of high-energy $\gamma$ rays.[13,14]

It follows from what we have said that the shape of the response function, in particular the width of the peak, depends on the geometrical configuration of the detector. Because sources of low-energy $\gamma$ rays with $E_\gamma > 7$ MeV are not readily available, theoretical Monte Carlo calculations of the response functions (using, for example, the programs GEANT[15] or JACKET[16]) are used. The results of the calculations are verified in separate test experiments with the same detectors. Besides calibration of the detectors by means of tagged bremsstrahlung $\gamma$ rays from facilities of MAMI A type,[17] high-energy $\gamma$ transitions from $(p, \gamma)$ reactions on light targets are often used (Refs. 11, 12, 18, and 19). The energy calibration during the experiments is usually made by means of $\gamma$ rays from the $^9$Be$(\alpha, n\gamma)$ $^{12}$C reaction in neutron sources, giving energy $E_\gamma = 4.43$ MeV, or by measurement of the energy losses of cosmic-ray muons in the detector. For example, the mean energy loss of a "cosmic" muon after passage through a $BaF_2$ layer of thickness 1 cm is 6.5 MeV (Ref. 5).

In heavy-ion reactions, the yield of $\gamma$ rays with $E_\gamma \geqslant 8$ MeV is only $10^{-4}$ of the total yield of $\gamma$ rays with energy below 2 MeV (see Fig. 8). This corresponds to yield cross sections of order $100 \times 10^{-30}$ cm$^2$ and less. Simultaneously, the mean energy of the neutrons evaporated from the highly excited products of the nuclear reactions with the heavy ions is about 2 MeV. As the energy of the incident ions is increased in the range $E/A_1 = 10$–$100$ MeV/nucleon, the temperature in the highly excited reaction product varies in the range $T = 1$–$5$ MeV, and the mean energy of the evaporated neutrons varies in the range $\langle E_n \rangle = 2$–$10$ MeV. With increasing $E/A_1$, the yield at small angles of pre-equilibrium neutrons and protons with mean energy of order $E/A_1$ increases up to values that are comparable with the reaction cross section. At such cross sections, it is necessary to take into account carefully the contribution of fast neutrons and protons to the instrumental spectrum detected by the $\gamma$-ray detector. Therefore, it is necessary to select detectors that possess not only a high $\gamma$-ray detection efficiency but also a low efficiency for detection of the main background radiations, i.e., neutrons and light charged particles, so that their contribution to the experimental data can be suppressed in the analysis. In this connection, we shall now comment on some features of the detection of neutrons and charged particles by means of scintillators.

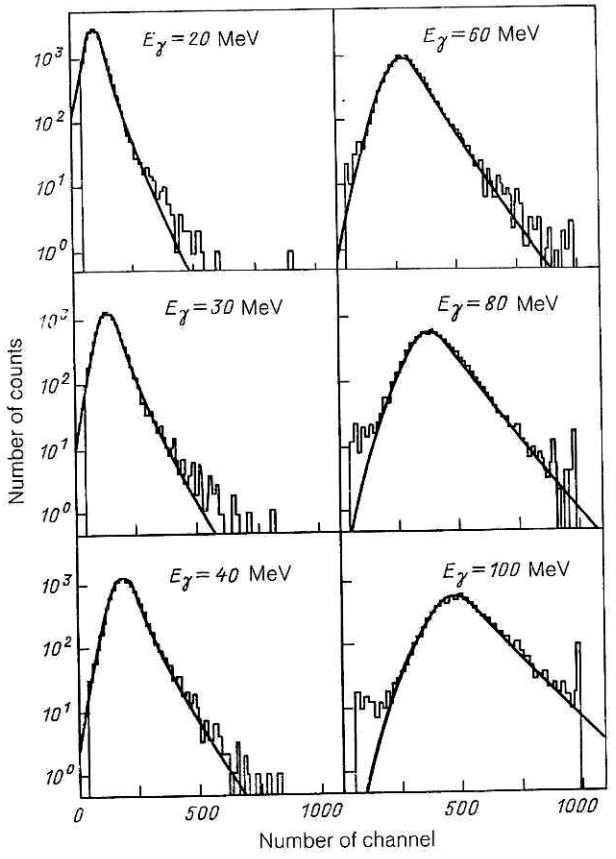


FIG. 4. Instrumental spectra obtained with the MAMI A facility in detection of monoenergetic $\gamma$ rays with different energies by a lead glass detector.[7] The continuous curves are the envelopes of the experimental data.

### Neutrons

The mechanism of detection of fast neutrons in scintillators with large $Z$ is at present not well understood. It is clearly at least a two-step process. One of the mechanisms is moderation of the neutrons in the material of the scintillator with subsequent capture of the neutrons in the $(n, \gamma)$ reaction and detection of the secondary photon. In the employed scintillators the cross section for the radiative capture of only thermal neutrons is at present well known. It is largest for CsI(Tl) and smallest for lead glass (see Table I). But time-of-flight measurements in the study of Ref. 13 showed that the efficiency of fast-neutron detection by lead glass is not so low as was hitherto assumed on the basis of data on the reaction cross section $(n_{\text{therm}}\gamma)$. Moreover, as regards this parameter, lead glass is comparable with other scintillators. This can be seen by comparing the time-of-flight spectra shown in Fig. 5. On the other hand, measurements of the amplitude spectra of scintillation detectors made of NaI(Tl), BGO, and $BaF_2$ corresponding to the detection of fast neutrons showed that:

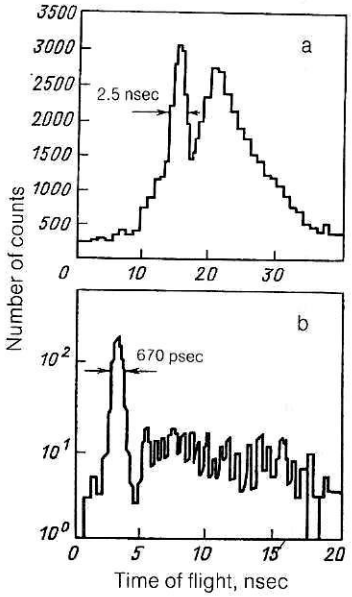


FIG. 5. Time-of-flight spectra: a) for the $^{14}N(35$ MeV/nucleon$) + Ni$ reaction[13] with lead-glass detector 50 cm from the target; b) for the $^{40}Ar(44$ MeV/nucleon$) + {}^{155}Gd$ reaction[5] with $BaF_2$ detector 60 cm from the target (the arrows and numbers indicate the widths of the peaks at half their heights).

a) the shape of the amplitude spectra depends weakly on the energy of the neutrons (Fig. 6) in the case of $BaF_2$ (Ref. 20) and NaI(Tl) (Refs. 21 and 62);

b) the shape can be represented by a rapidly decreasing function with abrupt termination at an amplitude corresponding to $E_\gamma$ of about 8 MeV (Ref. 18);

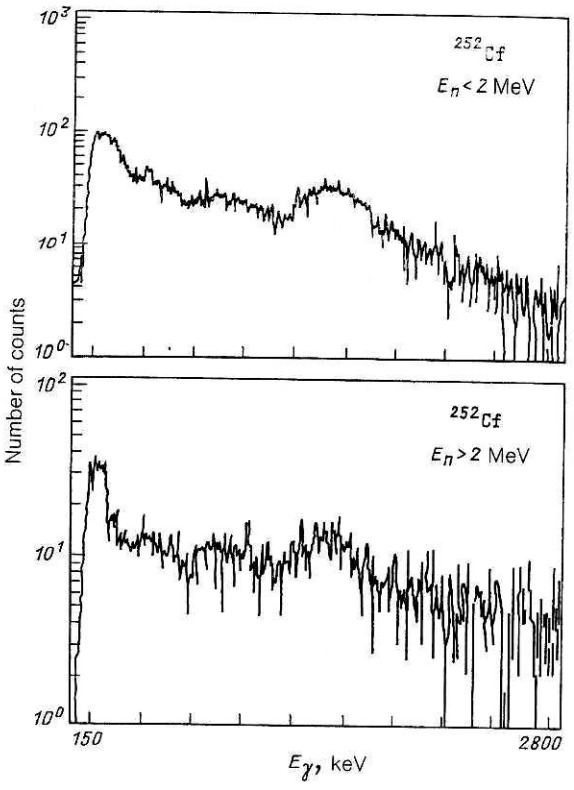


FIG. 6. Instrumental spectra corresponding to detection of neutrons with energy $E_n$ determined by the time-of-flight method over a 40-cm base in a hexagonal $BaF_2$ detector of diameter 10 cm and length 14 cm.[20]

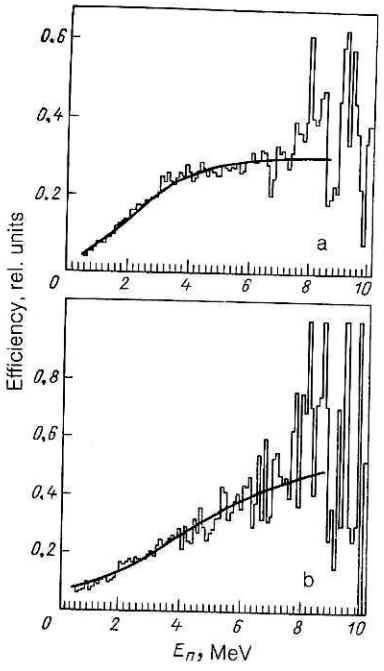


FIG. 7. Total neutron detection efficiency (i.e., the integral of the amplitude spectrum) normalized to the corresponding solid angle: a) for a hexagonal $BaF_2$ detector of diameter 10 cm and length 14 cm (Ref. 20); b) for a cylindrical NaI(Tl) detector of diameter 7.5 cm and height 7.5 cm.[21] The continuous curve is the envelope of the experimental data.

c) the total detection efficiency, i.e., the integral of the amplitude spectrum, increases slowly with the energy of the neutrons and reaches values of 40 and 30% for NaI(Tl) and $BaF_2$, respectively, at $E_n > 6$ MeV (Fig. 7).

Thus, the mechanism of detection of fast neutrons in scintillation detectors of $\gamma$ rays includes not only radiative capture of neutrons moderated to thermal energies but also a further, as yet poorly understood mechanism. From analysis of the shape of the corresponding amplitude spectra it can be assumed that in the region $E_\gamma > 8$ MeV the contribution from the detection of fast neutrons in the scintillation $\gamma$ detector is nevertheless small and does not depend on the neutron energies, although for reactions in which the energies of the incident ions are above 20 MeV/nucleon there are indications that the neutron contribution cannot be entirely ignored.[5] Therefore, an important parameter of the detector is still its time resolution, which is better in $BaF_2$ crystals, in which the scintillation flash has a fast component (see Table I), which permits a time resolution significantly shorter than 1 nsec (see Fig. 5b). In other materials, for example, NaI(Tl), a typical time resolution of the order of a few nanoseconds is achieved. On the other hand, compared with other materials, an advantage of BGO detectors is that their linear dimensions are almost two times smaller, and, accordingly, there is a reduction by a factor of two in the efficiency of detection of the evaporation and pre-equilibrium neutrons at the same $\gamma$-ray detection efficiency, i.e., in the same solid angle relative to the target. The use of BGO crystals made it possible to obtain satisfactory shapes of the response function up to $\gamma$-ray energies of 20 MeV for small crystals in the shape of cylinders of diameter 7.6 cm and heights 7.6 and 2.5 cm, respectively (see Figs. 18 and 19). The decrease in the

volume of the detector simultaneously led to a decrease of the contribution of background radiation to the measured spectra of the high-energy $\gamma$ rays compared with a standard large detector based on a NaI(Tl) crystal of diameter 15 cm and height 10 cm.

### Charged particles

The intensity of the light flash produced by entry of a charged particle into a scintillator is proportional to the energy of the particle and is equivalent to the detection of a $\gamma$ ray with an energy of about the same magnitude. If it is borne in mind that the range of light charged particles with energy 10 MeV/nucleon in aluminum is less than 1 mm, additional measures to eliminate the contribution of high-energy charged particles to the instrumental spectra must be undertaken only for heavy-ion reactions with energy above 10–20 MeV/nucleon.[13] Besides passive shielding, active shielding consisting of thin plastic placed in front of the detector is used for this purpose. Because the plastic is thin, the threshold for the detection of pulses in it can be arranged to be such that practically all the charged particles that enter the $\gamma$-ray detector are detected, and this can be used to abort detection.[13] Recent experiments have also exploited the possibility of identifying cases of charged-particle detection by the shape of the pulse in $BaF_2$ (see Refs. 4 and 10). A CsI(Tl) crystal also possesses such properties (see Fig. 6). As in the case of neutrons, measurement of the time of flight of the particle between the target and the detector is also used. Here the good time resolutions of $BaF_2$ and lead glass permit a short flight path and a corresponding increase of the detector efficiencies.

## 2. DISCOVERY OF A COMPLICATED NATURE OF THE EMISSION OF $\gamma$ RAYS WITH $8 < E_\gamma < 30$ MeV IN HEAVY-ION REACTIONS

Until 1981 the experimental study of the $\gamma$ rays emitted in heavy-ion reactions was restricted to energy $E_\gamma < 8$ MeV. During this time there was established the well-known picture in which the observed $\gamma$-ray spectra were associated with the process of de-excitation of the products of the nuclear reaction. In the statistical model, three main stages were distinguished in the process of de-excitation of highly excited nuclei.[22] In the first stage, neutrons and light charged particles $(\alpha, p)$ are "evaporated," while in the case of heavy nuclei fission into two fragments occurs. In the second stage, when the excitation energy sinks below the binding energy of the particles, there follows the emission of some "statistical" $\gamma$ rays, whose spectrum is described by a relation $\sigma(E_\gamma) \sim \exp(-E_\gamma/T)$ with temperature $T \sim 1$ MeV. Then comes a cascade of comparatively low-energy $\gamma$ rays, $E_\gamma = 0.5$–$1.5$ MeV, between states near the "yrast lines." The number of low-energy $\gamma$ rays and the sum of their energies (the total energy of the cascade) are directly proportional to the angular momentum of the state from which the cascade commences. The data of numerous experiments corresponded to this picture, and in the experimental spectra of the photons one could readily identify the regions of the dipole and quadrupole "bumps" or the cascades of low-energy $\gamma$ rays with $E_\gamma < 2$ MeV and the exponentially decreasing spectrum of the "statistical" $\gamma$ rays for $E_\gamma > 2$ MeV (see, for example, Ref. 22).

In 1981 the results of measurements of $\gamma$-ray spectra in the range $E_\gamma = 2$–$30$ MeV in nuclear reactions between accelerated $^{40}Ar$ ions (170 MeV) and target nuclei of the isotopes $^{82}Se$, $^{110}Pd$, and $^{124}Sn$ were published.[23] A new feature in the experimental data of Ref. 23 was the detection in the $\gamma$-ray spectra of characteristic breaks in the region of $E_\gamma \sim 8$ MeV. An excess in the yield of $\gamma$ rays over the values calculated using the relation $Y_\gamma \sim \exp(-E_\gamma/T)$ for $E_\gamma > 8$ MeV was also observed. The experimental spectra took the form of an exponential as far as $E_\gamma < 8$ MeV, but at higher energies the spectra differed strongly from the exponential, and their shape resembled a broad peak—a "bump." The spectra reached a plateau at $E_\gamma \sim 20$ MeV (Fig. 8). The appearance of this plateau in the experimental spectra was due to the method employed in the study to separate the nuclear-reaction channel (the so-called gamma-start method), and the authors of the study conjectured that the plateau was due to cosmic rays. It has subsequently shown experimentally[2] that the simultaneous arrival of $\gamma$ rays and particles from a cosmic-ray shower in the start detector and the detector of the high-energy $\gamma$ rays did indeed lead to the appearance of a constant background contribution to the experimental spectra.

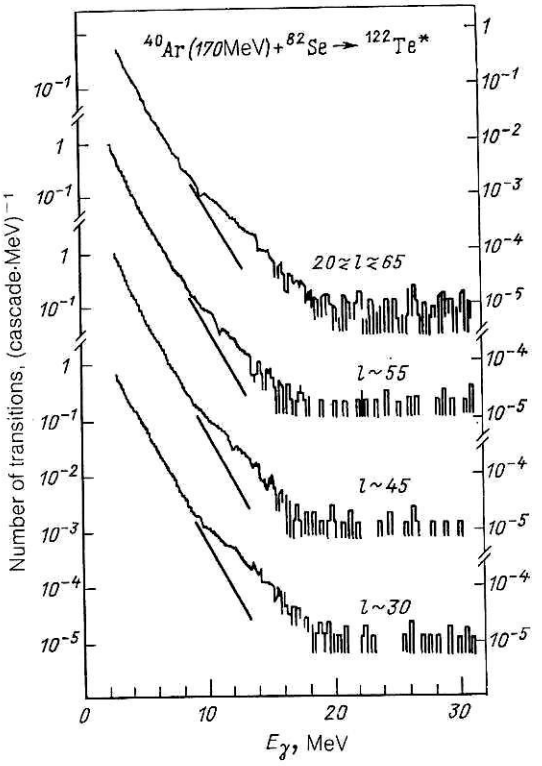


FIG. 8. Gamma spectra corresponding to different windows $E_\gamma = 10$–$40$ MeV in the total energy of the $\gamma$-ray transitions (see the text). The angular momenta corresponding to the spectra are indicated in the figure. The straight lines are the extrapolation of the lower-energy part of the spectra.

The observed bumps in the experimental $\gamma$-ray spectra at $E_\gamma > 8$ MeV and the conjecture that they were associated with excitation of a giant dipole resonance (GDR*) in the compound nucleus stimulated great interest in the study of high-energy photons from heavy-ion reactions that lead to the formation of compound nuclei. Several studies investigated different aspects of the change in the shape of the spectra of the high-energy $\gamma$ rays for different values of the pa-

rameters of the compound nuclei. A search was made for a possible double-hump shape of the spectra corresponding to splitting of the GDR* because of the large angular momentum of the compound nuclei, and the angular anisotropy of the emission of the high-energy $\gamma$ rays was studied. In parallel with the experimental studies there have in recent years been numerous theoretical investigations of the properties of heated and rapidly rotating GDR* nuclei[24–31] and of the giant quadrupole resonance (GQR*).[32,33]

During the following seven years several publications have given the results of investigation of $\gamma$-ray spectra measured in heavy-ion reactions by means of the gamma-start methods. These methods need special consideration, since they do not permit the direct separation of the channel of compound-nucleus formation that is customary when use is made of detectors of the characteristic $\gamma$- or x-ray radiation and of fission fragments, or accurate measurement is made of the charges and masses of the reaction fragments. The main difference between the various gamma-start methods is the number or the total efficiency of the $\gamma$ detectors that produce the start signal. This results in different sensitivities of these methods to the different reaction channels, which do not always differ strongly in the multiplicity of the low-energy $\gamma$ rays that accompany them.[34]

As will become clear from what follows, this may be the reason for the difficulties that arise when the results of different studies are compared. Therefore, in Sec. 2.1 we shall describe the arrangement of the experiments that yielded the data which are analyzed, in order to permit the readers to draw their own conclusions about the reliability of the separation of the compound-nucleus channel by means of these methods.

Particular attention must also be given to the extraction of the parameters that characterize the shape of the spectra and the yield of high-energy $\gamma$ rays. In all the studies that have used the gamma-start method, the analysis of the experimental data was based on the assumption of excitation of a giant resonance in highly excited states of compound nuclei.[23] For nonfissioning nuclei the shape of the $\gamma$-ray spectrum can be described in means of the expressions[35]

$$Y(E_\gamma) = \Gamma_\gamma(E_\gamma)/\Gamma_T;$$

$$\Gamma_\gamma(E_\gamma) = \frac{1}{2\pi\rho(E^*)}\left\{\frac{2E_\gamma^2}{\pi c^2\hbar^2}\,\sigma(E_\gamma)\,\rho(E^*-E_\gamma)\right\}.$$

If the total decay width of the excited nucleus is determined by the neutron width $\Gamma_n$ (this is the case for medium-mass nuclei), then

$$\Gamma_T \sim \Gamma_n = \frac{1}{2\pi\rho(E^*)}\left\{\frac{4M_nT^2}{\pi\hbar^2}\,\sigma_n\rho(E^*-B_n)\right\}.$$

Here, $B_n$, $M_n$, and $T$ are the binding energy and mass of the neutron and the nuclear temperature, respectively. Further, to good accuracy we can write

$$Y(E_\gamma) = \frac{E_\gamma^2\sigma(E_\gamma)}{2c^2T^2M_n\sigma_n}\exp((B_n-E_\gamma)/T).$$

The photoabsorption cross section $\sigma(E_\gamma)$ can be written as

$$\sigma(E_\gamma) = LE_\gamma f(E_\gamma),$$

where $L$ is the total cross section for absorption of $E1$ radiation. The ground-state strength function $Lf(E_\gamma)$ for a giant dipole resonance can be well reproduced by the Lorentzian form

$$f(E_\gamma) = \frac{\Gamma_g E_\gamma}{(E_\gamma^2-E_g^2)^2+E_g^2\Gamma_g^2},$$

where $E_g$ and $\Gamma_g$ are the energy and width of the resonance, respectively. Thus, the $\gamma$ yield at given excitation energy can be described in this simple statistical representation as

$$Y(E_\gamma) \sim \frac{E_\gamma^3}{T^2}\exp((B_n-E_\gamma)/T)\left\{\frac{\Gamma_g E_\gamma}{(E_\gamma^2-E_g^2)^2+E_g^2\Gamma_g^2}\right\}.$$

In general form $\sigma(E_\gamma)$ can be described with allowance for splitting of the giant resonance as follows:

$$\sigma(E_\gamma) = 60\cdot10^{-27}\,(\text{MeV}\cdot\text{cm}^2)\,(2/\pi)$$
$$\times(NZ/A)\sum_{i=1}^{2} S_g^i\Gamma_g^iE_\gamma^2\{(E_\gamma^2-(E_g^i)^2)^2+(E_g^i\Gamma_g^i)^2\}^{-1},$$

where $S_g^i$, $E_g^i$, and $\Gamma_g^i$ are the strength of the resonance (in units of the classical sum rule), its energy, and its width for the two components.

However, by no means all the studies were based on the assumption of splitting of the giant resonance for rapidly rotating nuclei (this assumption was justified in the theoretical study of Ref. 24). Figure 9a shows the $\gamma$-ray spectrum ($Y_\gamma$, which is measured in units of the number of transitions per decay of the compound nucleus by 1 MeV) calculated for the $^{124}$Sn + $^{40}$Ar reaction by means of the program GROGI 2 in the single-component approximation for $\sigma(E_\gamma)$.[23] It can be seen from this figure that without allowance for excitation of the giant dipole resonance (broken curve) the spectrum is roughly a sum of two exponentials of the form $\exp(-E_\gamma/T)$. In the region up to 8 MeV, we have $T\sim1$ MeV, while in the region $E_\gamma > 8$ MeV the nucleus has an effective temperature $T = T_{\text{eff}}$ that can be estimated from the initial excitation energy of the compound nucleus:

$$T_{\text{eff}} = (E^*/a)^{1/2},$$

where $a$ is the level-density parameter. Thus, for clarity, the spectrum calculated with allowance for the excitation of the GDR can be multiplied by $\exp(E_\gamma/T_{\text{eff}})$: $Y'_\gamma = Y_\gamma\exp(E_\gamma/T_{\text{eff}})$, in order to separate the contribution to the $\gamma$-ray spectrum of the $\gamma$ rays from the decay of the GDR* (see Fig. 9b). The resulting curve (in a linear scale; continuous curve) has a shape very close to a single-component Lorentzian profile (broken curve in Fig. 9b). This is the essence of the method used to separate the GDR* peaks from the experimental spectra that was used in a number of studies (see below) to obtain parameters characterizing the shape of the GDR* bump.

In accordance with the considerations mentioned earlier, i.e., with allowance for the differences in the experimental arrangements and in the methods of extracting the parameters of the giant resonances, it is not possible to make a systematic analysis of the experimental data obtained in the different studies on the dependence of such obvious physical parameters as $E_g$, $\Gamma_g$, and $S_g$ ($E1$), which are spectroscopic characteristics ascribed to the nuclei, on the excitation energy and angular momentum that characterize the state of the emitting nucleus. Where possible, such an analysis is made for the experimental data obtained in each separate study.

In all the investigations, the values of $E_g$, $\Gamma_g$, and $S_g$ obtained in the heavy-ion experiments were compared with

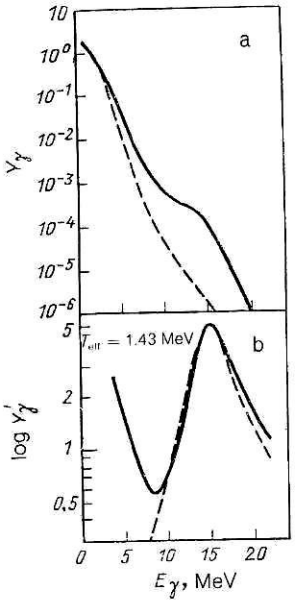


FIG. 9. Gamma spectrum calculated with the program GROGI2 (see the text).

the analogous values for the ground states of the investigated nuclei. A systematic compilation of the GDR, GQR, etc., parameters can be found in Ref. 36 for a wide range of nuclear masses. Figure 10 gives a systematic representation of the GDR parameters for the mass range $20 < A < 220$.

In this section we also give the results of measurements of the angular distribution of the high-energy $\gamma$ rays and of the dependence of the multiplicity of the low-energy $\gamma$ rays accompanying the emission of high-energy $\gamma$ rays together with the results of investigations directed at determining the position of the process of emission of the high-energy $\gamma$ rays on the axis of the interaction time of the complex nuclei.

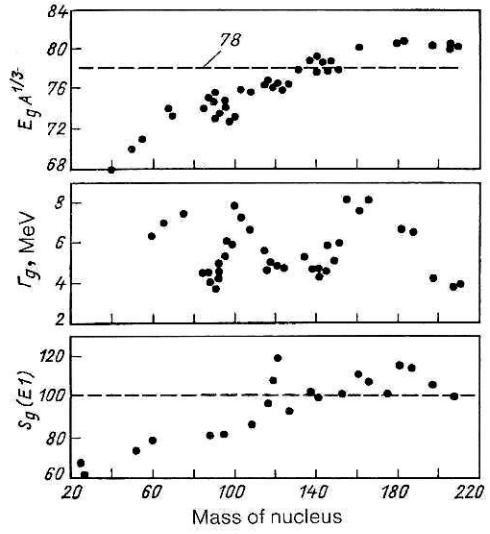


FIG. 10. Systematic representation of parameters[36] that characterize the bumps of the isovector giant dipole resonances for different nuclear masses. The top figure gives the energy at the maximum, approximated by the function $E_g A^{1/3}$, where $A$ is the mass of the emitting nucleus; the central part gives the width $\Gamma_g$ of the resonance; and the bottom part gives the strength of the $E1$ transition, $S_g$ ($E1$), as a percentage of the sum rule.

In investigations of the yield of high-energy $\gamma$ rays in heavy-ion reactions the investigations made at the Laboratory of Nuclear Reactions at the Joint Institute for Nuclear Research at Dubna occupy a particularly important place. In these studies the channel corresponding to the production of the residual nuclei, the reaction products, was separated by direct methods based on detection of characteristic x rays and fission fragments. In these studies it proved to be possible to systematize the data with respect to the ratio of the masses of the interacting nuclei, a parameter that characterizes the entrance channel of the reaction.

### 2.1. Investigation of the shape of the $\gamma$ spectrum in experiments using the gamma-start method

The investigation of Ref. 23 initiated the use of analysis of the shape of the $\gamma$-ray spectra as a new tool for studying nuclear dynamics for nuclei in states very far from the ground state.

The experimental arrangement described in Ref. 23 consisted of a sum spectrometer and eight NaI(Tl) detectors (measuring $12.7 \times 15.2$ cm) of high-energy $\gamma$ rays. These detectors were arranged at different angles. The detection threshold in the eight $\gamma$-ray detectors was set at values between 1.5 and 2.5 MeV according to the particular target in order to accommodate the existing restrictions on the rate of accumulation of data in the computer. This made it possible to detect in the $\gamma$-ray spectrum individual counts for $\gamma$ rays with $E_\gamma > 20$ MeV simultaneously with $10^6$ counts for $E_\gamma \approx 4$ MeV during one day.

The sum spectrometer consisted of two large NaI(Tl) detectors, which measured $33 \times 20$ cm and were placed 2.5 cm from the target, below and above it. Both detectors were divided optically into four sectors. This made it possible to use the sum spectrometer as a filter of the multiplicity of the low-energy $\gamma$ rays. A necessary condition for detection of a high-energy $\gamma$ ray was the presence of signals from at least six sectors of the sum spectrometer. Thus, a high-energy $\gamma$ ray corresponded to a nuclear reaction characterized by a multiplicity of the low-energy $\gamma$ rays greater than five (if rescattering of the $\gamma$ rays between neighboring sectors of the sum spectrometer is ignored).

In the opinion of the authors, this arrangement of the experiment guaranteed that the spectra obtained for the high-energy $\gamma$ rays were effectively freed from background processes such as reactions on light nuclei present as impurities in the target and cosmic-ray processes. The choice of the window in the total energy of the $\gamma$ rays in the interval $10 < E_s < 40$ MeV permitted separation of $\gamma$ rays from states of the compound nucleus with different spins in the interval $(20\text{–}60)\hbar$. Naturally, it was assumed that large values of the spin must correspond to large values of $E_s$.

Figure 8 shows $\gamma$-ray spectra corresponding to different $E_s$ windows for the $^{82}\text{Se} + {}^{40}\text{Ar} \rightarrow {}^{122}\text{Te}^*$ reaction. It is easy to note the increase in the yield of high-energy $\gamma$ rays with decreasing spin of the compound nucleus, as would be expected on the basis of the statistical approach to the description of the mechanism of emission of the high-energy $\gamma$ rays.

The experimental value found for the yield of high-energy $\gamma$ rays with $E_\gamma = 10\text{–}20$ MeV was $(2\text{–}3) \times 10^3$ $\gamma$ rays for one triggering. The excess of the $\gamma$-ray yield over the value calculated by means of the expression

$$Y_\gamma = \text{const}\ E_\gamma \exp\left(-E_\gamma / T_{\text{eff}}\right)$$

at $E_\gamma > 8$ MeV was interpreted in Ref. 23 as an observation of $\gamma$ rays corresponding to the decay of resonance nuclear states (GDR*) based on highly excited states of compound nuclei (see Ref. 37).

In Ref. 23 the procedure described earlier was used to find the shape of the $\gamma$-ray spectrum in the region 8–20 MeV. For $E_\gamma < 8$ MeV the shape of the $\gamma$ spectrum was well described by taking $T_{\text{eff}} \approx 1$ MeV for all three reactions. The fact that at $E_\gamma > 10$ MeV the $\gamma$-ray spectrum reached a plateau indicated emission of these $\gamma$ rays at significantly larger $T_{\text{eff}}$. For the reaction leading to the compound nucleus $^{164}$Er* (target $^{124}$Sn) the value $T_{\text{eff}} = 1.43$ MeV was chosen, and for the conversion of $T_{\text{eff}}$ for the other reactions the relation $T_{\text{eff}} \approx A^{-0.5}$ was used. The experimental spectra were multiplied by $\exp(E_\gamma / T_{\text{eff}})$. The results obtained in this manner are shown in Fig. 11, from which it follows that for the $^{124}$Sn + $^{40}$Ar reaction the energy spectrum has a maximum at 14 MeV and a width close to the width of the giant dipole resonance based on the ground state. At the same time, the energy at the maximum of the peaks (bumps) is displaced to larger values for smaller masses of the compound nuclei, in accordance with the relation $E_g \sim A^{-1/3}$ for the energies of the giant dipole resonances (see Fig. 10).

In the statistical model, by fitting the results of the calculation to the experimental spectra (see Fig. 9), the authors of Ref. 23 determined the energies and widths of the GDR* for the compound nuclei $^{122}$Te*, $^{150}$Gd*, and $^{164}$Er*. The values obtained for the energy $E_g$ corresponded to the known values for the giant dipole resonances on the ground states of the compound nuclei. At the same time, the authors drew attention to the complicated structure of the bumps, which was very different from a simple Lorentzian profile,

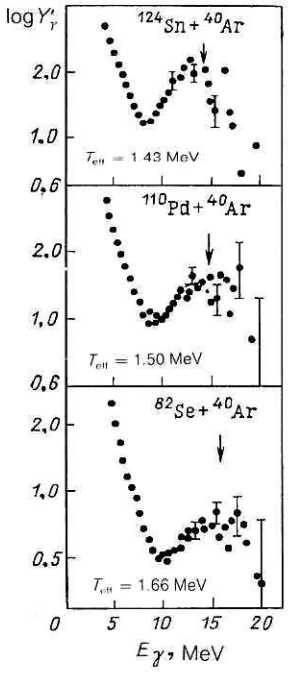


FIG. 11. Gamma spectra corresponding to the total window in $E_\gamma$ (see the text). The arrows indicate the position at the maximum of the isovector giant dipole resonances, calculated in accordance with the expression $E_g = 78/A^{1/3}$ MeV.

and also did not deny a possible contribution to the observed structures from $\gamma$ rays emitted in direct processes from coherent GDR states formed in the initial stages of the reaction.

Similar investigations, but in a wider range of masses of the compound nuclei ($^{154}$Er, $^{153}$Gd, $^{78}$Kr, and $^{46}$Ti), were made in the investigation of Ref. 38. In these experiments, the high-energy $\gamma$ rays were detected by the anti-Compton spectrometer BNL MARKIII (Ref. 12), placed at distance 87 cm from the target. To reduce the contribution of neutrons from nuclear reactions on the target the $\gamma$ rays and neutrons were separated by the time-of-flight method. The gamma-start method was used, and the start detector was a NaI(Tl) detector that measured 24×25 cm and was placed 3 cm from the target.

In the investigation of Ref. 38 the reactions $^{34}$S(141 MeV) + $^{130}$Tl, $^{29}$Si(127 MeV) + $^{124}$Sn, $^{18}$O(60 MeV) + $^{60}$Ni, and $^{18}$O(40 MeV) + $^{28}$Si were studied.

The spectra that were measured are shown in Fig. 12. The continuous curves in this figure are data calculated in accordance with the statistical model using the modified program CASCADE, which includes a unit Lorentzian distribution function. The values of the parameters $E_g$ and $S_g$

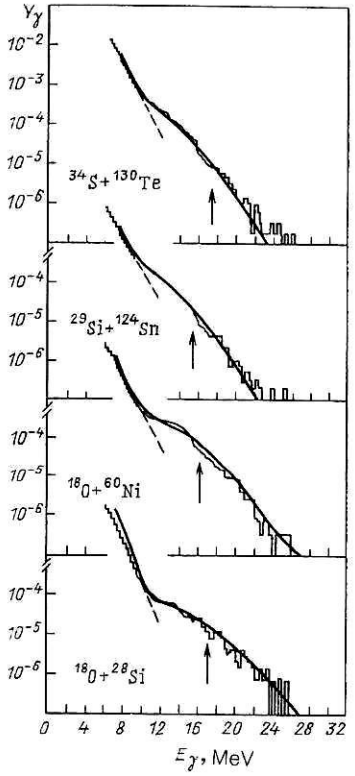


FIG. 12. Gamma spectra of four reactions. The values of $Y_\gamma$ were obtained with allowance for the total efficiency of the detector of the high-energy $\gamma$ rays, and also under the assumption of isotropy of the angular distribution of the $\gamma$-ray emission. The continuous curves are the result of calculation in accordance with the statistical theory for the following values of the parameters of the isovector giant dipole resonances (from top to bottom in the figure):

$S_g(E1) = 100\%$, $E_g = 17$ MeV, $\Gamma_g = 13$ MeV;
$S_g(E1) = 35\%$, $E_g = 15$ MeV, $\Gamma_g = 11$ MeV;
$S_g(E1) = 65\%$, $E_g = 16$ MeV, $\Gamma_g = 8$ MeV;
$S_g(E1) = 50\%$, $E_g = 17$ MeV, $\Gamma_g = 12$ MeV;

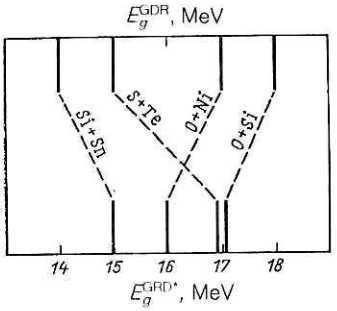


FIG. 13. Comparison of the values of the energies at the maxima of the GDR* optimized in the description of the experimental $\gamma$-ray spectra for four reactions (see Fig. 12) by means of the program CASCADE (at the bottom of the figure) with values of $E_g$ for the GDR (at the top of the figure) excited on the ground states of the nuclei in accordance with the systematic representation in Fig. 10.

corresponding to the best fit to the experimental data are indicated in Figs. 13 and 14. A tendency for the $\gamma$-ray yield to exceed the statistical decay in the region $E_\gamma \approx 11$ MeV with decreasing A was noted. The fitted values of $E_g$ and $\Gamma_g$ differed appreciably from the values of $E_g$ for the ground states of these nuclei and did not satisfy the well-known systematics $E_g \sim A^{-1/3}$ (see Fig. 13). In the opinion of the authors, this could have been due to a strong spin dependence of $E_g$. A similar deviation of $E_g$ from the systematics was observed in Ref. 35.

On the other hand, good agreement was observed between the fitted values of $S_g$ ($E1$) and the values of $S_g$ ($E1$) obtained for neighboring nuclei in the ground state in photoabsorption reactions (Fig. 14). This indicated that the statistical approach to the quantitative description of the yield of high-energy $\gamma$ rays was valid.

A detailed analysis of the $\gamma$-ray spectrum in the framework of the statistical theory in a wide range of masses of the compound nuclei, $63 < A < 127$, was also made in the study of Ref. 39. In this study particular attention was devoted to the influence of the angular momentum of the compound nucleus on the shape of the $\gamma$-ray spectrum in the high-energy region In the study of Ref. 39 the high-energy $\gamma$ rays were detected by a NaI(Tl) detector, which measured $25 \times 30$ cm and was placed in an anti-Compton shield at distance 72 cm from the target; the time-of-flight method was used to reduce the contribution of the neutrons from nuclear reactions on the target. Reactions of $^{12}$C ions (42–60 MeV) with the

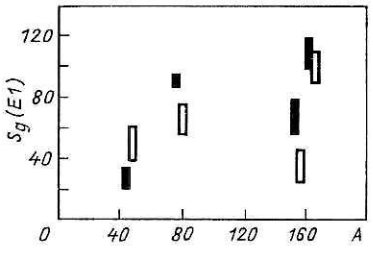


FIG. 14. Oscillator strengths as percentages of the sum rules (open rectangles) determined as a result of calculations (see Fig. 12). The black rectangles are the values of $S_g$ ($E1$) for the giant dipole resonances excited on the ground states of the nuclei in accordance with the systematic compilation of Fig. 10.

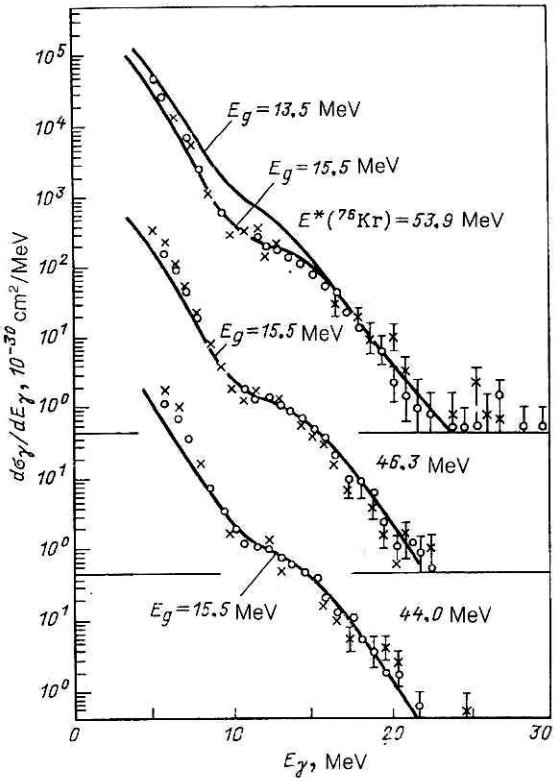


FIG. 15. Gamma spectra corresponding to decay of $^{76}$Kr at excitation energies 44.0, 46.3, and 53.9 MeV. The open circles are the data for the $^{18}O + ^{58}Ni$ reaction, and the crosses are for the $^{12}C + ^{64}Zn$ reaction. The cross sections are given for the reaction with $^{18}$O ions. The data of the other reaction are normalized to them. The continuous curves are the results of calculation in accordance with the statistical model with the indicated values of the parameters $E_g$ for $\Gamma_g = 7.0$ MeV.

nuclei $^{51}$V, $^{64}$Zn, and $^{115}$In, leading to the formation of the compound nuclei $^{63}$Cu, $^{76}$Kr, and $^{127}$Cs, respectively, with excitation energy about 50–60 MeV, were investigated. The same compound nuclei but with higher angular momentum were studied in reactions between $^{18}$O ions (42–60 MeV) and the nuclei $^{45}$Sc, $^{58}$Ni, and $^{109}$Ag.

The experimental shape of the $\gamma$-ray spectra shown in Figs. 15 and 16 was well reproduced in the region $E_\gamma > 8$ MeV in calculations in accordance with the statistical model (CASCADE program) with the fitted parameters $E_g$ and $\Gamma_g$ given in Table II.

In the study it was noted that the fitted values of $E_g$ were found to be 1.0–1.5 MeV lower than the values for the corresponding ground states of the nuclei, and that this effect could not be explained by the influence of the angular momentum on the shape of the compound nucleus. This was the case because the spins of the investigated compound nuclei were below the limit $l = 20\hbar$ given in the theoretical study of Ref. 26. Upper bounds were obtained for the variation of $E_g$ and $\Gamma_g$ with respect to the spin: $dE_g/dl < 0.1$ MeV and $d\Gamma_g/dl < 0.1$ MeV.

Contradictory conclusions about the agreement between the parameters of giant dipole resonances excited on the ground state of nuclei and in heavy-ion reactions, in which the excitation of the GDR* is necessarily associated with a high excitation energy and a broad angular-momentum distribution in the compound nucleus, raised the ques-

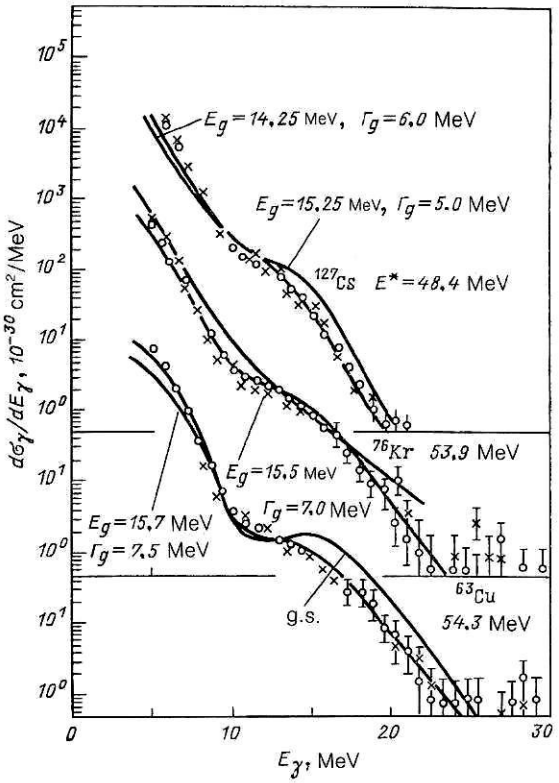


FIG. 16. Gamma spectra corresponding to decay of different compound nuclei. At the top, $^{137}$Cs and excitation energy 48.4 MeV with crosses for data on the $^{12}C + ^{115}I$ reaction and the open circles for data on the $^{18}O + ^{109}Ag$ reaction; at the center, $^{76}$Kr (53.9 MeV) with the crosses for the $^{12}C + ^{64}Zn$ reaction and the open circles for the $^{15}O + ^{58}Ni$ reaction; at the bottom $^{63}$Cu (54.3 MeV) with the crosses for the $^{12}C + ^{51}V$ reaction and open circles for the $^{18}O + ^{45}Sc$ reaction. The curves are the results of calculations made in accordance with the statistical model with the parameters indicated for the giant dipole resonances.

tion of the validity of the gamma-start method for separating the channel of compound-nucleus formation.

The validity of the gamma-start method for this purpose was tested in Ref. 40 by comparing the $\gamma$-ray spectra measured using this method and by using coincidence with the characteristic $\gamma$ line of the isomer level of the residual $^{144}$Gd nucleus with half-life $t = 190$ nsec.

In the experiment of Ref. 40 the high-energy $\gamma$ rays were detected by a NaI(Tl) detector which measured 25.4×30.5 cm and was placed in an anti-Compton shield of Ne 102 plastic at distance 60 cm from the target. The time-of-flight method was used to reduce the contribution of the neutrons from nuclear reactions on the target, a paraffin block of thickness 20 cm being used to moderate the neutrons. A study was made of reactions of 145-MeV $^{28}$Si ions with $^{120}$Sn nuclei, which led to the formation of compound $^{148}$Gd nuclei. The detector of the high-energy $\gamma$ rays was placed at angles 0, 38, and 90° to the direction of the beam of ions, but the experimental difficulties and poor statistics did not permit reliable conclusions to be drawn about the angular anisotropy of the emission of the high-energy $\gamma$ rays. The spectrum of the photons is shown in Fig. 17.

Four NaI(Tl) detectors, measuring 12.5×15 cm and placed in a lead shield, were used to determine the mean multiplicity $\langle M_\gamma \rangle$ of $\gamma$ rays accompanying the emission of the high-energy $\gamma$ rays. A small decrease of $\langle M_\gamma \rangle$ with increasing energy of the high-energy $\gamma$ ray (Fig. 18).

A condition of delayed coincidence of the trigger detector of the $^{144}$Gd isomer level with the detector of the high-energy $\gamma$ rays did not change at all the shape of the experimental spectra. The experimental value of the yield of high-energy photons with $E_\gamma = 9$–20 MeV, after subtraction of the exponential, was $(2.8 \pm 0.6) \times 10^{-3}$ $\gamma$ rays for one delayed triggering, in good agreement with the value given in Ref. 23.

The fit of the calculations to the experimental spectra led to the values $E_g = 12.2$ MeV and $\Gamma_g = 8.9$ MeV, which differ strongly from the parameters of the giant dipole resonance on the ground state of the compound nucleus. In particular, for $A = 144$ use of the relation $E_g = 78A^{-1/3}$ gives $E_g = 14.9$ MeV. The authors also succeeded in describing the experimental spectra by means of a two-component giant dipole resonance with $E_g^1 = 11.6$ MeV and $E_g^2 = 14.9$ MeV and width $\Gamma_g = 6.7$ MeV of both components (see Fig. 17).

As follows from what we have been saying, the study of Ref. 40 is by no means alone in not denying the possibility of describing the broad bump in the region of the giant dipole resonance by means of two components corresponding to longitudinal and transverse vibrations of deformed nuclei.

The experimental observation of a double-hump shape of the bump in the spectrum of the high-energy $\gamma$ rays for $E_\gamma > 8$ MeV was first reported in Ref. 41. A measurement was made of the direct spectrum of $\gamma$ rays in reactions of 63-MeV $^{12}$C ions with $^{148}$Sm and $^{154}$Sm nuclei, leading to the

TABLE II. Parameters characterizing compound nuclei formed in reactions with carbon and oxygen ions: $E^*$ is the excitation energy, $l$ is the angular momentum, and $E_g$ and $\Gamma_g$ are adjustable parameters obtained by attempting to reproduce the $\gamma$-ray spectra from the compound nuclei in accordance with the statistical model (see the text).

| Compound nucleus | $E^*$, MeV | $l$, $\hbar$ ($^{18}$O) | $l$, $\hbar$ ($^{12}$C) | $E_g^a$, MeV | $\Gamma_g^a$, MeV |
|---|---|---|---|---|---|
| $^{63}$Cu | 54.3 | 10 | 16 | 15.7 | 7.5 |
| $^{76}$Kr | 44.0 | 9 | 15 | 15.5 | 7.0 |
| $^{76}$Kr | 46.3 | 12 | 15 | 15.5 | 7.0 |
| $^{76}$Kr | 53.9 | 17 | 19 | 15.5 | 7.0 |
| $^{137}$Cs | 48.4 | 8 | 16 | 14.25 | 6.0 |

[a] The values of $E_g$ and $\Gamma_g$ were obtained with an error ± (0.5–0.75) MeV.

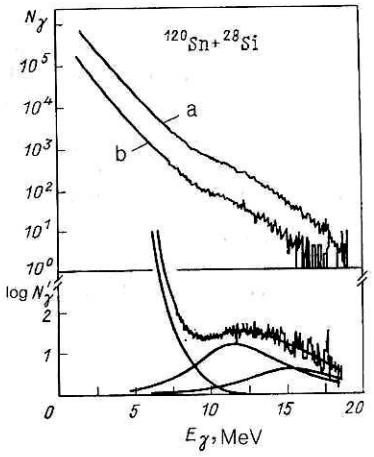


FIG. 17. Gamma spectra measured using $M_\gamma$ filter [curve (a)] and in the method of delayed coincidences with $\gamma$ rays from the decay of the isomer state of the residual nucleus [curve (b)] (see the text). The lower part of the figure shows the experimental data corresponding to curve (a) shown in the upper part of the figure in a comparison with a calculated curve that consists of three components, namely, an exponential "tail" and two Lorentzian curves. For better graphical representation the experimental $N_\gamma$ and the calculated data have been normalized, i.e., $N'_\gamma = N_\gamma / [E_\gamma^2 \exp(-E_\gamma/T_{\text{eff}})]$, and, therefore, the vertical scale of the lower part of the figure is represented in relative units.

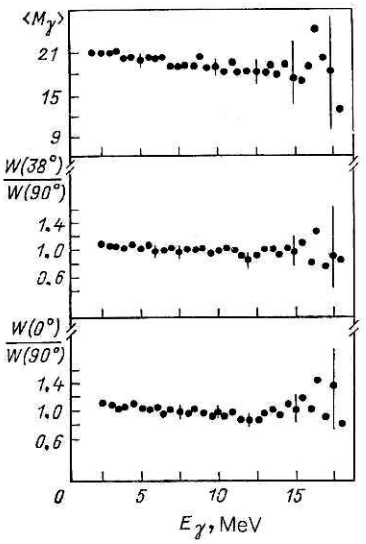


FIG. 18. Results of measurement of $\langle M_\gamma \rangle$ and W as functions of $E_\gamma$ by the method of delayed coincidences with $\gamma$ rays from decay of the isomer state of the residual nucleus [see the text and curve (b) in Fig. 17].

formation of the compound nuclei $^{160}$Er and $^{166}$Er, respectively. Determination of the time correlations between the detector of the high-energy $\gamma$ rays and the signal from the high-frequency master oscillator of the accelerator made it possible to reduce the contribution to the experimental spectra from cosmic-ray showers and other background processes.

In Fig. 19 the measured spectra are compared with calculations made by means of the modified program CASCADE. Comparing the theory with the experiment (Fig. 19), the authors of Ref. 41 concluded that the best agreement is observed if two components of the GDR* are used in the calculations. The optimized parameters are given in Table III.

Using the data of Ref. 44 and the hydrodynamic model of Ref. 45, which gives the specific ratio of the resonance strengths for a prolate nucleus, $S_g^2 : S_g^1 = 2:1$, and an oblate nucleus, $S_g^2 : S_g^1 = 1:2$, and also the ratio

$$E_g^2 : E_g^1 = 0.911d + 0.089,$$

where $d$ is the ratio of the largest symmetry semiaxis to the smallest, the authors succeeded in obtaining from the data of Table III the values $\delta = (d-1)d^{-1/3} = 0.3$ and 0.25, respectively, for the deformations of the compound nuclei $^{166}$Er* and $^{160}$Er*. These results agree well with the values obtained from measurements of the quadrupole moments for these nuclei at low energies ($\delta = 0.95\beta$ with the values of $\beta$ taken from Ref. 46; averaging over $^{164,166}$Er and $^{158,160}$Er yielded values of $\delta$ equal to 0.3 and 0.24, respectively).

The data of this study relate to nuclei with mean temperature $T \approx 1$ MeV (for level-density parameter $a = A/8$ in the Fermi-gas model). This is below the critical temperature $T_{\text{cr}} \approx 2$ MeV for such nuclei. In accordance with Ref. 47 an yrast-like deformation must persist for $T < T_{\text{cr}} = 40\delta A^{-1/3} \approx 2$ MeV, and thus the authors concluded that the shape of the GDR* $\gamma$-ray spectrum for heated deformed nuclei at mean temperature $T \approx 1$ MeV and spin $l = 0$–25h was remarkably similar to the shape of the $\gamma$-ray spectrum of the giant dipole resonance excited on the ground state of the same nuclei (Fig. 20).

The conclusions drawn in Ref. 41 contradict the data obtained with the Crystal Ball facility, which possessed great

TABLE III. Optimized parameters of GDR* (see the text).

| Nucleus | $E_g^1$, MeV | $\Gamma_g^1$, MeV | $S_g^1$ | $E_g^2$, MeV | $\Gamma_g^2$, MeV | $S_g^2$ |
|---|---|---|---|---|---|---|
| $^{166}$Er* | 12.15±0.09 | 3.69±0.23 | 0.43±0.07 | 15.77±0.17 | 5.75±0.71 | 0.74±0.11 |
| $^{160}$Er* | 12.21±0.09 | 3.13±0.21 | 0.39±0.07 | 15.17±0.18 | 4.81±0.51 | 0.64±0.09 |
| $^{154}$Sm[a] | 12.35±0.10 | 3.35±0.15 | 0.45±0.03 | 16.10±0.10 | 5.25±0.20 | 0.76±0.05 |
| Er[a] | 12.0 | 2.9 | 0.42 | 15.45 | 5.0 | 0.84 |

*Note.* The asterisk signifies that the data refer to an ensemble of the nuclei $^{164\text{-}166}$Er and $^{158\text{-}160}$Er with mean excitation energy $E^* \approx 30$ MeV and angular momentum $l = 0$–25$\hbar$; the superscript "$a$" indicates data of measurements for the ground state of the nuclei in $(\gamma, n)$ reactions from Refs. 42 and 43.

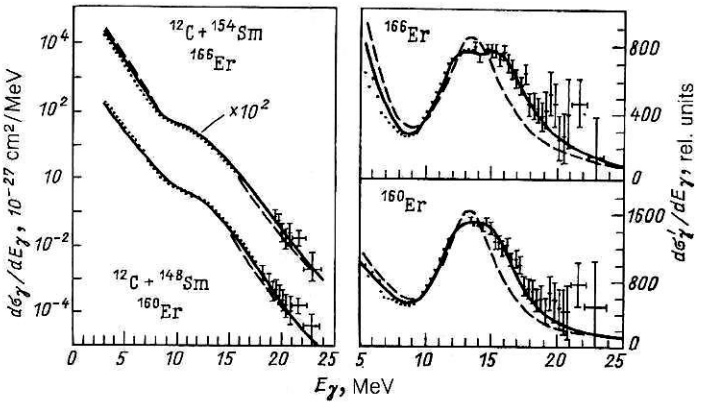


FIG. 19. Spectra of $\gamma$ rays from decay of $^{166}$Er nuclei at excitation energy $E^* = 49.2$ MeV and of $^{160}$Er nuclei at $E^* = 43.2$ MeV formed, respectively, in the $^{12}C + ^{154}Sm$ and $^{12}C + ^{148}Sm$ reactions at mean energy 61.2 MeV of the bombarding carbon ions. The broken and continuous curves are the rms fit of the spectra calculated in accordance with the statistical model (CASCADE program) for the region $E_\gamma = 9$–21 MeV under the assumptions, respectively, of a single-component and two-component form of the GDR*. The detector response function was used in the calculations. The ordinate gives the mean values of the cross section $\sigma_\gamma(E_\gamma)$ in the region of angles $\theta_\gamma = 65$–140°. The right-hand part of the figure shows the product $\sigma'_\gamma(E_\gamma) = \sigma_\gamma(E_\gamma)\exp(\alpha E_\gamma)$, where $\alpha^{-1} = 1.45$ MeV for $^{166}$Er and 1.40 MeV for $^{160}$Er.

methodological possibilities.[48] In the study of Ref. 48 an investigation was made of the $\gamma$-ray spectra in the reaction $^{34}S(155\text{ MeV}) + ^{128}Tl$, which leads, as in the study of Ref. 41, to formation of an erbium isotope with mass close to that of the nuclei studied in Ref. 41 and with excitation energy 71 MeV and angular momenta up to 65h. Gamma rays with energy $E_\gamma > 4.7$ MeV were detected in any of the 160 modules of the spectrometer in coincidence with $\gamma$ rays of any energy detected by other modules.

Because of the $4\pi$ geometry the multiplicity $N$ of the response of the modules was proportional to the angular momentum of the residual nucleus produced in the interaction event. The $\gamma$-ray spectra for different windows with respect to $N$, i.e., with respect to the angular momentum, are given in Fig. 21. The same procedure for separating the GDR bumps was used, namely, multiplication of the experimental spectrum by the factor $\exp(aE_\gamma)$, $a^{-1} = 1.6$ MeV. The data obtained in this manner are shown in Fig. 22. The authors succeeded in describing the data by introducing into the calculation of the $\gamma$-ray spectra (CASCADE code) just one GDR component. However, this approach necessitated a decrease of the energy and width of the resonance with increasing spin. For small values of the spins the energies $E_g$ agreed well with the data for the ground state. The optimized parameters are given in Table IV.

A study of the shape of the spectra of the high-energy photons for Er isotopes was also made in Ref. 49. Studies were made of the reactions $^{16}O(84\text{ MeV}) + ^{150}Nd$ and

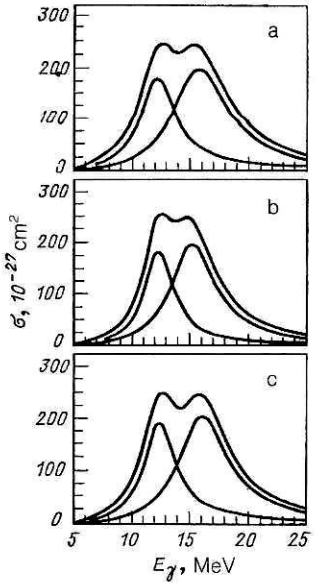


FIG. 20. Photoabsorption cross section $\sigma(E_\gamma)$ extracted from analysis of experimental data: a) best fit for the case of $\gamma$ decay of $^{166}$Er; b) for $^{160}$Er (see Fig. 19 and Table II); c) fit of calculated curve for the case of photoabsorption in the ground state in the $^{154}Sm(\gamma, n)$ reaction. The data are taken from Refs. 42 and 43 and Table III.

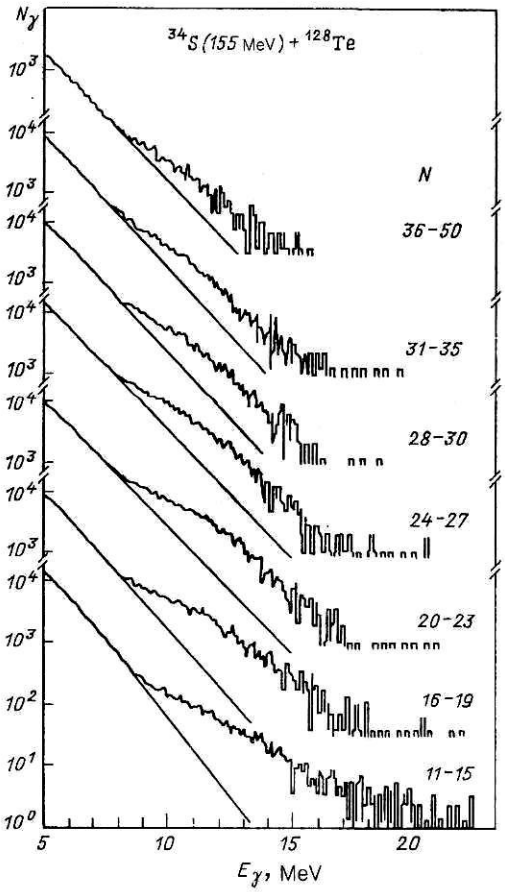


FIG. 21. Spectra of high-energy $\gamma$ rays for an individual detector corresponding to different numbers $N$ of $\gamma$ rays coincident with them in other detectors. The straight lines are the extrapolations of the low-energy part of the $\gamma$-ray spectra to the region of energies above 8 MeV.

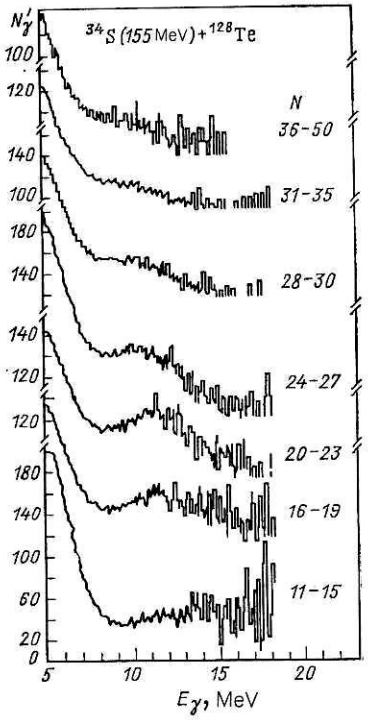


FIG. 22. The same as in Fig. 21, multiplied by an exponential factor (see the text).

$^{17}O$(72 MeV) + $^{148}Nd$, which lead, respectively, to the formation of compound nuclei $^{155}Er$ with excitation energy $E^* = 61.5$ MeV and angular momenta $l \leqslant 36\hbar$ and $^{165}Er$ with $E^* = 49.9$ MeV and $l \leqslant 23\hbar$. In this experiment, as in that of Ref. 48, only a single-hump structure of the bump in the region $E_\gamma \geqslant 10$ MeV was observed. By means of a special technique it was established that about 25% of the total cross section for $\gamma$-ray emission in the region 10–20 MeV was associated with the emision of $\gamma$ rays in competition with evaporation of the first neutron from the compound nucleus $^{166}Er$.

It should be noted that the differences in the shapes of the $\gamma$-ray spectra of neighboring Er isotopes found by comparing the data of different studies could be due to the significant differences in the excitation energies and angular momenta. A double-hump structure of the bump is most clearly observed at a relatively low excitation energy, around 30 MeV (Ref. 41). In the other studies of Refs. 23, 38, and 48–50 the erbium isotopes were studied at higher excitation energies, and the conclusions drawn in them about the number of peaks forming the bump are not unambiguous.

In the study of Ref. 35 a special investigation was made of the yield of high-energy $\gamma$ rays as a function of the energy of the residual nuclei. The high-energy $\gamma$ rays were detected by seven NaI(Tl) detectors that measured $12.7 \times 15.2$ cm and were placed at distance 50 cm from the target. Six of them lay in a single (the horizontal) plane at angles $\pm 90$, $\pm 120$, and $\pm 150°$ relative to the beam direction, and one was perpendicular to this plane. The $^{136}Xe$(1150 MeV) + $^{197}Au$ reaction was studied. Fragments close in mass to the Xe nuclei were detected at angle 29° near the classical grazing angle by eight silicon detectors ($\Omega = 6.4$ msr/detector), which were placed in a ring around the beam axis (Fig. 23). The photon spectra corresponding to different "windows" of $Q$ values of the reaction (the mean energies in windows 1–5 were 34, 80, 119, 159, and 199 MeV, respectively) are shown in Fig. 24. The spectra were corrected to take into account the Doppler effect and correspond to only two-body kinematics. In this experiment there was observed to be a sharp growth of the yield of high-energy $\gamma$ rays in the region 10–20 MeV with increasing degree of inelasticity of the interaction or, in other words, with increasing excitation energy of the fragments.

Comparison of the experimental spectra with spectra calculated using the statistical model showed that it was necessary to change the parameters $E_g$ and $\Gamma_g$ in order to describe the complete set of $\gamma$-ray spectra at different excitation energies. Thus, with increasing excitation energy of the fragments it was necessary, in order to achieve the best agreement between the calculations and the experiments, to reduce the energy of the resonance and increase its width relative to the values of these quantities for the ground state.

There have been several investigations in which measurements similar to those described earlier were made and the shape of the $\gamma$-ray spectra and the yield of high-energy $\gamma$ rays were analyzed. For example, the $^{12}C$(100 MeV) + $^{159}Tb$ reaction was studied.[51] An analysis of the shape of the photon spectra in a wide range of masses of the target nuclei and of the energies of the bombarding ions, $\varepsilon = (5 \pm 7)$ MeV/nucleon, in reactions with the light ions $^{3,4}He$, $^{12}C$, and $^{16}O$ was made in Ref. 52.

In Ref. 50 the results were given of investigations of the reactions $^{3}He$(12–26 MeV) + $^{25}Mg$, $^{16}O$(40 MeV) + $^{12}C$ and of the reactions $^{12}C + {}^{51}V \rightarrow {}^{63}Cu$ and $^{4}He + {}^{59}Co \rightarrow {}^{63}Cu$ with $^{63}Cu$ excitation energy from 17 to 52 MeV, and data for the reactions $^{12}C$(61.5 MeV) + $^{154}Sm \rightarrow {}^{166}Er^*$ and $\alpha$(27 MeV) + $^{149,154}Sm$ were analyzed.

The experimental data characterizing the shape of the $\gamma$-ray spectra and the yield of $\gamma$ rays in the region of energies of the giant dipole resonances and their analysis that we have

TABLE IV. Optimized parameters of GDR* used in calculation of the spectra of high-energy $\gamma$ rays for the reaction $^{34}S$(155 MeV) + $^{128}Te$ in various windows in the angular momentum $l$ of the residual nuclei (see the text).

| $N$ | $l$, $\hbar$ | $E_g$, MeV | $\Gamma_g$, MeV | $S_g$ |
|---|---|---|---|---|
| 29—40 | 45 | 12.0 | 6.50 | 0.56 |
| 25—28 | 36 | 12.5 | 5.75 | 0.56 |
| 21—24 | 30 | 13.0 | 5.00 | 0.67 |
| 17—20 | 23 | 14.0 | 5.00 | 0.52 |
| 13—16 | 16 | 15.0 | 7.00 | 0.44 |
| 9—12 | 10 | 14.5 | 9.00 | 0.30 |

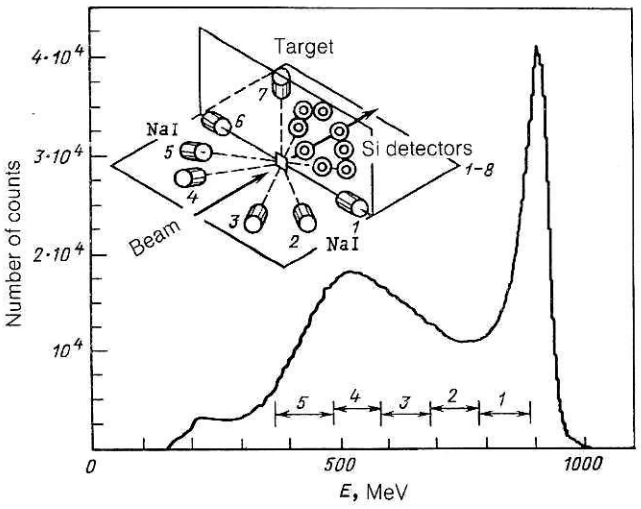


FIG. 23. Summed energy spectrum in the laboratory system of fragments that had mass and charge close to those of the bombarding Xe ion and were detected at angle 29° by eight silicon detectors. The geometry of the experiment is shown schematically in the inset.

given in this subsection are not, of course, complete, but they do reflect the general picture that has been obtained from the investigations of the high-energy $\gamma$ rays emitted in heavy-ion reactions and studied by means of the gamma-start method.

On the one hand, the shape of the spectra and the yield of the $\gamma$ rays in the GDR region can be satisfactorily described in the framework of the statistical theory under the assumption that the properties of the giant dipole resonances excited on the ground state or a higher-lying state of the nucleus are equivalent (Brink's hypothesis). On the other hand, the GDR* parameters deduced by analyzing the experimental data in the framework of the statistical theory differ significantly, as a rule, from the parameters of the GDR excited on the ground states of the same nuclei. They also differ for neighboring nuclei studied in different investigations, for example, for the erbium isotopes. The reason for these differences is not clear, and one cannot rule out the possibility of an influence on the final result of the actual arrangement of the experiments using the gamma-start method. The reason could lie in the parameters of the reactions—the excitation energy, the angular momenta, and the mass ratio of the interacting nuclei. As was noted in Ref. 50, after the euphoria associated with the apparently obvious fact of the statistical nature of the excitation of giant resonances on high-lying states of the compound nuclei additional detailed investigations in this field of heavy-ion physics are needed.

We give now data of experiments made using a fundamentally new approach to investigate the emission of high-energy $\gamma$ rays in heavy-ion reactions.

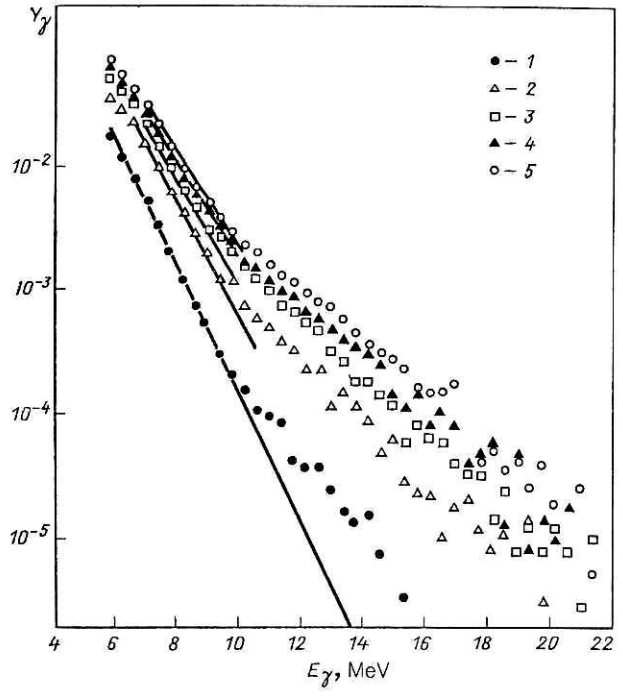


FIG. 24. Gamma-ray spectra corresponding to the five different regions of the energy spectrum of the fragments with parameters close to those of Xe as shown in Fig. 23 (see also the text).

### 2.2. Investigation of the yield of high-energy $\gamma$ rays by means of the characteristic x-ray radiation and the fission fragments

As we noted above, to separate the channel of the formation of the compound nucleus the authors of Refs. 23, 49, and 50 and other studies used the gamma-start method, i.e., they investigated the yields of $\gamma$ rays with energy $E_\gamma > 4$ MeV in coincidence with a cascade of low-energy ($E_\gamma \approx 1$ MeV) $\gamma$ rays corresponding to the final stage in the decay of the excited residual nuclei. However, in heavy-ion reactions highly excited nuclei are formed not only in the fusion channel but also in the majority of the other channels of deep inelastic interactions. This fact partly devalues the advantages of using the gamma-start method in these reactions and casts doubt on the correspondence between the high-energy $\gamma$ rays observed in this manner and the $\gamma$ decay of giant resonances in excited compound nuclei. In this connection it is necessary to use direct methods to separate the channel in which the compound nuclei are formed, basing these, for example, on detection of the characteristic x-ray radiation of the residual nuclei and fission fragments of the compound nuclei.

*a) The fission channel.* Results of experiments to observe the emission of high-energy $\gamma$ rays corresponding to the channel in which the compound nucleus Bi* is formed were presented in Ref. 53. The fusion channel in the reactions $^{159}$Tb + $^{40}$Ar(220, 300 MeV), $^{181}$Ta + $^{22}$Ne(155 MeV) and $^{192}$Os + $^{15}$N(147 MeV) was separated by detecting the fission fragments of the compound nuclei. It was established that the experimental $\gamma$-ray spectra obtained in the investigated reactions have the same shape in the region $E_\gamma < 10$ MeV (Ref. 54). This fact agrees with theoretical estimates of the yield of $\gamma$ rays accompanying decay of excited compound nuclei Bi* and excited Bi* fission fragments as calculated by means of the modified program CASCADE[55] and a Monte Carlo program,[56] respectively. The results of these calculations showed that the calculated yield of high-energy $\gamma$ rays depends mainly on the excitation energy of the compound nucleus Bi*, i.e., it is relatively larger for the reactions $^{192}$Os + $^{15}$N(147 MeV) and $^{159}$Tb + Ar(300 MeV) and relatively smaller for the reaction $^{159}$Tb + $^{40}$Ar(220

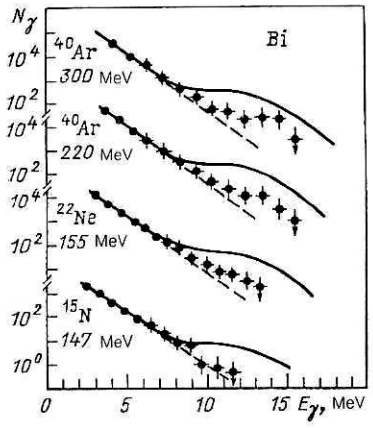


FIG. 25. Gamma-ray spectra. The points are the experimental data normalized at $E_\gamma < 8$ MeV to the theoretical curve (continuous line); see the text.

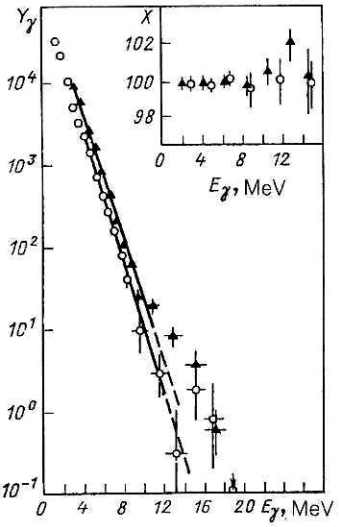


FIG. 27. Spectra of high-energy $\gamma$ rays measured in coincidence with characteristic x rays of products having $Z$ values close to that of the compound nucleus for the reaction $^{64}Zn + {}^{68}Zn$ (black circles) and the reaction $^{20}Ne + {}^{112}Sn$ (open circles). In the inset $X$ is the number of the channel of the spectrum of the $K$ x rays corresponding to the position of the centroid of the peak of the characteristic x rays measured in coincidence with the high-energy $\gamma$ rays.

MeV). However, this result is in manifest disagreement with experiment (Fig. 25).

*b) The evaporation channel.* The yield of high-energy $\gamma$ rays in the evaporation channel of the reactions was studied by means of the method of coincidence with characteristic x rays of the $K$ shell ($K$ x rays), which is described in Ref. 58. The advantages of detecting $K$ x rays to separate the reaction channel in a wide $Z$ range of the products of heavy-ion reactions were demonstrated.

A detailed study of the dependence of the high-energy $\gamma$ rays on the entrance channel was made for the reactions $^{20}Ne(220\ MeV) + {}^{112}Sn$ and $^{64}Zn(290\ MeV) + {}^{68}Zn$, which lead to the formation of the same compound nucleus $^{132}Nd$ with nearly the same excitation energies.[54] The experiments were made with thick targets, behind which the detector of the $K$ x rays was placed, ensuring a high efficiency of their detection.

The measurement of the $\gamma$-ray spectra by the gamma-start method did not reveal, to within the experimental error, any differences in the shape of the $\gamma$-ray spectra for the two reactions up to $E_\gamma \approx 19$ MeV (Fig. 26). The $\gamma$-ray spectra had rises at $E_\gamma > 8$ MeV like those observed in the studies of Refs. 23, 50, and others. In contrast, the $\gamma$ spectra measured in coincidence with $K$ x rays of reaction products with $Z$ near its value for the compound nucleus differed appreciably (Fig. 27). A theoretical analysis showed that the differences in the excitation energies and angular momenta of the compound nuclei, formed in different combinations, could not explain this difference in the $\gamma$-ray spectra. The results of calculations of the spectra of high-energy $\gamma$ rays accompanying decay of the compound nuclei, made for the studied reactions in the statistical model by the Monte Carlo method, are shown in Fig. 28. It can be seen that up to energy $E_\gamma \approx 14$

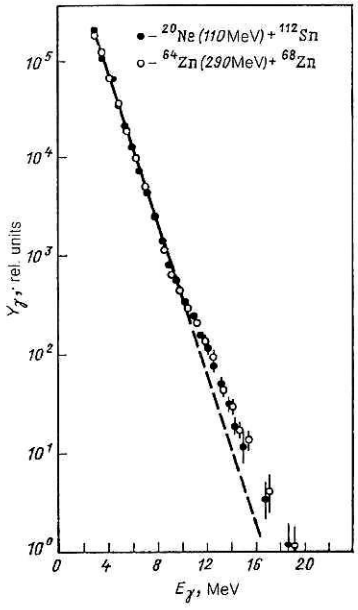


FIG. 26. Photon spectra measured by means of the gamma-start method.

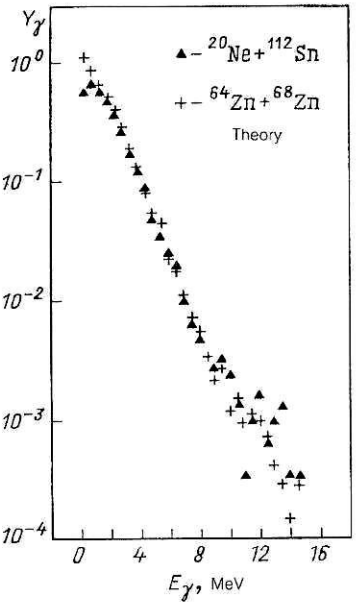


FIG. 28. Calculated $\gamma$-ray spectra (see the text).

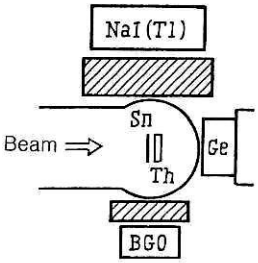


FIG. 29. Arrangement of experiment.

MeV the calculated spectra for the two reactions hardly differ.

To investigate the contribution of the different channels to the emission of high-energy $\gamma$ rays the experiments of Refs. 2 and 3 measured for the reaction $^{nat}Sn + ^{40}Ar$(300 MeV) the spectra of $\gamma$ rays with $E_\gamma = 4$–20 MeV in coincidence with $K$ x rays of the residual nuclei, and measurements were also made of the yield of the $K$ x rays in the wide range $Z = 50$–68 as a function of $E_\gamma$ . The angular anisotropy of the high-energy photons in a wide range of $E_\gamma$ was also measured for the same reaction. The experiments were made using an extracted beam of 300-MeV $^{40}Ar$ ions from the U-300 cyclotron of the Laboratory of Nuclear Reactions at the Joint Institute. The arrangement for measuring the spectra of $\gamma$ rays in coincidence with the $K$ x rays is shown in Fig. 29. The extracted beam of $^{40}Ar$ ions struck the target, a metallic foil of tin of the natural isotopic composition of thickness 15 mg/cm$^2$, and was completely stopped in an absorber in the form of a metallic thorium foil of thickness 47 mg/cm$^2$ set up behind the target. The x-ray detector, made of pure germanium, had an efficiency at the total-absorption peak of 5% in the region $E_{Kx} = 25$–80 keV. The energy resolution for this region was 600 eV. The high-energy $\gamma$ rays were detected by BGO and NaI(Tl) detectors, which measured $7.5 \times 2.5$ cm and $15 \times 10$ cm, respectively, and were placed at right angles to the direction of the beam at 10 cm and 20 cm from the target. The detection threshold in them was set above 4 MeV. The method of measurement is described in more detail in Ref. 57.

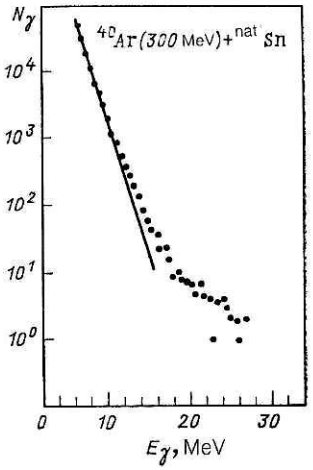


FIG. 30. Spectra of high-energy $\gamma$ rays measured by the gamma-start method.

Figure 30 shows the spectrum of $\gamma$ rays detected by the BGO detector in coincidence with the Ge detector, which detected $\gamma$ rays in the energy range 25–400 keV (Fig. 31) in the reaction $^{40}Ar + ^{nat}Sn$. In the region of energies $E_\gamma \leqslant 10$ MeV the $\gamma$ ray spectrum can be approximated by the function $\exp(-E_\gamma/T_{eff})$, with $T_{eff} = 1.1$ MeV. This low-energy region corresponds to the emission of statistical photons basically in the final stages of de-excitation of the residual nuclei.[50] At higher energies we observe a deviation from the exponential dependence, and the spectrum has the shape of a broad peak superimposed on an exponentially decreasing function, in qualitative agreement with the shape of the $\gamma$ spectra in the $^{nat}Sn + ^{40}Ar$ reaction measured by means of the gamma-start method in the study of Ref. 23. In accordance with the conclusions of Ref. 23, the GDR* $\gamma$ rays emitted by highly excited compound nuclei in equilibrium decay must make a large contribution to this region of the $\gamma$-ray spectrum. One could also expect an appreciable contribution of photons with $E_\gamma = 10$–14 MeV emitted in the initial stages of the fusion reaction.[59,60] However, as can be seen from the x-ray spectrum (Fig. 31), the spectrum shown in Fig. 30 corresponds to a spectrum of photons of products of not only the complete-fusion channel of the $^{nat}Sn + ^{40}Ar$ reaction but also channels leading to the formation of target-like products.

Figure 32 shows $\gamma$ spectra measured by the BGO and NaI(Tl) detectors in coincidence with $K$ x rays of nuclei with $Z$ values near that of the compound nucleus. It can be seen that for $E_\gamma \geqslant 10$ MeV this spectrum differs significantly in its shape from the spectrum in Fig. 30. The main distinctive feature is the presence of a minimum at an energy around 16 MeV, which makes it possible to identify in the spectrum three characteristic regions: a first $E_\gamma \leqslant 10$ MeV, a second $10 \leqslant E_\gamma \leqslant 16$ MeV, and a third $E_\gamma \geqslant 16$ MeV.

Figure 31 shows the x-ray spectra measured in coincidence with high-energy $\gamma$ rays in the different regions of the $\gamma$-ray spectrum. In the spectrum of the x rays in coincidence

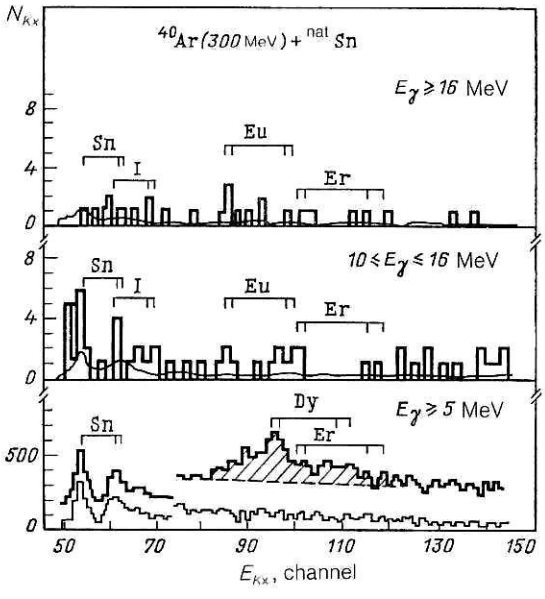


FIG. 31. Spectrum of $K$ x rays measured in coincidence with $\gamma$ rays of various energies (the range of $E_\gamma$ is shown in the figure).

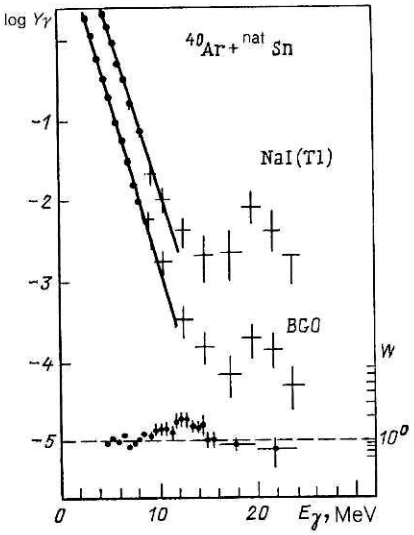


FIG. 32. Spectra of high-energy $\gamma$ rays measured in coincidence with $K$ x rays by two different detectors. The scale on the right gives $W$, the ratio of the yields of the high-energy $\gamma$ rays in the directions perpendicular to and parallel to the ion beam.

with the spectrum of the high-energy $\gamma$ rays of the second region there are both x-ray transitions corresponding to residual nuclei with $Z$ values close to that of the compound nucleus and transitions corresponding to nuclei with $Z$ values close to that of the target nucleus. From this it can be concluded that the processes that lead to the formation of these nuclei make a significant contribution to the second region of the high-energy spectrum. This fact is in disagreement with the assumption adopted in Ref. 23 and other studies that the main source of the high-energy $\gamma$ rays responsible for the excess above the exponential decay in the spectrum at $E_\gamma \geqslant 10$ MeV is statistical decay of the compound nucleus.

It follows from the x-ray spectrum measured in coincidence with the spectrum of $\gamma$ rays with $E_\gamma \geqslant 16$ MeV that the $\gamma$ rays of the third region come mainly from processes that lead to the formation of residual nuclei with $Z$ values near those of the compound nucleus. Thus, an excess of the yield of $\gamma$ rays that are associated with decay of the compound nucleus above the exponential decay is observed in the complete range of energies $E_\gamma \geqslant 10$ MeV. But a corresponding excess for nuclei that are neighbors of the target nucleus is observed mainly only in the region $E_\gamma = 10$–16 MeV.

Thus, the method of direct separation of the channel of the reaction accompanied by the emission of high-energy photons gave basically new results. From the experiments made in this way it can be concluded unambiguously that the bump observed when the gamma start method is used consists of several constituent peaks belonging to different reaction channels. Like the complete-fusion channel, the other channels of inelastic interaction of complex nuclei (incomplete fusion, many-nucleon transfer reactions, etc.) are accompanied by a large number of low-energy $\gamma$ rays.[34] A change in the mass ratio of the interacting nuclei and in the energy of the bombarding ions results in a change in the ratio of the cross sections in the different reaction channels and, as a consequence, must lead to a change in the contributions of the peaks to the overall bump. This could be a reason for the deviation of the values of the energies at the maxima of the bump from the GDR energies of the corresponding compound nuclei that is observed to different degrees in the experiments described in Sec. 2.1.

A more detailed analysis will be made in Sec. 2.6. In the following sections we give experimental data on measurement of the angular anisotropy of the high-energy $\gamma$ rays; these data cast light on the nature of this emission and its multipolarity. We also give data on the measurement of the multiplicity distribution the mean multiplicity of the low-energy $\gamma$ rays accompanying the high-energy $\gamma$ rays. This work relates to attempts to determine the region of angular momenta in the nuclei responsible for the emission of the high-energy $\gamma$ rays.

### 2.3. Angular anisotropy of the high-energy $\gamma$ rays

In deformed axisymmetric nuclei the giant dipole resonance is split at low angular momenta into two components, and the energy of the splitting is proportional to the deformation. At higher angular momenta, the resonance is split into five components through the effect of Coriolis forces on the nucleus, which has a triaxial shape. The vibrations of the protons relative to the neutrons along the spin axis (the $x$ axis) are de-excited by the emission of "nonaligned" dipole radiation ($m_x = 0$, $\Delta I = 0$), which takes place predominantly at right angles to the spin. The vibrations in the plane perpendicular to the spin are de-excited by emission of "aligned" dipole radiation ($|m_x| = 1$, $|\Delta I| = 1$), which takes place mainly along the spin axis. Thus, one of the components of the giant dipole resonance can, in principle, be separated from the others in the angular distribution of the corresponding high-energy $\gamma$ rays.

Because the spin direction of a nucleus formed in a heavy-ion reaction has an uncertainty in the plane perpendicular to the beam direction, the expected anisotropy of the $\gamma$-ray yield with respect to the direction of the ion beam cannot be large in experiments in which it is directly measured. Such measurements were made for the $^{16}O + ^{92}Mo$ reaction at 84 MeV (Ref. 61) and the $^{28}Si + ^{120}Sn$ reaction at 144 MeV (Ref. 40). The quoted studies did not draw definite conclusions about the anisotropy of the $\gamma$ radiation apart from finding some indications that at $E_\gamma < 11$ MeV the emission takes place mainly along the spin axis and is perpendicular to it at higher energies.

The effect may be significantly greater in correlation measurements in which the directions of emission of at least two $\gamma$ rays are measured. The results of such experiments were published in Ref. 48. The Crystal Ball facility was used to detect all $\gamma$ rays from the $^{34}S$(155 MeV) + $^{130}Te$ reaction. The low-energy $\gamma$ rays corresponding to the quadrupole bump were used to determine the spin direction of the nucleus for each individual event, and the direction of emission of the high-energy $\gamma$ rays was then determined relative to this direction. The data obtained in this manner are shown in Fig. 33. Gamma rays with energy up to about 10 MeV (Fig. 33) were emitted mainly at right angles to the spin direction for $\langle M_\gamma \rangle < 30$ and along the spin direction for $\langle M_\gamma \rangle = 31$–50. At larger values of the multiplicity $\gamma$-ray emission perpendicular to the spin direction of the nucleus was dominant in the range of $E_\gamma$ from 8 to 10 MeV.

The angular distribution of the high-energy $\gamma$ rays can be expressed by the relation

$$W(\theta) = 1 + \sum_k A_k P_k(\cos\theta), \quad k = 2, 4 \ldots,$$

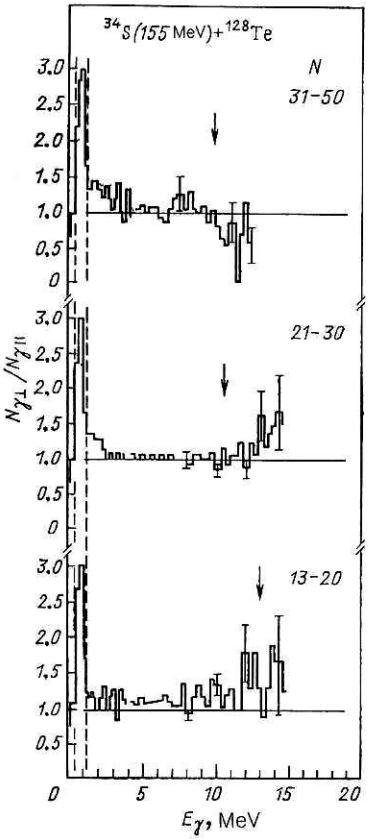


FIG. 33. Angular anisotropy of the high-energy $\gamma$ rays as the ratio of the $\gamma$-ray yields perpendicular to and parallel to the direction of the spin of the nucleus in the range of angles $\pm 30°$ for three windows in the number $N$ of detectors that responded. The arrows indicate the positions of the center of the peak of the giant resonance in the given $N$ window.

where the $P(\theta)$ are Legendre polynomials, and $\theta$ is the angle of emission relative to the spin direction. Figure 34 gives the coefficient $A_2$ as a function of $E_\gamma$ for the $^{12}C(100\text{ MeV}) + {}^{159}Tb \rightarrow {}^{171}Dy^*$ reaction.[51] In this investigation correlation measurements of the low-energy and high-energy $\gamma$ rays were made. Analyzing the dependence shown in Fig. 34, the authors of Ref. 51 noted the negative value of $A_2$ in the region $E_\gamma \approx 3$ MeV and in the region $10 < E_\gamma < 13$ MeV, and also the isotropic distribution in the region between 3 and 10 MeV. For a GDR* excited directly in a heavy-ion reaction along the spin direction the authors expected the excitation mode to be weakly populated, since the collective electric dipole moment lies near the reaction plane. In this case, the value of $A_2$ must be about 0.5, a value that differs strongly from the one obtained (Fig. 34). For a GDR* excited statistically in an elongated compound nucleus, the low-energy component must have a value $A_2 > 0$. Therefore, it was concluded in Ref. 51 that in the studied reaction an appreciable fraction of the $\gamma$-ray spectrum up to $\approx 10$ MeV was not due to GDR* decay in the complete-fusion channel.

To elucidate the nature of the $\gamma$ emission measured in the $^{nat}Sn + {}^{40}Ar$ reaction[2] and corresponding to the $E_\gamma$ regions described in Sec. 2.2, measurements were made of its yield at angles 90 and 0° to the direction of the ion beam. Since the investigation of Ref. 51 had not revealed a distinguished direction of emission of the $\gamma$ rays for $E_\gamma \leqslant 8$ MeV in the $^{12}C + {}^{159}Tb$ reaction, which leads to the formation of a

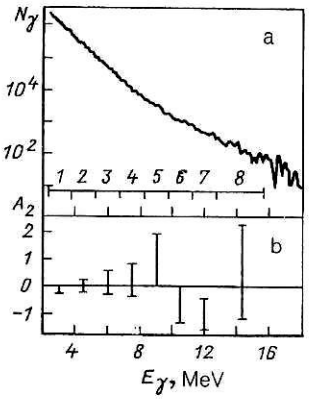


FIG. 34. Gamma-ray spectrum (a) and the coefficient $A_2$ (b) as a function of $E_\gamma$ (see the text).

compound nucleus with neighboring mass, the observed spectra were normalized to each other in the region $E_\gamma \leqslant 8$ MeV. This automatically introduced a correction for the Doppler shift of the energy of $\gamma$ rays observed along the beam direction relative to the energy of the $\gamma$ rays observed at right angles to the beam. The observed ratio of the $\gamma$-ray yields, $W = N_\gamma(90°)/N_\gamma(0°)$, is shown as a function of $E_\gamma$ in Fig. 32. In the range of energies $E_\gamma = 10$–16 MeV we observe an increase in the yield of $\gamma$ rays emitted at right angles to the beam direction, and this may correspond to aligned dipole transitions. In the range of energies $E_\gamma = 16$–22 MeV a distinguished direction of emission of the $\gamma$ rays is not observed to within the experimental errors. The data obtained on the anisotropy of the $\gamma$-ray emission relative to the beam direction are an additional indication of different natures of the sources of their emission in the different energy ranges.

We made analogous measurements for the $^{22}Ne + {}^{nat}Sn$ reaction. The observed $E_\gamma$ dependence of the anisotropy of the $\gamma$-ray emission repeats the data for the $^{40}Ar + {}^{nat}Sn$ reaction (Fig. 35; cf. Fig. 32).

In the study of Ref. 53 data were obtained on the angular anisotropy of high-energy $\gamma$ rays in the fission reaction with Bi compound nuclei. Determination of the plane of emission of the Bi fission fragments made it possible to determine the ratio of the yields of $\gamma$ rays with $E_\gamma > 12$ MeV perpendicular to the direction of the spin **I** (Fig. 36a) and along the direction of the fissioning nucleus Bi (Fig. 36b) in the reactions $^{40}Ar(220, 300\text{ MeV}) + {}^{159}Tb$. The high-energy $\gamma$

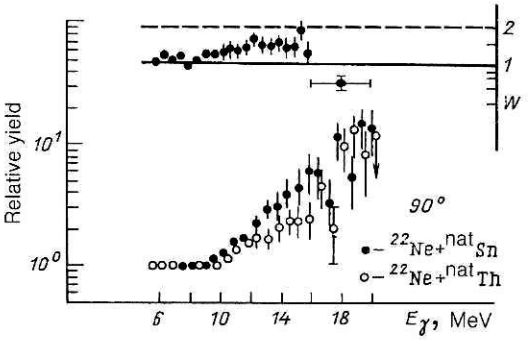


FIG. 35. Gamma-ray spectrum normalized to the function $\exp(-E_\gamma/T_{eff})$ for two reactions. At the top, the angular anisotropy of radiation for the $^{22}Ne(178\text{ MeV}) + {}^{nat}Sn$ reaction is shown.

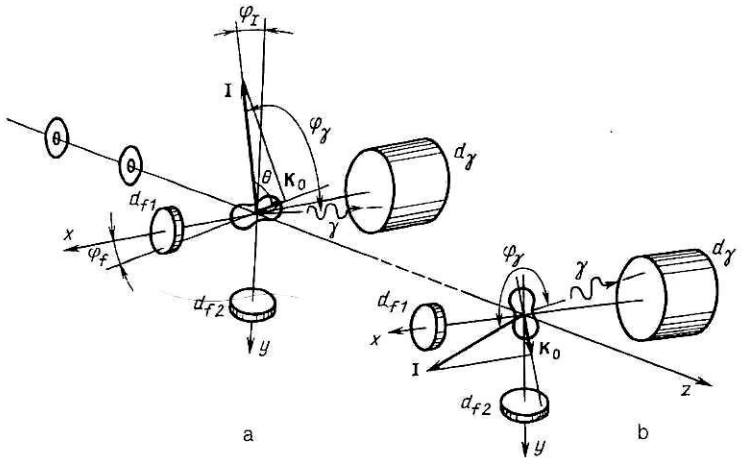


FIG. 36. Arrangement of experiment to measure the angular anisotropy of high-energy $\gamma$ rays: a) measurement in the direction perpendicular to the direction of the spin of the nucleus; b) measurement parallel to this direction. The $\gamma$-ray and fragment detectors are $d_\gamma$ and $d_f$, respectively, and **I** is the spin of the nucleus.

rays emitted along the spin direction of the fissioning nuclei and perpendicular to it were observed by a single detector. This arrangement of the experiment eliminated methodological errors associated with comparison of $\gamma$-ray spectra measured by different detectors. For the region of energies $E_\gamma > 12$ MeV the ratio of the $\gamma$-ray yields along and at right angles to the spin direction of the Bi nuclei was found to be approximately the same $(0.5 \pm 0.3)$ for the two energies of the Ar ions. The experimental data are in agreement with the assumption that the $\gamma$ rays with $E_\gamma > 12$ MeV corresponded to aligned dipole transitions.

Thus, the results of most experiments to measure the angular anisotropy of the high-energy component of the $\gamma$ emission confirm the assumption of its dipole nature. The data of the experiments of Ref. 53 do not preclude a possible contribution to the $\gamma$-ray spectrum at $E_\gamma > 16$ MeV of $\gamma$ rays from decay of the giant quadrupole resonance, which could be excited in the nuclei of the bombarding particle and target in the interaction process. More details about this contribution are given in Sec. 3.

### 2.4. Multiplicity of $\gamma$ rays accompanying emission of high-energy $\gamma$ rays in heavy-ion reactions

In some studies the multiplicities of the $\gamma$ rays were measured as functions of the $\gamma$-ray energies in order to obtain estimates of the angular momenta of the nuclei emitting the high-energy $\gamma$ rays. For example, in the study of Ref. 40 $\langle M_\gamma(E_\gamma)\rangle$ was measured in the range of energies $2 < E_\gamma < 20$ MeV in the reaction $^{28}$Si(145 MeV) + $^{120}$Sn (see Fig. 18). To within the statistical errors, constancy of $\langle M_\gamma(E_\gamma)\rangle$ was observed in this reaction.

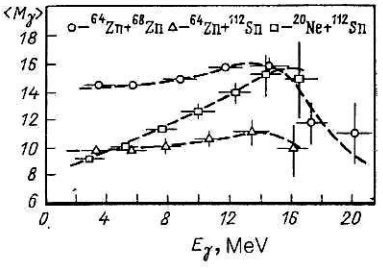


FIG. 37. The value of $\langle M_\gamma \rangle$ as a function of $E_\gamma$ measured for three reactions.

Investigations of the dependence of $\langle M_\gamma \rangle$ on $E_\gamma$ in the range of energies $E_\gamma = 3$–$24$ MeV in the three reactions $^{64}$Zn(290 MeV) + $^{68}$Zn, $^{20}$Ne(110 MeV) + $^{112}$Sn, and $^{64}$Zn(358 MeV) + $^{112}$Sn were made in the study of Ref. 58. In the first and third of these reactions a slow increase of $\langle M_\gamma \rangle$ with increasing energy $E_\gamma$ was observed (Fig. 37).

In the $^{20}$Ne + $^{112}$Sn reaction, a sharp growth of $\langle M_\gamma \rangle$ with variation of $E_\gamma$ from 3 to 12 MeV was observed, this being different from the $\langle M_\gamma(E_\gamma)\rangle$ dependence observed for the Si + Sn reaction.[40]

Analysis of these data showed that in the region $E_\gamma = E_g$ the observed $\langle M_\gamma \rangle$ corresponds mainly to the evaporation channel of the fusion reaction for the Zn + Zn reaction, while for the Ne + Sn reaction it corresponds to the reaction channel in which "sticking" is followed by breakup of the fragments (sticking process). The main conclusion of the study was that the experimental dependence of $\langle M_\gamma \rangle$ on $E_\gamma$ does not agree with the model of dominant GDR* excitation in the channel of complete fusion of the nuclei (Ref. 23 and other studies; see Sec. 2.2).

### 2.5. Experimental investigations of the de-excitation time associated with high-energy $\gamma$ rays

To understand the mechanism of formation of the high-energy $\gamma$ rays, investigations aimed at determining the de-excitation time for them are important. A number of studies made in recent years have indicated the existence of $\gamma$-ray emission in the first stages of the reactions between complex nuclei. In the studies of Refs. 59 and 60 an experimental observation was made of a "cooling" of the spectra of protons and $\alpha$ particles measured in coincidence with $\gamma$ rays ($E_\gamma > 14$ MeV) in the $^{58}$Ni + $^{16}$O(76 MeV) reaction, and the same thing was observed for the spectra of neutrons in coincidence with $\gamma$ rays ($E_\gamma > 10$ MeV) in the reaction $^{159}$Tb + $^{12}$C(100 MeV).

In Ref. 63 the yield of evaporation products of the $^{87}$Ru + $^{65}$Cu → $^{148}$Dy reaction was measured. This resulted in the observation of an unexpectedly large (compared with the results of a calculation in accordance with the statistical theory) yield of the products of evaporation of a small number of neutrons (1n, 2n) at a relatively high thermal excitation energy of the compound nucleus around 50 MeV. The mechanism of reactions like those studied in Refs. 59, 60, and 63

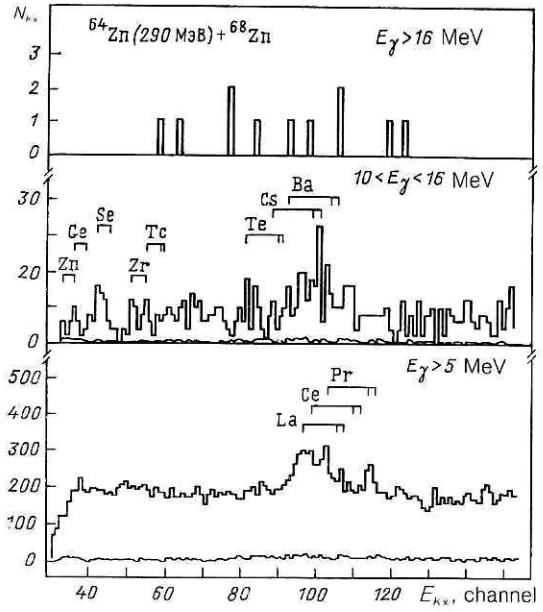


FIG. 38. Spectra of $K$ x rays measured in coincidence with $\gamma$ rays of different energies (the ranges of energy $E_\gamma$ are indicated).

has not yet been definitively established. Therefore a possible mechanism is pre-equilibrium emission of high-energy $\gamma$ rays ($E_\gamma > 10$ MeV).

At the same time, as we have shown in the foregoing subsections, the study of the yields of $\gamma$ rays with $E_\gamma > 10$ MeV in heavy-ion reactions in recent years has been associated mainly with the assumption of the presence of $\gamma$-decay giant resonances constructed on highly excited states of compound nuclei. The analysis made in Ref. 54 of experimental data obtained for the $^{68}$Zn + $^{64}$Zn reaction showed that in the energy spectrum of the $K$ x rays (Fig. 38) the centroid of the peak corresponding to the products of the fusion channel and measured in coincidence with the high-energy $\gamma$ rays is displaced when $E_\gamma > 10$ MeV to higher energies. This displacement is shown in the inset of Fig. 27. It corresponds to a smaller number of evaporated charged particles. For the $^{20}$Ne + $^{112}$Sn reaction no such correlation was found to within the experimental errors (see the inset in Fig. 27). Calculations made by means of the modified ALICE program[64] showed that the observed correlation between the $Z$ values of the residual nuclei and the energy of the $\gamma$ rays for the $^{64}$Zn + $^{68}$Zn reaction indicates that the emission of $\gamma$ rays with $E_\gamma > 10$ MeV occurs in the first steps of the evaporation cascade or before it, reducing thereby the excitation energy of the compound nucleus and, accordingly, the number of evaporated particles (protons).

### 2.6. Theoretical approaches to the explanation of the mechanism of emission of high-energy $\gamma$ rays with energy $E_\gamma < 30$ MeV

We summarize some conclusions that follow from the foregoing analysis. The data obtained on the yield of high-energy $\gamma$ rays in the channels corresponding to formation of a compound nucleus (Refs. 2, 3, 53, 54, and 65) indicate the existence of a mechanism of their emission different from that assumed earlier (Refs. 23, 50, and others). Noteworthy is the fact that the $\gamma$-ray spectra measured in a distinguished channel corresponding to formation of a compound nucleus do not always have the characteristic breaks in the region of 8 MeV (see Figs. 25, 27, and 32), and they thus cast doubt on the method used to separate the GDR bump based on multiplication of the $\gamma$ spectrum by the factor $\exp(E_\gamma/T_{\text{eff}})$. As was shown in Ref. 2, the use of the gamma-start method may, unless special measures are adopted (the signals in the gamma-start detectors bounded above), have the consequence that "$\gamma$ rays" of cosmic-ray origin will make a large contribution to the high-energy part of the $\gamma$-ray spectrum.

For the qualitative interpretation of the results, we consider one of the possible mechanisms of emission of such "cosmic" $\gamma$ rays. It is known that in heavy-ion reactions the excitation of various modes of giant resonances (GDR, GQR, GMR) is observed already at a comparatively small contact of the interacting nuclei, i.e., in inelastic reactions.[36] The excitation of giant resonances was noted in Refs. 66 and 67 as one of the possible mechanisms of kinetic-energy dissipation in the interaction of complex nuclei. It is natural to assume that giant resonances are also excited in the process of mass transfer in the double nuclear system of interacting nuclei that is formed in the first stages of deep inelastic reactions and fusion reactions.

It has been established experimentally that the decay of giant resonances leads in approximately a proportion $10^{-3}$–$10^{-4}$ of the cases to the emission of $\gamma$ rays with energy $E_\gamma \approx E_{\gamma'}$.[36] On the basis of data obtained in photonuclear reactions it can be asserted that for comparable probabilities of excitation of the various giant-resonance modes it is the decay of the giant dipole resonance that will make the main contribution to the $\gamma$-ray emission.[44] Since in the initial stages of the existence of the double nuclear system the giant dipole resonances must be excited mainly along the symmetry axis of the system,[51] i.e., at right angles to the direction of its spin, the corresponding $\gamma$ rays will be emitted mainly parallel to the spin direction. For such $\gamma$ rays, the energy $E_g$ is determined by the dimension $2r''$ of the double nuclear system along the symmetry axis. In the initial stage of the interaction

$$r^{\parallel} = r^{\max\ \parallel} \sim (A_1^{1/3} + A_2^{1/3}),$$

where $A_2$ is the mass number of the target nucleus, and this relation makes it possible to obtain a lower bound on the GDR* energy (MeV):

$$E_g^{\min\ \parallel} \approx \frac{78}{(A_1^{1/3} + A_2^{1/3})}. \qquad (1)$$

Subsequently, the double nuclear system can decay into two excited fragments (target-like and ion-like) or form a prolate ellipsoid that gradually acquires the equilibrium configuration of a compound nucleus. For the compound nucleus

$$r^{\parallel} = r^{\min\ \parallel} \sim (A_1 + A_2)^{1/3},$$

and one can estimate the maximal energy of the GDR* (MeV) corresponding to vibrations of the nucleus perpendicular to the spin:

$$E_g^{\max\ \parallel} \approx \frac{78}{(A_1 + A_2)^{1/3}}. \qquad (2)$$

In the region of energies $E_\gamma = (E_g^{\min\parallel}, E_g^{\max\parallel})$ contributions must be made not only by the $\gamma$ rays corresponding to

decay of the compound nucleus but also by the $\gamma$ rays corresponding to decay of the double nuclear system into target-like and ion-like fragments. Since the spin of the double nuclear system is most probably oriented at right angles to the direction of the beam, the $\gamma$ rays with $E_\gamma = E_g^{\min\|} - E_g^{\max\|}$ must be emitted at right angles to the beam direction.

As the shape of the nucleus is transformed from a prolate ellipsoid to an equilibrium, nearly spherical configuration, there may also be excitation of GDR* in the plane perpendicular to the symmetry axis of the system, i.e.,

$$E_g^{\perp} > E_g^{\max\|}. \tag{3}$$

In the energy range $E_\gamma > E_g^{\max\|}$ the main contribution must be made by $\gamma$ rays that correspond to the transverse GDR mode in the compound nucleus that has been formed and do not have a distinguished direction of emission relative to the beam direction.

Using the relations (1)–(3), one can establish for the $^{40}Ar + {}^{nat}Sn$ reaction that the $\gamma$ rays corresponding to the formation of a compound nucleus and of the decay products of the double nuclear system and emitted mainly at right angles to the beam direction must have energy $E_\gamma = 8$–16 MeV. The $\gamma$ rays emitted isotropically relative to the beam direction and corresponding mainly to the formation of a compound nucleus must have energy $E_\gamma > 16$ MeV. These estimates agree well with the results of the measurements given in Fig. 32.

The data show that in the spectrum of $\gamma$ rays associated with the interaction of the nuclei in the $^{40}Ar(300\ MeV) + {}^{nat}Sn$ reaction an appreciable contribution in the range of energies $E_\gamma = 8$–16 MeV is made by $\gamma$ rays that correspond to many-nucleon transfer reactions. This conclusion disagrees with the conclusions drawn by authors of earlier studies (Refs. 23 and 52, for example). In the region of energies $E_\gamma = 16$–22 MeV the contribution of the $\gamma$ rays corresponding to fusion of the nuclei was dominant. There was observed to be an increase in the yield of $\gamma$ rays in the energy range $E_\gamma = 8$–16 MeV emitted at right angles to the beam direction, while an isotropic angular distribution was observed in the energy range $E_\gamma = 16$–22 MeV. The model proposed for the formation of the high-energy part of the $\gamma$-ray spectrum in heavy-ion reactions on the basis of the assumption of excitation of giant dipole resonances in dissipative processes in the double nuclear system explains qualitatively the presence of three regions of the energy $E_\gamma$ in the $\gamma$-ray spectrum and the contributions to them of the various channels of the $^{40}Ar + {}^{nat}Sn$ reaction. In the framework of the model the $E_\gamma$ dependence of $W$ (see Fig. 32) finds a transparent interpretation.

If we assume that the break in the dependence $W(E_\gamma)$ in the region $E_\gamma \approx 8$ MeV and 16–17 MeV for the Sn + Ne and Sn + Ar reactions (see Figs. 32 and 35) is due to deformation of the emitting nucleus,[51] then we can estimate the deformation $\delta$ of such a system (see Sec. 2.1). For $E_g^1 : E_g^2 \approx 0.6$–0.7, we readily obtain $\delta = 0.35$–0.4. Such a large deformation cannot correspond to the target nuclei, Sn, or to the nuclei of the incident ions Ne and Ar. It is also too large for the putative compound nuclei Nd and Er.

The assumption of emission of high-energy $\gamma$ rays from the double nuclear system, for which deformations such as 0.5 are not unusual,[34] can explain the dependences $W(E_\gamma)$ observed for both reactions.

In the framework of this approach, the $\gamma$-ray spectra measured in the gamma-start method must be a superposition of GDR* that are excited in different stages of evolution of the nuclear system and have, thus, different energies. We then recognize as obvious the fact that with increasing angular momentum of the interacting nuclei the mean energy of the superposition must decrease, as was noted, for example, in Ref. 48. This may also be related to the broadening of the GDR* bumps and the shift of their energy to lower values compared with the values obtained in the systematics for the ground states (see Fig. 10), an effect noted in the overwhelming majority of studies. Excitation of giant dipole resonances in the sticking channel with subsequent breakup of the double nuclear system is indicated by measurements of the $\gamma$-ray multiplicity in the Ne + Sn reaction.[58]

We note also that the existence of a mechanism leading to excitation of GDR* mainly at right angles to the spin of the compound system was suggested in Ref. 48 to explain the relatively large yield of $\gamma$ rays in the region $E_\gamma \geqslant 7$ MeV in the $^{34}S + {}^{128}Te$ reaction.

A certain contribution to the spectrum of $\gamma$ rays with $E_\gamma \geqslant 16$ MeV may be made by the process of pre-equilibrium excitation and decay of an isovector giant quadrupole resonance. The quantitative estimate of such a contribution of order $10^{-6}$ for a compound nucleus was given in Ref. 68 for the $^{90}Zr + {}^{90}Zr$ radiative-capture reaction. Another possible mechanism responsible for this part of the $\gamma$-ray spectrum is the bremsstrahlung process in the collision of complex nuclei. This mechanism is considered in detail in the following section. Good agreement of the data calculated in accordance with this model with the experimentally measured $\gamma$-ray spectra was found in Ref. 69 for the reactions $^{22}Ne(155MeV) + {}^{181}Ta$ and $^{40}Ar(300\ MeV) + {}^{159}Tb$ (see Sec. 4).

Everything said above applies to reactions with sufficiently large mass asymmetry in the entrance channel. With regard to reactions between nuclei with nearly equal masses, comparison of data on the Zn + Zn and Ne + Sn reactions, which lead to the same compound nucleus, shows that there are grounds for supposing the picture of the formation of the high-energy $\gamma$ rays to be still more complicated. In Fig. 39 the yields $\Sigma Y_\gamma$ of $\gamma$ rays with energy in the GDR energy

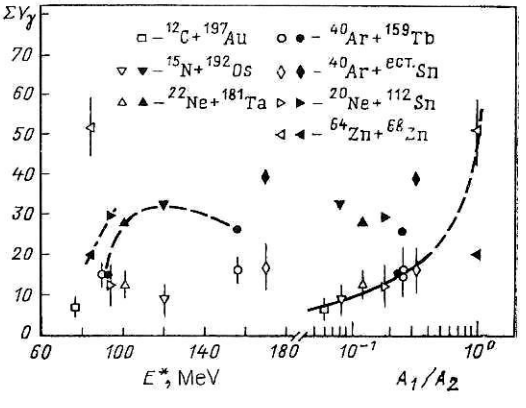


FIG. 39. Experimental and theoretical yields of high-energy $\gamma$ rays (see the text) in units of the number of transitions per nucleus, multiplied by $10^4$, in the energy range $12 \leqslant E_\gamma \leqslant 14$ MeV.

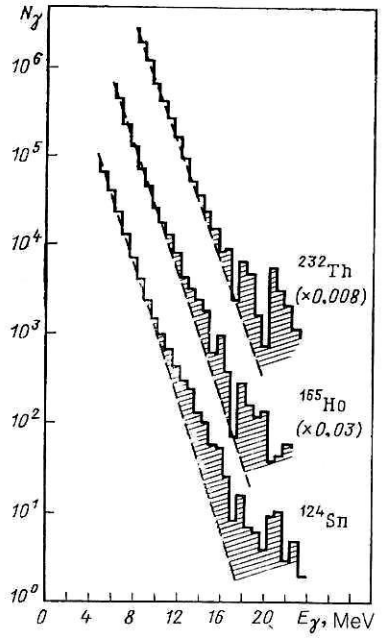


FIG. 40. Gamma-ray spectra measured in reactions of accelerated $^{22}$Ne ions of energy 178 MeV on different targets.

range $12 \leqslant E_\gamma \leqslant 14$ MeV are systematized with respect to two parameters: the excitation energy $E^*$ and the ratio of the mass numbers of the projectile nucleus, $A_1$, and the target nucleus, $A_2$ (Ref. 54).

Figure 39a demonstrates the strong dependence of the calculated values of $\Sigma Y_\gamma$ on $E^*$ and the absence of any systematic dependence of the experimental values of $\Sigma Y_\gamma$ on E*. Figure 39b shows a monotonic increase of the experimental values with increasing $A_1/A_2$, i.e., it reveals a systematic dependence of $\Sigma Y_\gamma$ on a parameter which characterizes the reaction in the entrance channel.

We used the gamma-start method to investigate the yield of high-energy $\gamma$ rays as a function of the mass-asymmetry parameter in the entrance channel of the reaction, keeping the mass of the bombarding ion constant. Figure 40

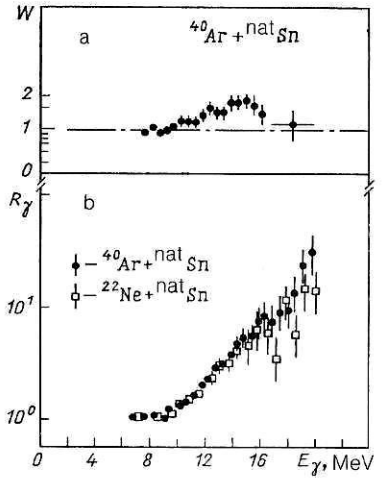


FIG. 41. Angular anisotropy of $\gamma$ rays measured by the gamma-start method for the $^{40}$Ar + $^{nat}$Sn reaction (a) and $\gamma$-ray spectra for the reaction between the target nucleus $^{nat}$Sn and ions of different masses ($^{22}$Ne and $^{40}$Ar) measured by the gamma-start method and normalized to $\exp(-E_\gamma/T)$ (b) (see the text).

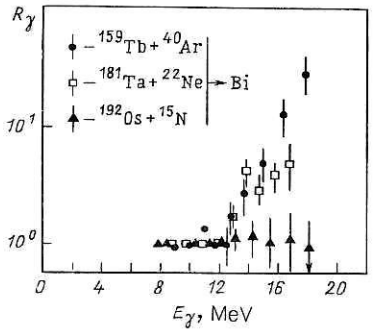


FIG. 42. Gamma ray spectra measured in the separated fission channel of Bi nuclei and normalized to $\exp(-E_\gamma/T)$ (see the text).

shows the spectra of $\gamma$ rays measured in reactions with 178-MeV $^{22}$Ne ions on the targets $^{232}$Th, $^{165}$Ho, and $^{124}$Sn. The hatched region in the $\gamma$-ray spectra corresponds to an excess of the $\gamma$-ray yield above the exponential decay. Figure 41 gives the dependence of the excess $R_\gamma$ of the $\gamma$-ray yield above the exponential decay as calculated under the assumption of a single-exponential decay,

$$R_\gamma = Y_\gamma/\exp(-E_\gamma/T) \approx E_\gamma^3 f(E_\gamma),$$

for the two reactions $^{22}$Ne(175 MeV) + $^{nat}$Sn and $^{40}$Ar(220 MeV) + $^{nat}$Sn. It follows from Figs. 40 and 41 that the yield of $\gamma$ rays with $E_\gamma > 10$ MeV increases with increasing mass ratio $A_1/A_2$ when the mass of the target nucleus is kept the same. An even clearer growth of $R_\gamma$ with increasing $A_1/A_2$ is shown in Fig. 42 for the distinguished fusion channel in the experiment of Ref. 53 described in the foregoing.

It would be natural to assume that the yield of high-energy $\gamma$ rays could also be associated with pre-equilibrium mechanisms like those proposed to explain the emission of fast charged particles.[70] Then the values of $\Sigma Y_\gamma$ should increase as the energy per nucleon of the bombarding ions is increased above the Coulomb barrier of the interaction with the target nucleus. However, as can be seen from Fig. 43, the dependence of $\Sigma Y_\gamma$ on $\epsilon$ differs strongly from the expected growth of the yield of pre-equilibrium particles with increasing $\epsilon$.[70] In Ref. 71 the high-energy part of the $\gamma$-ray spectra measured for the Zn + Zn reaction[54] was interpreted on the basis of calculations using an exciton model.

Thus, there are grounds for supposing that some of the

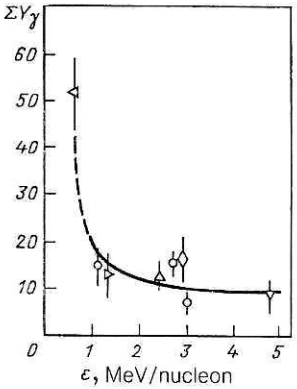


FIG. 43. Yields of high-energy $\gamma$ rays as functions of the energy $\epsilon$ of the incident ion (see the text).

high-energy $\gamma$ rays with $E_\gamma > 10$ MeV are associated with a new mechanism of interaction of complex nuclei that depends strongly on the mass asymmetry of the interacting nuclei in the entrance channel of the reaction. In Ref. 72 the emission of $\gamma$ rays in the process of the evolution of the shape of the double nuclear system was considered in the framework of the hydrodynamic approach. Two emission mechanisms were investigated. In the first the density of nucleons was assumed to be constant and the emission to be quadrupole in nature. In the second it was assumed that there was excitation in the system of isovector density vibrations, and allowance was made for only the lowest mode, which was described as a giant dipole resonance in a spherical nucleus with a time-dependent radius equal to the length of the composite system. The yields of $\gamma$ rays in the region of energies $12 \leqslant E_\gamma \leqslant 14$ MeV calculated for the $^{64}Zn + {}^{68}Zn$ and $^{20}Ne + {}^{112}Sn$ systems in the framework of the first approach were $5 \times 10^{-8}$ and $10^{-6}$, respectively, while in the second they were $43 \times 10^{-4}$ and $34 \times 10^{-4}$. These last data agree with the tendency of the systematics of Ref. 54 shown in Fig. 39, and, moreover, the $\gamma$-ray yield for the Zn + Zn reaction is close to the experimental value. Thus, in Ref. 72 quantitative confirmation was found for the idea that high-energy $\gamma$ rays could be emitted as the shape of the double nuclear system evolves, as was proposed in Ref. 21.

### 2.7. Experimental investigations of the spectra of $\gamma$ rays with $E_\gamma > 30$ MeV

We now consider the main results of experimental studies of the spectra of $\gamma$-ray emission accompanying collisions of ions at intermediate energies ($E/A_1 > 20$ MeV/nucleon). Although for this region of energies the number of published studies is as yet small, it has recently been increasing steadily. This is due to both the commissioning of new accelerators and the significant interest shown by theoreticians in the elucidation of the reaction mechanism, which was found to be not particularly simple. In Table V we summarize the properties of reactions with ions of intermediate energies in which the yield of high-energy photons for specific reactions was determined. Table V gives only the range of approximate values of the differential cross section $d^2\sigma_\gamma/dE_\gamma d\Omega_\gamma$ at the beginning and end of the spectrum. The more accurate behavior of the experimental cross section $d^2\sigma/dE\ d\Omega$ for the majority of the reactions listed in Table V will be presented in Sec. 4 in a comparison with the results of theoretical calculations. Here we only give a general characterization of these spectra.

At $\gamma$-ray energies $E_\gamma > 30$ MeV the dependence of $d^2\sigma/dE_\gamma d\Omega_\gamma$ on $E_\gamma$ can be approximated for all the reactions by a function $\exp(-E_\gamma/E_0)$, where $E_0$ is a parameter that determines the rate of decay of the curve (or the slope of the straight line when plotted on a logarithmic scale). As follows from Table V, the range of $E_0$ values is fairly small, and $E_0$ has a tendency to increase with increasing $E/A_1$ (for example, for the $^{14}N + C$, Zn, Pb reactions) and depends very weakly on the mass of the colliding nuclei. In individual cases the deviation of $E_0$ from the value averaged over all the $\gamma$-ray spectra, $\langle E_0 \rangle = 11.5 \pm 0.5$ MeV, is due to the use, in the approximation of the spectrum, of a function more complicated than $\exp(-E_\gamma/E_0)$ (for example, in Ref. 75). The $\gamma$-ray yield has a certain tendency to increase with increase both of the beam energy and of the masses of the colliding nuclei (Fig. 44, which is taken from Ref. 78). Figure 44 shows the cross section for the total yield of $\gamma$ rays with $E_\gamma > 50$ MeV, normalized to the geometrical cross sections of the colliding nuclei, as a function of the beam energy $E/A_1$.

The angular distributions of $\gamma$ rays emitted in the reaction process were investigated in the studies of Refs. 13, 14, and 74, and, in contrast to the energy distributions, an unambiguous picture was not obtained in this case. For example, whereas for the reactions $^{86}Kr$(44 MeV/nucleon) + C, Ag, Au and $^{12}C$(48, 60, 74 and 84 MeV/nucleon) + $^{12}C$ an isotropic $\gamma$-ray distribution was observed,[14,77] and for the $^{14}N$(20–40 MeV/nucleon) + C, Zn, Pb reactions a small peak at small angles was noted,[74] the angular distribution of the $\gamma$ rays in the $^{14}N$(35 MeV/nucleon) + $^{58}Ni$ reactions exhibited a pronounced anisotropy with a maximum at $\theta_\gamma = 90°$ (Ref. 13). In this last case the position of the maximum did not depend on the $\gamma$-ray energy.

Since the beam energies and masses of the colliding nuclei in some of these reactions differed only slightly [for example, in the reactions $^{14}N$(30 and 40 MeV/nucleon) + Zn, $^{86}Kr$(44 MeV/nucleon) + $^{12}C$, and $^{14}N$(35 MeV/nucleon) + $^{55}Ni$], the pronounced difference between the results of Refs. 74 and 77, on the one hand, and Ref. 13, on the other, poses the question of their origin. However, irrespective of its solution, it would be interesting, in order to obtain general conclusions, to continue the investigation of the angular distributions, which are as yet not sufficiently well established.

## 3. THEORETICAL APPROACHES TO THE DESCRIPTION OF THE EMISSION OF HIGH-ENERGY $\gamma$ RAYS

The main question that arises in the theoretical analysis of the experimental $\gamma$-ray spectra in heavy-ion reactions is the manner of formation of the high-energy $\gamma$ rays in a collision of nuclei if each nucleon has a relatively low energy of translational motion ($E/A_1 < E_\gamma \ll E$). It is therefore obvious that any microscopic mechanism of formation of high-energy radiation must be based on some method of taking into account the internucleon interaction. The manifestations of this interaction may be quite varied—from the formation of an average nuclear field and an optical potential to redistribution of the nucleons in the energy or phase spaces through collision terms in kinetic equations. However, it is unfortunately by no means always possible to relate unambiguously the observed properties to parameters of the internucleon potential. This gives rise to the variety of theoretical approaches to the description of the same phenomenon in the case considered here—the properties of the high-energy $\gamma$-ray emission.

Depending on the way in which the interaction of the nucleons is taken into account, the known theoretical approaches[69,79–96] can be divided nominally into four main groups:

1) thermodynamic models[79,80];

2) first-collision models[81–87];

3) statistical models[88–93];

4) quantum models of electromagnetic radiation in an optical potential.[69,94–96]

In what follows we shall analyze the basic ideas of each of these approaches and formulate in more detail the quan-

TABLE V. Properties of reactions with ions of intermediate energies accompanied by emission of $\gamma$ rays with $E_\gamma > 30$ meV.

| Reaction | $E/A_1$, MeV/nucleon | Range of $E_\gamma$, MeV | Angle of observation of $\gamma$ rays, deg | Range of $d^2\sigma/dEd\Omega$, $10^{-30}$ cm$^2$·MeV$^{-1}$·sr$^{-1}$ | $E_0$, MeV | Detector | Reference |
|---|---|---|---|---|---|---|---|
| $^{40}Ar+^{70}Ge$ | 15<br>24 | 5—45<br>5—55 | —<br>— | —<br>— | 8±2<br>10±2 | NaI(Tl) | [73] |
| $^{14}N+^{12}C$ | 20<br>30<br>40 | 20—75<br>20—85<br>20—105 | 30; 60; 90; 120; 150 | $10^2-10^{-1}$<br>—<br>— | 7.7<br>11.1<br>13.3 | CsI(Tl) | [74] |
| $^{14}N+Zn$ | 20<br>30<br>40 | 20—75<br>20—85<br>20—105 | 30; 60; 90; 120; 150 | $10^2-10^{-1}$<br>—<br>— | 8.3<br>11.8<br>13.7 | CsI(Tl) | [74] |
| $^{14}N+^{208}Pb$ | 20<br>30<br>40 | 20—75<br>20—85<br>20—105 | 30; 60; 90; 120—150 | $10^2-10^{-1}$<br>— | 10.0<br>12.0<br>14.2 | CsI(Tl) | [74] |
| $^{40}Ar+^{197}Au$ | 30 | 20—55 | 40; 90; 157 | $10-10^{-1}$ | 7.3 | $BaF_2$<br>NaI(Tl) | [75] |
| $^{14}N+^{58}Ni$ | 35 | 20—150 | 30; 60; 90; 120 | $10-10^{-1}$ | 14.5±1.0 | Lead glasses | [13] |
| $^{14}N+Cu$ | 40 | 20—140 | — | — | — | — | [76] |
| $^{40}Ar+^{158}Gd$ | 44 | 5—80 | 90;<br>145 | $10-10^{-1}$ | 12.6±0.6<br>10.5±0.7 | $BaF_2$ | [4] |
| $^{86}Kr+^{12}C$<br>$^{86}Kr+Ag$<br>$^{86}Kr+^{197}Au$ | 44<br>44<br>44 | 30—80<br>—<br>— | 40; 90; 150<br>40; 65; 100; 153,5<br>30; 90; 153,5 | $10-10^{-1}$<br>—<br>— | 11.6±0.5<br>12.5±0.3<br>12.1±0.2 | $BaF_2$<br>NaI(Tl) | [77] |
| $^{12}C+^{12}C$ | 48<br>60<br>74<br>84 | 30—80<br>30—120<br>30—140<br>30—200 | 90 in c.m.s.<br>—<br>—<br>— | $10-10^{-2}$<br>—<br>—<br>— | — | Lead glasses | [14] |
| $^{12}C+^{238}U$ | 84 | 30—200 | 52,5; 90 | $10-10^{-2}$ | — | The same | [14] |

tum model of electromagnetic radiation in an optical potential.

### 3.1. Thermodynamic models

In this group we put the approaches in which an entire compound nucleus (or part of it) formed as a result of the reaction is in a state of thermodynamic equilibrium and has a definite temperature. It is usually assumed that at relatively low energies of the colliding ions (8–12 MeV/nucleon) the entire compound system is uniformly heated. At a collision energy above 20 MeV/nucleon the formation of a strongly heated individual region in the compound system—a fireball—becomes possible. In both cases the source of the electromagnetic radiation is the random thermal motion of the nucleons.

We shall not here make an analysis of the theoretical studies of the $\gamma$-ray spectra in reactions of ions with $E/A_1 = 8$–12 MeV/nucleon in the framework of evaporation models, since they were reviewed in Sec. 2, and we shall restrict ourselves to considering just the fireball model. We

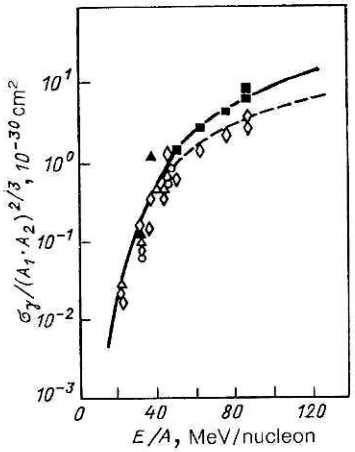


FIG. 44. Yield of $\gamma$ rays with $E_\gamma \geqslant 50$ MeV as a function of the energy of the bombarding ions. The experimental points are taken from Ref. 78 (open diamonds), Ref. 74 (open triangles), Refs. 75 and 77 (open circles), Ref. 14 (black squares), and Ref. 13 (black triangles).

merely note that in the range $E_\gamma < 25$ MeV it is necessary to investigate not only the evaporation spectra but also the electromagnetic emission due to decay of giant resonances excited in the reaction process in the colliding nuclei, in the compound nucleus, and in the reaction products. The procedure of the corresponding calculations is known and implemented in the form of various standard programs (for example, ALICA, CASCADE, GROGI, etc.).

The fireball model supposes that a collision of nuclei leads to the formation of a heated region that constitutes a Boltzmann gas with temperature $T_F$. The nucleons of the gas collide with each other randomly, and this gives rise to incoherent electromagnetic radiation. As was shown in Ref. 79, in the classical description of the bremsstrahlung resulting from individual *np* collisions the differential cross section for emission by the fireball of a high-energy $\gamma$ ray is determined by the expression

$$\frac{d\sigma}{dE_\gamma} \approx 8{,}73\cdot 10^{-4}\,\frac{\sigma_R}{E_\gamma}\,(2\nu+1)\,\frac{N_F Z_F}{A_F} \times \frac{T_F}{mc^2}\,e^{-E_\gamma/T_F}\left[2\left(\frac{E_\gamma}{T_F}\right)^{3/2}+3\left(\frac{E_\gamma}{T_F}\right)^{1/2}+\frac{3}{2}\left(\frac{E_\gamma}{T_F}\right)^{1/2}\right]. \quad (4)$$

Here, $\sigma_R$ is the total reaction cross section, $m$ is the nucleon mass, $N_F$ and $Z_F$ are the numbers of neutrons and protons in the fireball, and $A_F = N_{F+}Z_F$. The parameter $\nu$ determines the mean number of collisions undergone by each nucleon in the fireball. In the case of greatest interest, when $T_F/\epsilon_F \sim 1$ ($\epsilon_F$ is the Fermi energy)

$$\nu \approx 4{,}6\cdot 10^{-2}\,\sigma_T R_F \exp(B/T) \times [1-\exp(-0{,}8\cdot 10^{-6}\,T^4\,(16+8\pi\varepsilon_F/T)^{1/2})], \quad (5)$$

where $R_F$ is the radius of the fireball in fermis, $B$ is the mean separation energy of a nucleon, and $\sigma_T$ is the mean cross section of nucleon–nucleon collisions (in units of $10^{-27}$ cm$^2$).

The fireball model was used to describe the low-energy part (below 50 MeV) of the electromagnetic spectrum in the $^{12}C + ^{238}U$ reaction at 84 MeV/nucleon. Agreement with the experimental data was obtained under the assumption that the thermalized source has temperature 6 MeV and that the mean number of collisions per nucleon is about 30.

A simplified fireball model, augmented by a quantum calculation of the cross section for emission of a $\gamma$ ray in an individual *np* collision was also used in Ref. 80. We shall consider the results of this study later in our discussion of the statistical approaches.

We note that the presence of several free parameters ($R_F$, $T_F$, $\nu$, and $B$) and the absence of a clear physical justification of equilibrium thermalization in a strongly nonequilibrium situation prevent, despite certain successes, the wide use of the fireball model to describe the emission of high-energy $\gamma$ rays.

### 3.2. First-collision models

The properties of the bremsstrahlung resulting from the scattering of nucleons by nuclei have been fairly well studied (see, for example,the review of Ref. 97). This circumstance provided the basis for a number of approaches to the solution of the problem of the electromagnetic radiation in nucleus–nucleus collisions.[81–87] In these approaches, as a rule, one considers the emission of high-energy $\gamma$ rays in the initial stage of the collision of the ions, the emitters being either a complete ion or individual protons of the colliding nuclei. In the latter case the emission process can be regarded as either due to the deceleration of the nucleons of the incident ion in the average field of the target nucleus (this field may vary with the time) or due to nucleon–nucleon collisions (usually, only *np* collisions, which give the greatest radiation intensity, are considered).

There are two possible ways of treating nuclear bremsstrahlung—classical and quantum. We consider below the main results of each of these approaches.

*a) Classical bremsstrahlung models.* The approaches developed in the studies of Refs. 79 and 81–84 can be included among these models. In them it is assumed that the ions move along classical trajectories and that the radiation is due to a change of the relative velocity of the nuclei in the collisions. The differential cross section for $\gamma$-ray emission, $d^2\sigma_\gamma/dE_\gamma d\Omega_\gamma$, can be calculated in accordance with the expression[81]

$$\frac{d^2\sigma_\gamma}{dE_\gamma d\Omega_\gamma} = \frac{e^2}{4\pi^2}\,\frac{\sigma_0}{E_\gamma}\left|\sum_{j=a,\,b}\int_{-\infty}^{+\infty}\frac{d}{dt} \times\left[\rho(\mathbf{p}_j)\,\frac{\mathbf{n}\times\mathbf{v}_j(t)}{1-\mathbf{n}\cdot\mathbf{v}_j(t)}\right]\exp[i\omega(t-\mathbf{n}\cdot\mathbf{R}_j(t))]\,dt\right|^2. \quad (6)$$

Here, $\rho(\mathbf{r})$ is the nuclear density; $\rho(\mathbf{p}) = \int\rho(\mathbf{r})e^{ip\cdot r}d^3r$ is its Fourier transform; $\sigma_0 = 4\pi R^2$, where the radius $R$ is determined by the condition $\rho(R) = 1/2\rho(0)$; $v_j$ and $\mathbf{p}_j$ are the velocity and momentum of the ion; $j = a$ or $b$ is the index that identifies the incident ion or target, respectively; $\mathbf{n}$ is the unit vector in the direction of emission of the $\gamma$ ray, and $\mathbf{R}_j(t)$ is the radius vector that determines the trajectory of ion $j$. The collision dynamics is determined by the time of deceleration of the ion, $\tau$, or, if a hydrodynamic model of the nucleus is used, this time can be related to the coefficient of friction $k$ of the nuclear medium. These quantities are parameters of the theory that cannot be calculated. In Refs. 81–84 such a model was used to calculate the yield of $\gamma$ rays and ions from collisions of heavy ions of different masses and energies (from 20 to 84 MeV/nucleon). It was found that for a value of the parameter $k$ that was the same for all the reactions it

was possible to explain all the pion spectra, but the calculated $\gamma$-ray yields were on the average half of the experimental yields. However, the authors did not regard this defect as critical because of the discrepancies between the results of the different experimental groups.

Although the classical models do have some heuristic value, this method of describing the reactions is unsatisfactory, since it does not permit one to relate the observable properties of the high-energy $\gamma$ rays to details of the nuclear structure and to the properties of the internuclear interaction of the specific nuclear systems that participate in the reaction.

*b) Quantum models.* The calculation of the bremsstrahlung cross section in Refs. 88 and 86 took into account the time evolution of the average nuclear field as a result of the encounter of the two nuclear systems. To find the single-particle wave functions $\varphi_\alpha$ $(\mathbf{r},t)$ a time-dependent Hartree–Fock equation was solved. In Ref. 85 the distribution function

$$f(\mathbf{r},\ \mathbf{k},\ \omega,\ t)=\sum_\alpha \int d^3s\, d\tau\, e^{-i\mathbf{k}s+i\omega\tau} \times \varphi_\alpha\left(\mathbf{r}+\tfrac{1}{2}s,\ t+\tfrac{1}{2}\tau\right)\varphi_\alpha^*\left(r-\tfrac{1}{2}s,\ t-\tfrac{1}{2}\tau\right) \quad (7)$$

(the summation is over the occupied single-nucleon states) was then calculated and used, after averaging over the volume of the region and the time during which the reaction takes place, to find the momentum distribution $g(\mathbf{k})$. The results were found to be not very sensitive to the parameters that characterize the chosen intervals of averaging. For the doubly differential cross section for emission of a $\gamma$ ray due to an *np* collision the expression

$$\frac{d^2\sigma_\gamma}{dE_\gamma d\Omega_\gamma}=\int d^3k_1\, d^3k_2\, g(\mathbf{k}_1)\, g(\mathbf{k}_2) \times \int \frac{d\Omega_q}{4\pi}\frac{E_\gamma}{E_{\gamma'}}\frac{d^2\sigma_\gamma^{(0)}}{dE'_\gamma\, d\Omega'_\gamma}(1-g(\mathbf{k}'_1))(1-g(\mathbf{k}'_2)), \quad (8)$$

where $\mathbf{q}=1/2(\mathbf{k}'_1-\mathbf{k}'_2)$, was used.

For the elementary reaction $n+p\to n'+p'+\gamma$, the cross section $d^2\sigma_\gamma^{(0)}/dE_\gamma d\Omega_\gamma$ was determined by the classical relation

$$\frac{d^2\sigma_\gamma^{(0)}}{dE_\gamma\, d\Omega_\gamma}=\alpha\frac{R^2}{12\pi}\frac{1}{E_\gamma}(2\beta_f^2+3\beta_i^2\sin^2\theta_\gamma). \quad (9)$$

Here, $\alpha=1/137$ is the fine-structure constant, and $\beta_i$ and $\beta_f$ are the initial and final velocities of the proton (in units of the velocity of light c) in the center-of-mass system. The value of the parameter $R=2.1$ F was chosen on the basis of an analysis of the $(p, n\gamma)$ reaction with 140-MeV and 200-MeV protons. To determine the total yield of $\gamma$ rays as a result of the nucleus–nucleus collision, an integration was performed over the impact parameter in a simplified geometry, and this yielded the result in the form

$$\frac{d^2\sigma_\gamma^{\text{tot}}}{dE_\gamma\, d\Omega_\gamma}\approx 2{,}3\,[(N_aZ_b+N_bZ_a)/(A_aA_b)^{1/3}]\frac{d^2\sigma_\gamma}{dE_\gamma\, d\Omega_\gamma}. \quad (10)$$

In the framework of this model a satisfactory description of the total yield of $\gamma$ rays with energy above 50 MeV was obtained for the reaction $^{12}C+{}^{12}C$(48, 60, 74, and 84 MeV/nucleon). This success was the justification for the conclusion that the initial stage of the collision makes the dominant contribution to the process of formation of the electromagnetic radiation.

In the study of Ref. 86 of the same group the formalism of the time-dependent Hartree–Fock equation was also used to estimate the contribution of the electromagnetic radiation produced as a result of coherent deceleration of the nucleons of one nucleus in the field of the other. In this case a direct quantum-mechanical calculation was made of the probability of $\gamma$-ray emission by a nucleon moving in a time-dependent potential field with separation both of the collective component in the bremsstrahlung due to the time and space variation of the single-nucleon current and of the component due to electromagnetic transitions of nucleons between populated and free time-dependent single-particle states. Because of the complications, calculations could be made only for reactions of light nuclei ($^{12}C+{}^{12}C$) in a simplified geometry, and this made it difficult to estimate the accuracy of the results. Nevertheless, the authors asserted that this mechanism could not give a $\gamma$-ray yield sufficient to explain the experimental data. Although, in our view, the method of describing the reaction proposed in Ref. 86 is the most consistent, at the present time it does not appear to be realizable in three-dimensional geometry, particularly for investigation of reactions involving ions more massive than $^{12}C$ or $^{16}O$

In Ref. 87, in which the approximations of infinite and semi-infinite nuclear matter were used, a comparative analysis was made of two mechanisms of formation of the high-energy $\gamma$ rays in ion collisions—through deceleration of the nucleons of the incident ion in the average field of the target nucleus and through *np* collisions. From the model estimates that were made it was concluded that the second mechanism plays a more important part in the formation of the radiation, although an attempt to calculate quantitatively the shape of the $\gamma$-ray spectrum for $^{14}N+{}^{298}Pb$ (40 MeV/nucleon) reactions gave a $\gamma$-ray yield three times smaller than the observed value. Since rather crude approximations (infinite nuclear matter, zero-range *np* interaction) were used in the model, it is rather difficult to draw a definite conclusion about the adequacy of the model for describing the process.

We note that in the quantum description of first-collision processes the coherent production of $\gamma$ rays as a result of *np* collisions was in essence considered only in Ref. 86, in which the amplitudes for $\gamma$-ray production, outside the cross section were summed. However as we have already noted, the approximations used in Ref. 86 to simplify the calculations and the uniqueness of the reaction for which comparison of the results of the calculation with experiment was made do not permit an unambiguous conclusion about the part played by coherent processes to be drawn. This question evidently requires further investigation.

### 3.3. Statistical models

In the statistical models the main problem is to calculate a time-dependent single-particle distribution function in the phase space or energy space of the system of two colliding nuclei. For this purpose various modifications of the Boltzmann equation are used. The emission of a $\gamma$ ray in these models takes place as a result of individual *np* collisions, and the total $\gamma$-ray yield is calculated using the single-nucleon distributions that have been found. In such calcula-

tions the contribution of the electromagnetic radiation from *pp* and *nn* collisions is usually ignored in the considered range of energies.

To determine the single-particle distribution of the nucleons in the phase space, $f(\mathbf{r}, \mathbf{k}, t)$, the authors of Ref. 88 solved the Boltzmann–Uehling–Uhlenbeck equation[98,99]:

$$\frac{\partial f_1}{\partial t}+\mathbf{v}\cdot\nabla_r f_1-\nabla_r u\cdot\nabla_p f_1=\frac{4}{(2\pi)^3}\int d^3k_2\, d^3k_3\, d\Omega v_{12}\,\frac{d\sigma^{(0)}}{d\Omega}$$
$$\times\,\delta^3(\mathbf{k}_1+\mathbf{k}_2-\mathbf{k}_3-\mathbf{k}_4)\,[f_1f_2(1-f_3)(1-f_4)$$
$$-f_3f_4(1-f_1)(1-f_2)]. \qquad (11)$$

Here, $d\sigma^{(0)}/d\Omega$ is the differential cross section for nucleon–nucleon scattering, $v_{1,2}$ is the relative velocity of the colliding nucleons, and $u$ is the potential of the average field in which the nucleons move. For this the parametrization

$$u(\rho) = a'\rho/\rho_0 + b'(\rho/\rho_0)^{4/3}, \qquad (12)$$

where $\rho(r)$ is the nuclear density, $a' = -218$ MeV, and $b' = 164$ MeV, was used.

To find the differential cross section for the emission of $\gamma$ rays when the ions collide the following expression was used:

$$\frac{d^2\sigma_\gamma^{(\mathrm{tot})}}{dE_\gamma\, d\Omega_\gamma}=\int d^2b\sum\int\frac{d\Omega_q}{4\pi}\,\frac{E_\gamma}{E_{\gamma'}}$$
$$\times\,\frac{1}{\sigma_{NN}}\,\frac{d\sigma_\gamma^{(0)}}{dE'_\gamma\, d\Omega'_\gamma}\,(1-f(\mathbf{r},\mathbf{k}_3,t))\,(1-f(\mathbf{r},\mathbf{k}_4,t)), \qquad (13)$$

where $b$ is the impact parameter, $\sigma_{NN} = 30\times10^{-27}$ cm$^2$, and $\theta_q$ and $\varphi_q$ are the angles that determine the direction of the vector $\mathbf{q} = 1/2(\mathbf{k}_3 - \mathbf{k}_4)$. The summation is over all possible *np* collisions. The cross section $d^2\sigma_\gamma^{(0)}/dE_\gamma d\Omega_\gamma$ is determined by the relation (9), but in this study the parameter $b$ was taken equal to $3F^2$.

Calculations of $d^2\sigma_\gamma^{(\mathrm{tot})}/dE_\gamma d\Omega_\gamma$ were made for the reactions $^{12}C + {}^{12}C$(84 MeV/nucleon) and $^{14}N + {}^{12}C$(20, 30, and 40 MeV/nucleon). It was found that, to order of magnitude, the model reproduces the shape of the energy spectrum and the dependence on the initial energy of the colliding ions, and also on the direction of emission of the $\gamma$ ray. Analysis of the time evolution of the process showed that the high-energy $\gamma$ rays are emitted in the initial stage of the reaction.

In our view, an advantage of the model is the absence of free parameters, but a shortcoming is the essentially classical method of description and the obvious complications in the practical realization of the method.

A different approach to the solution of the problem was proposed in Refs. 89–91. This used a system of quantum Boltzmann equations of the form

$$\frac{dn_i^x}{dt}=g_i^x\sum_y\Big\{\sum_{jkl}[\omega^{xy}_{kl\to ij}g_k^x g_l^y g_j^y n_k^x n_l^y(1-n_i^x)(1-n_j^y)$$
$$-\omega^{xy}_{ij\to kl}g_j^y g_k^x g_l^y n_i^x n_j^y(1-n_k^x)(1-n_l^y)]-n_i^x\omega^x_{i\to i'}\Big\}+f_i(p,n). \qquad (14)$$

Here, the indices $x$ and $y$ identify the nucleon species ($n$ or $p$); $g_i^x$ is the density of the single-particle states with energy $i$ (the Fermi-gas model was used for its determination); $n_i^x$ are the population numbers; $\omega^{xy}_{kl\to ij}$ is the probability of transition of nucleons $x$ and $y$, respectively, from the states $k$, $l$ to the states $i$, $j$ due to collisions; and $\omega^x_{i\to i'}$ gives the probability of transition of nucleon $x$ with energy $i$ to the continuum state with energy $i'$. The term $f_i(p,n)$ takes into account the probability of transition of a nucleon with energy $i$ in the incident nucleus into a bound state of the target nucleus (in the calculations it was assumed that the mass of the incident nucleus is significantly less than the mass of the target nucleus). One of the main approximations in the solution of Eq. (14) was that the energy carried by the incident ion into the compound system is distributed statistically in the initial stage among $n_0$ excitons. The number $n_0$ is a parameter of the theory to which the results of the calculations are particularly sensitive. From analysis of the pre-equilibrium neutron spectra and calculations of the yield of pions in heavy-ion reactions made on the basis of the solution of Eqs. (14) in Refs. 100 and 101 it was concluded that $n_0 = A_1$.

To find the $\gamma$-ray yield resulting from collision of the ions the following quantity was calculated:

$$\frac{d^2N_m^\gamma}{dE_\gamma\, dt}=\sum_{ijkl}\omega^{pn\gamma}_{ij\to klm}g_i^p g_j^n g_k^p g_l^n n_i^p n_j^n(1-n_k^p)(1-n_l^n). \qquad (15)$$

Here, $\omega^{pn\gamma}_{ij\to klm}$ is the probability of emission of a $\gamma$ ray with energy $m$ as a result of an individual *np* collision. For this the classical expression for dipole bremsstrahlung analogous to relation (9), but with the introduction of an additional numerical factor to take into account quantum corrections, was used. The value of the factor was determined by analyzing bremsstrahlung spectra for the *pd* reaction. The approach permitted a successful explanation of both the angular and energy distributions of the $\gamma$ rays in the reactions $^{14}N + {}^{12}C$, $^{208}Pb$(20, 30, and 40 MeV/nucleon), $^{40}Ar + {}^{197}Au$(30 MeV/nucleon), and $^{86}Kr + {}^{12}C$, Ag(44 MeV/nucleon). The results for the reactions $^{12}C + {}^{12}C$, $^{238}U(E/A_1$ above 50 MeV/nucleon) and $^{14}N + {}^{58}Ni$(35 MeV/nucleon) were not quite so good. As one of the possible reasons for the excess found in these last reactions in the experimental $\gamma$-ray yield above the theoretical value the authors drew attention to the use in the measurements of $\gamma$-ray detection by lead glasses, the detection efficiency of which was not sufficiently well known.[102] Of course, there may also have been a certain inadequacy of the description proposed for treating reactions with a fairly high energy of the relative motion of the ions (above 50 MeV/nucleon).

It should be noted that the model proposed in Refs. 89–91 is very sensitive, as the authors themselves note, to the parameter $n_0$, which determines the number of excitons in the compound system, and there do not exist clear physical grounds for its choice apart from agreement between the results of the calculations and the experiments.

Close to the models that we have already discussed is the approach proposed in Ref. 92, in which the yield of the $\gamma$ rays is determined by an intranuclear cascade. Calculating the angular and energy distributions of the bremsstrahlung $\gamma$ rays resulting from collisions of symmetric systems ($^{16}O + {}^{16}O$, $^{40}Ca + {}^{40}Ca$, $^{90}Zr + {}^{90}Zr$, $^{208}Pb + {}^{208}Pb$), the authors demonstrated the sensitivity of the process of $\gamma$-ray emission to the dynamics of the unfolding nuclear reaction. It was shown that an incoherent dipole component is dominant in the radiation spectrum at $\gamma$-ray energies above 30

MeV. In Ref. 92 the theory was not compared with definite experiments, since the authors saw its main aim as a methodological study of the reaction mechanism.

In Ref. 80 the fireball model was combined with the statistical approach. A formula analogous to (13) was used to determine the $\gamma$-ray yield, but the cross section $d\sigma_\gamma^{(0)}/d\,\mathbf{k}$ was calculated quantum-mechanically with allowance for the higher orders of the *np* interaction and without restriction to the dipole approximation. The distribution function $f(\mathbf{r}, \mathbf{k}, t)$ was chosen in accordance with the simplified fireball model in the form

$$f(\mathbf{r},\ \mathbf{k},\ t) = \frac{A_F}{4\,(mT_F)^{3/2}\,R_F^3} \exp\left[-\frac{\mathbf{p}^2}{2mT_F} - \frac{1}{2R_F^2}\left(\mathbf{r} - \frac{\mathbf{p}t}{m}\right)^2\right], \qquad (16)$$

where $T_F$ and $R_F$ are the initial temperature and radius of the fireball, and $A_F$ is the mean number of nucleons in it. Comparison of the results of the calculation of the $\gamma$-ray spectrum with the experimental data for the reactions $^{14}N + {}^{208}Pb$ (40 MeV/nucleon) and $^{12}C + {}^{238}U$(84 MeV/nucleon), and also with the data of Ref. 79, showed that the use of the exact value of the bremsstrahlung cross section for the individual *np* collisions significantly improved the agreement between the theory and experiment, although, in our view, all the advantages of the exact calculation of the cross section $d\sigma_\gamma^0/d\,\mathbf{k}$ are reduced to nothing by the use of the evaporation model with its numerous parameters.

The study of Ref. 93 occupies a special place in the statistical approaches. In this study it was assumed that the high-energy $\gamma$ rays are emitted as a result of the interaction of virtual clusters formed in the colliding nuclei. The probability of formation of a cluster of a definite number of nucleons was determined by the poisson distribution. Unfortunately, in the published studies[93,103] the actual mechanism of emission by the clusters of $\gamma$ rays (and also pions) was not described, and the expressions that were given suggest that it was not included in the calculation, although one would think that this mechanism must be the thing of greatest interest. Therefore, it is not clear what, apart from the conservation laws, ultimately controls the reaction nor what parameters are ultimately put into the calculation.

### 3.4. Quantum models of electromagnetic radiation in an optical potential

In Refs. 69 and 94–96 the optical-potential formalism was used to study different versions of a microscopic model of the emission of high-energy $\gamma$ rays in a collision of heavy ions with energy $E/A_1 < 100$ MeV/nucleon. This model does not have free parameters, and its use does not require lengthy calculations associated with solution of time-dependent Hartree–Fock equations or kinetic equations. The model is based on the assumption that the initial stage of the collision, when the distance between the centers of mass of the colliding ions still satisfies $|\mathbf{R}| \gtrsim R_a + R_b$, where $R_a$ and $R_b$ are, respectively, the radii of the incident nucleus and the target nucleus (the "deceleration" stage preceding nuclear fusion), plays the essential role in forming the yield of high-energy $\gamma$ rays. This stage corresponds to a situation in which several nucleons of one of the ions are simultaneously present in the region in which the gradient of the nuclear potential of the other ion acts, and then these nucleons can coherently emit a $\gamma$ ray. In such an approach the probability of the process will depend on the charge distributions and the two-nucleon correlation functions of the colliding nuclei, and also on the properties of the potential of the internuclear interaction.

Thus, for the production of high-energy $\gamma$ rays this process requires the simultaneous participation of several nucleons present together in the region of action of the gradient of a potential which is produced by some "external" field (for the peripheral process that we shall consider, this is the nuclear field of the collision partner). In our view this condition is satisfied by the real nuclear density and by the single-nucleon potentials known from experiments on the scattering of nucleons by nuclei (these optical potentials can be used to model the nuclear field). Indeed, the range of influence of the gradient of a single-nucleon optical potential with coordinate dependence of the real part in the form of the Woods–Saxon potential has a diameter of about 1 F. This is sufficient, given the real values of the nuclear density, for several nucleons of the incident ion to be present at once in this region, and therefore the emission of a $\gamma$ ray by the entire group simultaneously becomes possible.

The process of $\gamma$ emission is treated in the first order of perturbation theory in the internuclear interaction. Such an approximation is valid for an energy of the relative motion of the ions above 30 MeV/nucleon. The potential gradient needed to form the high-energy radiation ($E_\gamma > 30$ MeV) is achieved only in a narrow region near the surface of the nucleus. The typical value of the optical potential that acts in this region on an incident nucleon is 15–20 MeV for energy 30 MeV of the nucleon and decreases when that energy increases.[104] This is significantly less than the kinetic energy of the nucleon in the incident ion and is what justifies the use of perturbation theory. In our treatment we also bound $E/A_1$ above by the value 100 MeV/nucleon. At energies $\gtrsim 100$ MeV/nucleon the description of the scattering by means of the optical-potential formalism becomes much poorer because of the strong growth of the effects of bulk absorption. In fact, in this case the de Broglie wavelength of the incident nucleon is $\lambda \lesssim r_0$, where $r_0$ is the mean distance between the nucleons, and the picture of diffraction by many centers becomes more realistic.

For the matrix element of the process of electromagnetic emission of colliding nuclei *a* and *b* with interaction potential energy $U$ we obtain in this approximation the result

$$M^{(\gamma)} = \sum_{\lambda=a,\,b}\ \sum_{m_\lambda} \left\{ \frac{\langle f_\lambda \mid H_\lambda^{(\gamma)} \mid m_\lambda\rangle \langle m_\lambda \mid u \mid i_\lambda\rangle}{\varepsilon_{f_\lambda} - \varepsilon_{m_\lambda} + E_\gamma} + \frac{\langle f_\lambda \mid u \mid m_\lambda\rangle \langle m_\lambda \mid H_\lambda^{(\gamma)} \mid i_\lambda\rangle}{\varepsilon_{i_\lambda} - \varepsilon_{m_\lambda} - E_\gamma} \right\}. \qquad (17)$$

Here, the indices $i$, $m$, and $f$ label the initial, intermediate, and final states of the colliding nuclei; $\epsilon_s$ ($s = i, m, f$) are their corresponding energies; and $H^{(\gamma)}$ is the operator of the interaction of the nucleus with the electromagnetic radiation.

The further treatment involved separation in the operators and wave functions of the coordinates $\mathbf{R}_a$ and $\mathbf{R}_b$ of the centers of mass of the nuclei and of the relative coordinates of the nucleons in the nuclei, $\boldsymbol{\xi}^{(a)} = \mathbf{r}^{(a)} - \mathbf{R}_a$ and $\boldsymbol{\xi}^{(b)} = \mathbf{r}^{(b)} - \mathbf{R}_b$, where $\mathbf{r}^{(\lambda)}$ is the coordinate of a nucleon in nucleus $\lambda$

in the laboratory coordinate system. Thus, the wave functions of each of the colliding nuclei, $a$ or $b$, were expressed in the following form ($s = i, m, f$):

$$|s_\lambda\rangle \equiv |\mathbf{k}_s^{(\lambda)},\ \beta_s^{(\lambda)}\rangle = \exp(i\mathbf{k}_s^{(\lambda)}\mathbf{R}_\lambda)\,\Psi^\lambda_{\beta_s}(\xi^{(\lambda)}), \tag{18}$$

where $(\xi) \equiv (\xi_1, \xi_2, \ldots, \xi_A)$; $\mathbf{k}_s = \hbar^{-1}\mathbf{P}_s$; $\mathbf{P}_s$ is the momentum of the nucleus; and $\beta_s$ are the quantum numbers that describe the internal states of the ion. The form of the operator and of the matrix elements, calculated using the functions (18), is given in the Appendix, which also shows some details of the calculations.

We consider the form of the matrix elements $\langle S'_\lambda | u | S_\lambda \rangle$. The potential energy of the interaction of nuclei $a$ and $b$ was represented as follows:

$$V = \sum_{j,l} W_{j,l}(\mathbf{r}_j^{(a)} - \mathbf{r}_l^{(b)}), \tag{19}$$

where $W_{j,l}$ is the potential energy of the interaction of nucleon $j$ of nucleus $a$ with nucleon $l$ of nucleus $b$. Suppose that when $\gamma$ rays are emitted by one of the nuclei the other does not change its internal state (the use of the first order of perturbation theory justifies such an assumption). Then, for example, nucleus $b$ acts on the nucleons of nucleus $a$ with the following field:

$$u = \langle \mathbf{k}_f^{(b)},\ \beta_i^{(b)} \mid V \mid \mathbf{k}_i^{(b)},\ \beta_i^{(b)} \rangle$$
$$= \sum_j \int d^3R_b V_j^{(b)}(\mathbf{R}_b - \mathbf{R}_a + \xi_j^{(a)}) \exp[i(\mathbf{k}_i^{(b)} - \mathbf{k}_f^{(b)})\mathbf{R}_b], \tag{20}$$

where

$$V_j^{(b)}(\mathbf{r}) = \langle \beta_i^{(b)} | \sum_l W_{j,l}(\mathbf{r} - \xi_l^{(b)}) | \beta_i^{(b)} \rangle. \tag{21}$$

Introducing the relative coordinate $\mathbf{R}_{ba} = \mathbf{R}_b - \mathbf{R}_a$ and the coordinate $\mathbf{R}_c$ of the center of mass of the system, we can, using (20), represent the matrix element $\langle s'_a | u | s_a \rangle$ in the form

$$\langle s'_a \mid u \mid s_a \rangle = \delta(\mathbf{k}_i^{(b)} - \mathbf{k}_f^{(b)} + \mathbf{q}_{s_a s'_a})$$
$$\times \int d^3R_{ba} \exp(i\mathbf{q}_{s_a s'_a}\mathbf{R}_{ba}) \left\langle \beta_{s'}^{(a)} \left| \sum_{j=1}^{A_a} V_j^{(b)}(\mathbf{R}_{ba} + \xi_i^{(a)}) \right| \beta_s^{(a)} \right\rangle. \tag{22}$$

The matrix element $\langle s'_b | u | s_b \rangle$ is obtained accordingly from (22) by the substitution $a \rightleftarrows b$..

In Refs. 69, 95, and 96 more detailed analyses were made of two different physical situations:

a) a $\gamma$ ray is emitted in the initial stage of the collision without interpenetration of the nuclei, which corresponds to the condition $R_{ba} > \xi_j^{(a)}, \xi_j^{(b)}$ (Ref. 96);

b) the $\gamma$ ray is emitted after complete penetration of the nucler as a result of fusion.[69]

As we noted above, it is assumed in the model that the high-energy $\gamma$ rays are emitted only in the first stage of the collision, before the energy of the incident ion has been distributed over many degrees of freedom. The second situation is realized in the low energy part of the spectrum, and here the $\gamma$ decay of nuclear states excited in the collision process may also play an important part. In what follows, each of these situations is considered separately.

*a) Emission during the initial stage of the collision.* Adopting the condition $R_{ba} > \xi_j^{(a)}, \xi_l^{(b)}$, we can make an expansion in (22) in powers of $\xi_j^{(a)}$:

$$V_j^{(b)}(\mathbf{R}_{ba} + \xi_j^{(a)}) = V_j^{(b)}(\mathbf{R}_{ba}) + \left(\frac{\partial V_j^{(b)}}{\partial \xi_j^{(a)}}\right)_{\xi_j^{(a)}=0} \xi_j^{(a)} + \ldots \tag{23}$$

The individual terms of this expansion lead to excitation in nucleus $a$ of internal states of a definite multipolarity. The contribution of these states is most important in the case of the emission of $\gamma$ rays with energies near the energies of the corresponding giant resonances. Since we consider high-energy $\gamma$ rays ($E_\gamma > 30$ MeV), the contribution of the virtual nuclear excitations in the expression (17) can be ignored. Then

$$V_j^{(b)}(\mathbf{R}_{ba} + \xi_j^{(a)}) \approx V_j^{(b)}(\mathbf{R}_{ba}), \tag{24}$$

and the form of the matrix element simplifies to

$$\langle s'_a | u | s_a \rangle = u_0^{(b)}(\mathbf{q}_{s_a s'_a})\,\delta(\mathbf{k}_i^{(b)} - \mathbf{k}_f^{(b)} + \mathbf{q}_{s_a s'_a})\,\delta_{\beta_s^{(a)}, \beta_{s'}^{(a)}}, \tag{25}$$

where

$$u_0^{(b)}(\mathbf{q}) = \sum_{j=1}^{A_a} V_j^{(b)}(\mathbf{q}). \tag{26}$$

Making the substitution $a \rightleftarrows b$ in (25), we can obtain an analogous expression for the matrix element $\langle s'_b | u | s_b \rangle$.

In a collision of symmetric systems, for example, $^{12}C + {}^{12}C$, we have $V_l^{(a)}(\mathbf{R}_{ba}) = V_j^{(b)}(\mathbf{R}_{ba})$, and, therefore, $U_0^{(a)}(\mathbf{q}) = U_0^{(b)}(\mathbf{q}) \equiv U_0(\mathbf{q})$. It is easy to show [see Eq. (44) in the Appendix] that the emission matrix element $M^{(\gamma)}$ is determined by the Fourier transform of the interaction potential of the colliding nuclei, which depends only on the relative internuclear distance. In principle, if this potential were well known, the calculation of $U_0(\mathbf{q})$ ($\mathbf{q}$ is the momentum transfer to the target nucleus) would not be particularly complicated. However, data on the optical interaction potential of heavy nuclei are very ambiguous, although in recent years attempts have been made to obtain a universal formula (see, for example, the review of Ref. 105). Under these conditions it appears more consistent to model the internuclear potential by a sum of single-nucleon optical potentials, whose parameters are known with much greater accuracy.[104] Therefore, in what follows we take

$$U_0(\mathbf{q}) = \sum_j V_{0j}(\mathbf{q}). \tag{27}$$

where $V_0(\mathbf{q})$ is the Fourier transform of the single-nucleon optical potential.

For completely symmetric systems of two colliding nuclei (or for ones with nearly equal masses) the single-nucleon optical potential of either of the colliding nuclei can be taken as $V_0(\mathbf{r})$. For strongly asymmetric systems, for example, $^{12}C + {}^{238}U$, the single-nucleon optical potentials of the heavier ion are used to model $U_0$. Only in this case can the relative coordinates $\xi$ of the emitting nucleus be assumed to be less than the internuclear separation $R_{ba}$ and the approximation (24) be used. The validity of this method of modeling the function $U_0$ is justified *a posteriori* by comparing the results of the calculation with experiment.

Finally, for the differential cross section $d^2\sigma_\gamma/dE_\gamma d\Omega_\gamma$ we obtain the expression[96]

$$\frac{d^2\sigma_\gamma}{dE_\gamma\, d\Omega_\gamma}=\frac{\alpha E_\gamma}{(2\pi\hbar c)^4\, k_i^{(a)}}\int d\Omega_f^{(a)} k_f^{(a)} |u_0(\mathbf{q})|^2$$
$$\{|\mathbf{B}|^2-|\mathbf{k}_0\mathbf{B}|^2+Z_a(Z_a-1)$$
$$\times G_a(\mathbf{k})(|\mathbf{B}|^2-|\mathbf{k}_0\cdot\mathbf{B}_a|^2)+(A_a/A_b)^2$$
$$\times Z_b(Z_b-1)G_b(\mathbf{k})(|\mathbf{B}_b|^2-|\mathbf{k}_0\cdot\mathbf{B}_b|^2)\}. \quad (28)$$

Here, $\mathbf{q}=\mathbf{k}_i^{(a)}-\mathbf{k}_f^{(a)}-\mathbf{k}$, where $\mathbf{k}$ is the wave vector of the $\gamma$ ray, $k_0=\mathbf{k}/k$, and

$$\mathbf{B}=Z_a f_a^{(p)}(\mathbf{k})B_a+(A_a/A_b)Z_b f_b^{(p)}(\mathbf{k})\mathbf{B}_b; \quad (29)$$

$$\mathbf{B}_\lambda=\hbar c\left\{\mathbf{k}_i^{(\lambda)}\left[E_\gamma-\frac{\hbar^2}{2M_\lambda}(2\mathbf{k}_i^{(\lambda)}\cdot\mathbf{k}-\mathbf{k}^2)\right]^{-1}\right.$$
$$\left.-(\mathbf{k}_f^{(\lambda)}+\mathbf{k})\left[E_\gamma-\frac{\hbar^2}{2M_\lambda}(2\mathbf{k}_f^{(\lambda)}\cdot\mathbf{k}+\mathbf{k}^2)\right]^{-1}\right\}; \quad (30)$$

$G_\lambda(\mathbf{k})$ and $f_\lambda^{(p)}(\mathbf{k})$ are, respectively, the form factors of the proton–proton correlation function $G_\lambda^{(p)}(\mathbf{r})$ and the proton density $\rho_\lambda^{(p)}(\mathbf{r})$:

$$G_\lambda(\mathbf{k})=\int d^3r G_\lambda^{(p)}(\mathbf{r})\,e^{i\mathbf{kr}},\quad f_\lambda^{(p)}(\mathbf{k})=\int d^3r\rho_\lambda^{(p)}(\mathbf{r})\,e^{i\mathbf{kr}}; \quad (31)$$

$d\Omega_f^{(a)}=\sin\theta_f^{(a)}d\theta_f^{(a)}d\varphi_f^{(a)}$, $\theta_f^{(a)}\varphi_f^{(a)}$ are the angles that determine the direction of the vector $\mathbf{k}_f^{(a)}$ (the direction of the vector $\mathbf{k}_i^{(a)}$ is chosen as the quantization axis). In the derivation of (28) it was assumed for the sake of definiteness that nucleus $a$ is incident on nucleus $b$ at rest, and $M_\lambda$ is the mass of nucleus $\lambda$.

*b) Allowance for the effects of penetration.* In the original matrix element $\langle s_a'|u|s_a\rangle$ [see Eq. (22)], we can integrate over the magnitude and direction of the vector $\mathbf{R}_{ba}$ without recourse to the approximation (24):

$$\langle s_a'|u|s_a\rangle=\delta(\mathbf{k}_i^{(b)}-\mathbf{k}_f^{(b)}+\mathbf{q}_{s_a s_a'})$$
$$\times\left\langle\beta_{s'}^{(a)}\left|\sum_{j=1}^{A_a}V_{0,j}^{(b)}(\mathbf{q}_{s_a s_a'})\,e^{-i\mathbf{q}_{s_a s_a'}\xi_j^{(a)}}\right|\beta_s^{(a)}\right\rangle. \quad (32)$$

The emission process may take place either without excitation of the internal degrees of freedom of the colliding nuclei or with their excitation. Use of the well-known multipole expansion of the exponential gives

$$\langle s_a'|u|s_a\rangle=\delta(\mathbf{k}_i^{(b)}-\mathbf{k}_f^{(b)}+\mathbf{q}_{s_a s_a'})\sum_{LM}\frac{4\pi}{2L+1}Y_{LM}^*(\mathbf{q}_{s_a s_a'}^{(0)})$$
$$\times\langle\beta_{s'}^{(a)}|\hat{Q}_{LM}(\mathbf{q}_{s_a s_a'},\,\xi^{(a)})|\beta_s^{(a)}\rangle, \quad (33)$$

where

$$\hat{Q}_{LM}(\mathbf{q},\,\xi^{(a)})=\sum_{j=1}^{A_a}V_{0,j}^{(b)}(\mathbf{q})\,j_L(q,\,\xi_j^{(a)})\,Y_{LM}(\xi_j^{(0,\,a)}), \quad (34)$$

in which $\mathbf{q}^{(0)}$ and $\xi^{(0)}$ are unit vectors, and $j_L(x)$ is a spherical Bessel function. If in the emission process the internal state of the nucleus does not change, $\beta_{s'}^{(a)}\neq\beta_s^{(a)}$, then in (33) there remains only the first term of the expansion, and it is proportional to the nuclear form factor $f_a(\mathbf{q}_{s_a s_a'})$. If $\beta_{s'}^{(a)}\neq\beta_s^{(a)}$, then each term in the sum over $L$ leads to the excitation of nuclear states of a definite multiplicity. Among the possible nuclear excitations we shall retain in what follows only states of the type of giant resonances (dipole and quadrupole). After separation of states of this kind from the intermediate states in the expression for the matrix element of the emission $M^{(\gamma)}$ [see Eq. (17)] we obtain for the cross section for $\gamma$-ray emission[69]

$$d\sigma_\gamma=d\sigma_\gamma^{(T)}+\sum_{\lambda=a,\,b}d\sigma_{\gamma,\lambda}^{\mathrm{res}}, \quad (35)$$

where

$$\frac{d^2\sigma_\gamma^{(T)}}{dE_\gamma\, d\Omega_\gamma}=\frac{\alpha E_\gamma}{(2\pi\hbar c)^4\, k_i^{(a)}}\int d\Omega_{f_a}k_f^{(a)}(|\mathbf{C}|^2-|\mathbf{k}_0\cdot\mathbf{C}|^2); \quad (36)$$

$$\mathbf{C}=A_a[Z_a f_a^{(p)}(\mathbf{k})V_0^{(b)}(\mathbf{q})f_a^{(A)}(\mathbf{q})\mathbf{B}_a$$
$$+Z_b f_b^{(p)}(\mathbf{k})V_0^{(a)}(\mathbf{q})f_b^{(A)}(\mathbf{q})\mathbf{B}_b]; \quad (37)$$

$$\frac{d^2\sigma_{\gamma,\lambda}^{\mathrm{res}}}{dE_\gamma d\Omega_\gamma}=\sum_{L=1,\,2}\frac{\alpha}{(g^{L-1}\pi)^2}\left(\frac{Z_\lambda N_\lambda}{A_\lambda}\right)^{2(L-2)}$$
$$\times\frac{k^{2(L+1)}B_{J_i^{(\lambda)}\to J_f^{(\lambda)}}(EL)}{E_\gamma[(E_\gamma-\varepsilon_{\lambda,L}^{\mathrm{res}})^2+\Gamma_{\lambda,L}^2/4]}\frac{[(2L+1)!!]^2}{(2L+1)^3}\begin{Bmatrix}LJ_i^{(\lambda)}J_r^{(\lambda)}\\LJ_i^{(\lambda)}J_r^{(\lambda)}\end{Bmatrix}$$
$$\times\int d\Omega_f^{(a)}[(\mathbf{k}_f^{(\lambda)})^2-(\mathbf{k}_0\cdot\mathbf{k}_f^{(\lambda)})^2]\,|P_L(\cos\theta_q)|^2\,D_{J_i^{(\lambda)}\to J_r^{(\lambda)}}^{(\lambda)}(\mathbf{q},\,L). \quad (38)$$

Here, $V_0^{(a)}(\mathbf{q})$ and $V_0^{(b)}(\mathbf{q})$ are the Fourier transforms of the single-nucleon optical potentials of nuclei $a$ and b, respectively [in contrast to case (a), these are now different potentials if the colliding nuclei have different masses];

$$f_\lambda^{(A)}(\mathbf{q})=\int d^3r\rho_\lambda^{(A)}(\mathbf{r})\,e^{-i\mathbf{qr}}, \quad (39)$$

$\rho^{(A)}(\mathbf{r})$ is the nuclear mass density;

$$D_{J_i^{(a)}\to J_r^{(a)}}^{(a)}(\mathbf{q},\,L)$$
$$=\left|\left\langle J_r^{(a)}\right\|\sum_{j=1}^{A_a}V_{0,j}^{(b)}(\mathbf{q})\,j_L(q\xi_j^{(a)})\,Y_L(\xi_j^{(0,\,a)})\left\|J_i^{(a)}\right\rangle\right|^2; \quad (40)$$

$P_L(x)$ is a Legendre polynomial; $\theta_q=(\mathbf{k},\mathbf{q})$; $\epsilon_L^{\mathrm{res}}$ is the energy at the maximum of the corresponding giant resonance, and $\Gamma_L$ is its width; $B_{J_i\to J_r}(EL)$ is the reduced probability of the electromagnetic transition $J_i\to J_r$, where $J_i$ and $J_r$ are the total spins of the corresponding nuclear states. The method of calculating the reduced probabilities $B_{J_i\to J_r}(EL)$ and $D_{J_i\to J_r}(\mathbf{q},L)$ is described in the Appendix.

We shall consider the results of the calculation of $d^2\sigma_\gamma/dE_\gamma d\Omega_\gamma$ in accordance with the quantum model of electromagnetic radiation in an optical potential when we make a comparison with the experimental data and other theoretical approaches.

## 4. RESULTS OF THEORETICAL CALCULATIONS OF THE SPECTRA OF HIGH-ENERGY γ RAYS AND COMPARISON WITH EXPERIMENTS

In this section we consider the results of calculations of $d^2\sigma_\gamma/dE_\gamma d\Omega_\gamma$ in the framework of the quantum model of electromagnetic radiation in an optical potential, and we make a comparison with the experimental data and other approaches. The form of the single-nucleon optical potential $V_0(\mathbf{r})$, the analytic expressions for its Fourier transform and for the binary correlation function $G^{(p)}(\mathbf{r})$, and the final computational formula for the cross section $d^2\sigma_\gamma/dE_\gamma d\Omega_\gamma$ are given in the Appendix.

In comparing the theory with the experiments, we also give the results of calculations from Refs. 88 and 90. The

most extensive calculations were made in Ref. 90 on the basis of the alternative model of incoherent emission (see Sec. 3). With regard to the other theoretical studies, in them only selected reactions were analyzed, and the results obtained do not create an integral picture (we have already given a general characterization of these studies and their results in Sec. 3).

In our quantum model of electromagnetic radiation in an optical potential the basic quantity that determines the $\gamma$-ray yield is the single-nucleon optical potential. The form of this potential is usually taken to be a Fermi distribution, but for a given nucleon energy there are, as a rule, different sets of parameters that permit satisfactory description of the data on nucleon scattering by nuclei. Therefore, the cross sections of specific reactions were calculated for several sets, but in the comparison with the experiments we give only the parameters for which the best description of the experimental data is obtained. Here we note merely that the slope of the theoretical curves depends strongly on the values of the diffuseness parameters of the real and imaginary parts of the volume optical potential, and the spread of the theoretical values, particularly at the high-energy end of the spectrum, may reach an order of magnitude. This circumstance may provide an additional criterion for testing the single-nucleon optical potentials.

With some exceptions, which will be mentioned specially, the charge and density form factors were calculated with Fermi distributions in which the diffuseness parameter and radius were taken to be $a = 0.56$ F and $R = 1.07A^{1/3}$ F.[106] The investigation of the part played by pair correlations of the protons in the colliding nuclei made in Ref. 95 showed that such correlations become important when one is calculating the yield of $\gamma$ rays with energy above 100–120 MeV, increasing this yield in individual cases by 2–3 times. Therefore, in the cases in which $\gamma$ rays with energy above 120 MeV were not observed in the experiments the calculation was made in accordance with the simplified scheme in which the values of $G_a(\mathbf{k})$ and $G_b(\mathbf{k})$ were taken to be zero.

We begin the discussion of the results of the calculations with the nuclear reactions in which the energy of the relative motion of the ions was 30 MeV/nucleon and higher. We analyzed the following reactions, in which the yield of high-energy $\gamma$ rays has up to the present time been observed: $^{14}N + {}^{12}C$, $^{208}Pb$ ($E/A_1$ equal to 30 and 40 MeV/nucleon), $^{40}Ar + {}^{197}Au$ (30 MeV/nucleon), $^{14}N + {}^{58}Ni$ (35 MeV/nucleon), $^{40}Ar + {}^{158}Gd$ (44 MeV/nucleon), $^{86}Kr + {}^{12}C$, $^{nat}Ag$, $^{197}Au$ (44 MeV/nucleon), $^{12}C + {}^{12}C$ (48, 60, 74, and 84 MeV/nucleon), and $^{12}C + {}^{238}U$ (84 MeV/nucleon). As we already pointed out, the proposed model does not contain free parameters, and in the calculation we used single-nucleon optical potentials obtained by different authors who analyzed nucleon–nucleus scattering (these are summarized in the review of Ref. 104). In the cases when the necessary nucleon energy was not found in the summary table of Ref. 104, we used the parameters of the optical potentials of nearby energies for the given isotope or an isotope with neighboring mass number. Their values which give the best description of the experimental data are given in Table VI. We consider in what follows the results for each of the reactions just listed.

***The reactions $^{14}N + {}^{12}C$ and $^{14}N + {}^{208}Pb$ at energies 30 and 40 MeV/nucleon.***

Experimental data are given in Ref. 74 for the $\gamma$-ray emission angle $\theta_\gamma = 90°$ in the laboratory system. The results of the calculations are compared with the experiment in

TABLE VI. Parameters of single-nucleon optical potentials used in calculation (references to the corresponding sources are given in Ref. 104, and the form of the potentials is given in the Appendix).

| Parameter | Reaction | | | | | | | | | |
|---|---|---|---|---|---|---|---|---|---|---|
| | $^{4}He + {}^{154}Sm$ | $^{3}He + {}^{148}Sm$ | $^{12}C + {}^{154}Sm$ | $^{40}Ar + {}^{70}Ge$ | | $^{14}N + {}^{12}C$ | | $^{14}N + {}^{208}Pb$ | | $^{40}Ar + {}^{197}Au$ |
| $E/A$, MeV/nucleon | 6.75 | 9 | 10 | 15 | 24 | 30 | 40 | 30 | 40 | 30 |
| $V$, MeV | 53.5 | 59.8 | 53.5 | 50.3 | 54.2 | 50.0 | 55.1 | 69.6 | 49.0 | 47.9 |
| $r_0$, $F$ | 1.25 | 1.20 | 1.25 | 1.24 | 1.11 | 1.15 | 1.00 | 1.03 | 1.21 | 1.20 |
| $a_0$, $F$ | 0.65 | 0.72 | 0.65 | 0.65 | 0.77 | 0.63 | 0.62 | 0.77 | 0.77 | 0.70 |

Continuation of Table VI

| Parameter | Reaction | | | | | | | | | |
|---|---|---|---|---|---|---|---|---|---|---|
| | $^{14}N + {}^{58}Ni$ | $^{40}Ar + {}^{158}Gd$ | $^{86}Kr + {}^{12}C$ | $^{86}Kr + (nat)_{Ag}$ | $^{86}Kr + {}^{197}Au$ | $^{12}C + {}^{12}C$ | | | | $^{12}C + {}^{238}U$ |
| $E/A$, MeV/nucleon | 35 | 44 | 44 | 44 | 44 | 48 | 60 | 74 | 84 | 84 |
| $V$, MeV | 42.2 | 36.5 | 49.6 | 45.4 | 50.0 | 37.1 | 41.3 | 25.4 | 25.4 | 41.4 |
| $r_0$, $F$ | 1.25 | 1.25 | 1.15 | 1.24 | 1.24 | 1.11 | 1.08 | 1.13 | 1.13 | 1.22 |
| $a_0$, $F$ | 0.65 | 0.65 | 0.91 | 0.67 | 0.55 | 0.70 | 0.69 | 0.49 | 0.49 | 0.57 |

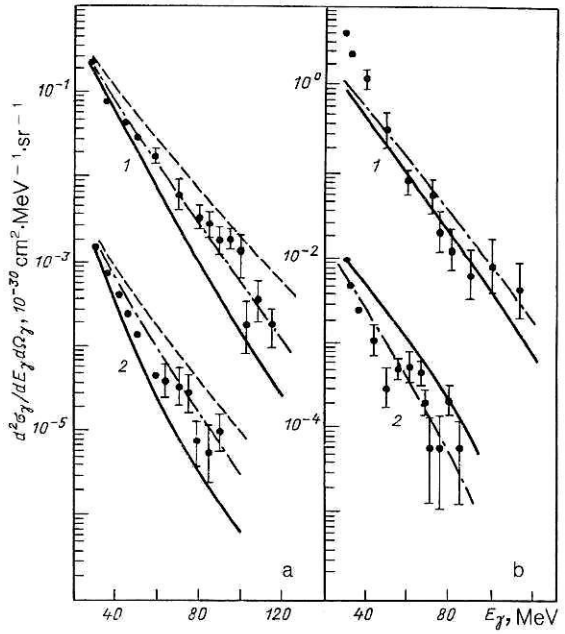


FIG. 45. Values of $d^2\sigma_\gamma/dE_\gamma d\Omega_\gamma$ for the reactions $^{14}N + {}^{12}C$ (a) and $^{14} + {}^{208}Pb$ (b) at $\theta_\gamma = 90°$: 1) $E/A_1 = 40$ MeV/nucleon; 2) $E/A_1 = 30$ MeV/nucleon (the theoretical and experimental values have been reduced by a factor $10^2$). The broken and chain curves represent the results of calculations from Refs. 88 and 90, respectively.

Fig. 45. Note that whereas for the reactions $^{14}N + {}^{12}C$(30 and 40 MeV/nucleon) and $^{14}N + {}^{208}Pb$(30 MeV/nucleon) the best agreement with the experiment was obtained for the values of the optical-potential parameters indicated in Table VI, for the reaction $^{14}N + {}^{208}Pb$(40 MeV/nucleon) values of $d^2\sigma_\gamma/dE_\gamma d\Omega_\gamma$ close to those given were also obtained for some other sets, for example, $V = 51$ MeV, $r_0 = 1.20$ F, and $a_0 = 0.65$ F, or $V = 52.8$ MeV, $r_0 = 1.15$ F, and $a_0 = 0.76$ F.

***The reaction $^{40}Ar + {}^{197}Au$(30 MeV/nucleon).***

Experimental data for this reaction are given in Ref. 75 for different $\gamma$-ray emission angles ($\theta_\gamma$ equal to 40, 90, and 157° in the laboratory system). The results of the calculations are presented in Fig. 46. We note a certain excess of the theoretical yield of the $\gamma$ rays above the experimental value for angles $\theta_\gamma$ equal to 40 and 90°. Since in this reaction $\gamma$ rays of comparatively moderate energies ($E_\gamma < 55$ MeV) were detected, the region of formation of the $\gamma$ rays is relatively larger, and effects of the interpenetration of the ions become more important. In Fig. 46 the broken curves show the values of $d^2\sigma^{(T)}/dE_\gamma d\Omega_\gamma$ calculated with allowance for the interpenetration effect in accordance with (36). It can be seen from Fig. 46 that for $\theta_\gamma$ equal to 40 and 90° the calculations with and without allowance for the penetration effect form a corridor within which the experimental data are situated.

***The reaction $^{14}N + {}^{58}Ni$(35 MeV/nucleon).***

Experimental data for this reaction from Ref. 13 and the results of calculations of $d^2\sigma_\gamma/dE_\gamma d\Omega_\gamma$ for angles $\theta_\gamma$ equal to 30, 60, and 90° in the laboratory system are presented in Fig. 47. We note that the theory and experiment agree less well at $\theta_\gamma = 90°$.

***The reaction $^{40}Ar + {}^{158}Gd$(44 MeV/nucleon).***

Experimental data for this reaction were obtained in Ref. 4 for $\theta_\gamma$ equal to 90 and 145° in the laboratory system. The results of theoretical calculations are presented in Fig. 48 for $\gamma$-ray energies above 30 MeV. As in the preceding case, the experimental data are described somewhat less well at the larger value of the angle $\theta_\gamma$.

***The reactions $^{86}Kr + {}^{12}C$ ($\theta_\gamma$ equal to 90 and 150°), $^{86}Kr + {}^{nat}Ag$ ($\theta_\gamma$ equal to 65, 100, and 153.5°), and $^{86}Kr + {}^{197}Au$ ($\theta_\gamma$ equal to 90 and 153.5°) at 44 MeV/nucleon).***

Experimental data for these reactions were obtained in the study of Ref. 77. The results of theoretical calculations of $d^2\sigma_\gamma/dE_\gamma d\Omega_\gamma$ are given in Fig. 49. We note a slight excess of the theoretical yield of $\gamma$ rays above the experimental value in the region of relatively low energies for the $^{86}Kr + {}^{12}C$ reaction. This may indicate that the interpenetration of the nuclei may play a more important part in this case.

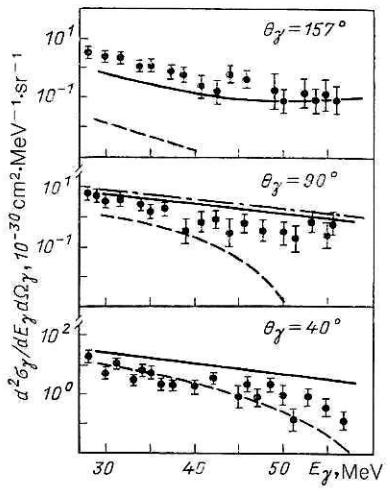


FIG. 46. Values of $d^2\sigma_\gamma/dE_\gamma d\Omega_\gamma$ for the reaction $^{40}Ar + {}^{197}Au$ at $E/A_1 = 30$ MeV/nucleon. The broken curve represents calculations with allowance for-interpenetration of the ions, and the chain curve gives the results of calculations from Ref. 90.

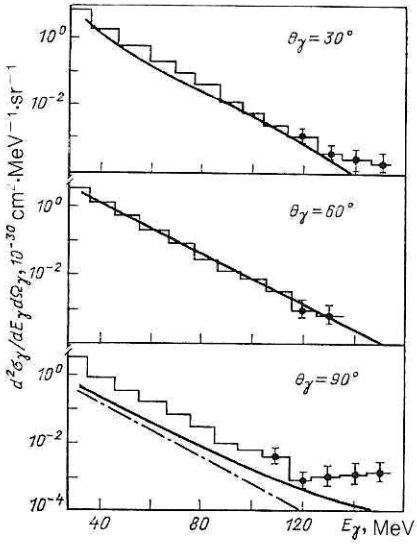


FIG. 47. Values of $d^2\sigma_\gamma/dE_\gamma d\Omega_\gamma$ for the reaction $^{14}N + {}^{58}Ni$ at $E/A_1 = 35$ MeV/nucleon for different emission angles. The chain curve represents the results of calculations from Ref. 90.

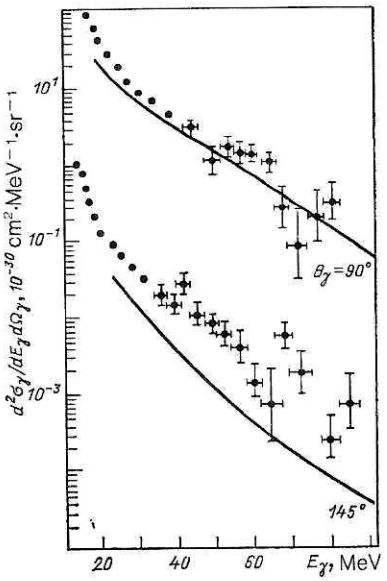


FIG. 48. Values of $d^2\sigma_\gamma/dE_\gamma d\Omega_\gamma$ for the reaction $^{40}$Ar + $^{158}$Gd at $E/A_1$ = 44 MeV/nucleon (the theoretical and experimental values have been reduced by a factor $10^2$).

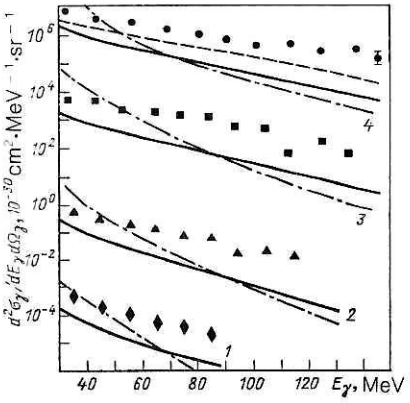


FIG. 50. Values of $d^2\sigma_\gamma/dE_\gamma d\Omega_\gamma$ for the reaction $^{12}$C + $^{12}$C at $\theta_\gamma$ = 90° in the center-of-mass system: 1) $E/A_1$ = 48 MeV/nucleon (all values reduced by a factor $10^3$); 2) $E/A_1$ = 60 MeV/nucleon; 3) $E/A_1$ = 74 MeV/nucleon (all values increased by a factor $10^4$); 4) $E/A_1$ = 84 MeV/nucleon (all values increased by a factor $10^7$). The broken curve gives the results of calculations from Ref. 88; the chain curve, from Ref. 90.

***The reaction $^{12}$C + $^{12}$C(48, 60, 74, and 84 MeV/nucleon).***

Experimental data for this reaction are given in Refs. 14 and 16 for the angle $\theta_\gamma$ = 90° in the center-of-mass system. The results of calculations of $d^2\sigma_\gamma/dE_\gamma d\Omega_\gamma$ are given in Fig. 50. Since in this case $\gamma$ rays of high energies (above 120 MeV) were also detected, nucleon–nucleon correlations were also taken into account. However, this was done by replacing the charge form factor $f^{(p)}(\mathbf{k})$ of the $^{12}$C nucleus by the dynamical form factor $f_d^{(p)}(\mathbf{k})$, for which the experimental value obtained in the investigation of Ref. 107 (see Ref. 95) was used. In contrast to all the reactions considered so far, in this case we observe a systematic and appreciable excess of the experimental $\gamma$-ray yield over the theoretical yield. This result appears surprising, since in our mechanism the $\gamma$-ray emission is maximally coherent. We recall that an analogous systematic discrepancy between theory and experiment for the same reaction was noted in Ref. 90 which reports the investigation of the incoherent component of the emission (see Fig. 50 and Sec. 3.3). The discrepancy between the theoretical and experimental values of $d^2\sigma_\gamma/dE_\gamma d\Omega_\gamma$ is still appreciable after summation of the $\gamma$-ray yields obtained in our calculations and in Ref. 90. One of the possible reasons for the discrepancy could be shortcomings in the method of detecting the high-energy $\gamma$ rays that was used in the measurements (see Sec. 2).

***The reaction $^{12}$C + $^{238}$U(84 MeV/nucleon).***

Experimental data for this reaction were obtained in Ref. 14 for angles $\theta_\gamma$ equal to 52.5° in the laboratory system (case 1) and 90° in the center-of-mass system (case 2). The results of the calculations are given in Fig. 51. Here, as for

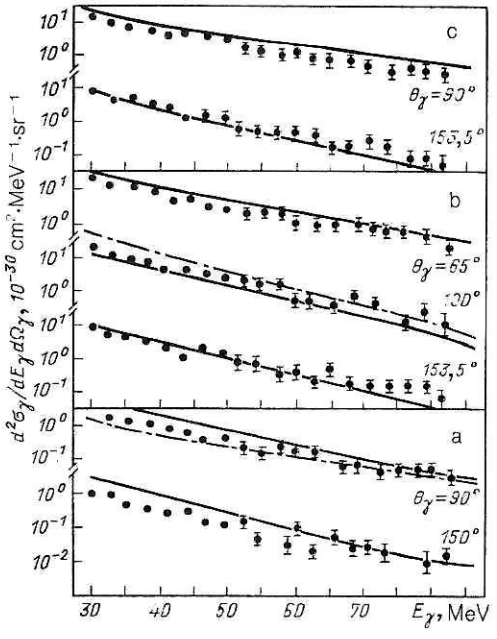


FIG. 49. Values of $d^2\sigma_\gamma/dE_\gamma d\Omega_\gamma$ for the reactions $^{86}$Kr + X at $E/A_1$ = 44 MeV/nucleon: a) $^{86}$Kr + $^{12}$C; b) $^{86}$Kr + $^{nat}$Ag; c) $^{86}$Kr + $^{197}$Au The chain curve represents the results of calculations from Ref. 90.

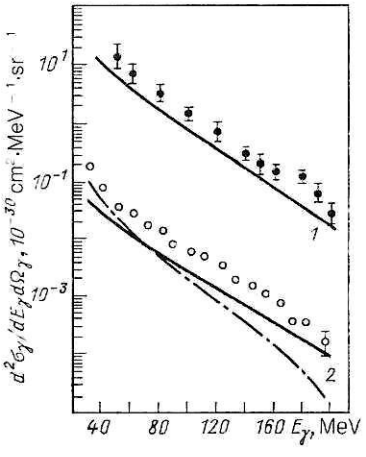


FIG. 51. Values of $d^2\sigma_\gamma/dE_\gamma d\Omega_\gamma$ for the reaction $^{12}$C(84 MeV/nucleon) + $^{238}$U (all values decreased by a factor $10^2$). The chain curve represents the results of calculations from Ref. 90.

the foregoing reaction, the calculation of the yield of high-energy $\gamma$ rays took into account two-nucleon correlations by replacing the static charge form factor of the $^{12}C$ nucleus by the dynamical form factor. We note an excess of the experimental $\gamma$-ray yield over the theoretical yields, as in the $^{12}C + {}^{12}C$ reaction, though in this case the discrepancy between theory and experiment is not so great.

The expression (28) for the cross section $d\sigma_\gamma$ permits the use of the Fourier transform of the ion–ion optical potential as $U_0(\mathbf{q})$. We made such calculations using the ion–ion potentials from the review of Ref. 105 for some of the reactions listed above. The results of the calculations show that with these potentials the experimental data are not reproduced well for either the shape of the $\gamma$-ray spectrum or the absolute magnitude of the yield. As a rule, the calculated shape of the spectrum is much flatter than observed, and the $\gamma$-ray yield is less than the experimental yield by one or two orders of magnitude or more. This fact can be understood. The parameters of the ion–ion potentials are chosen to describe the elastic scattering of ions in the region of relatively large values of the momentum transfer $q(q > 3\ F^{-1})$, and these potentials are not intended to explain phenomena with small values of $q$. In the process of $\gamma$ emission accompanying ion collisions the effective values of q are less than $3\ F^{-1}$. Therefore, it is not surprising that the use of the ion–ion potentials in this problem leads to worse results than the use of the single-nucleon potentials, the parameters of which make it possible to describe the region of small momentum transfers much better.

From the analysis of reactions in which the energy of the relative motion of the ions was fairly high (30 MeV/nucleon and more) and high-energy $\gamma$ rays ($E_\gamma = 30$–150 MeV) were detected, some conclusion can be drawn.

First, the proposed microscopic model, which does not use adjustable parameters and does not require lengthy calculations, can give a perfectly satisfactory description of a quite wide range of experimental data on the energy distributions of $\gamma$ rays emitted in ion–ion collisions. In our view, this can indicate that the adopted reaction mechanism is one of the main mechanisms, at least for $\gamma$ rays emitted in the forward hemisphere, though, of course, we cannot rule out a possible contribution to the total $\gamma$-ray yield from other mechanisms. Among such mechanisms, the most important part is probably played by incoherent *np* collisions. Comparison with the results of calculations based on the kinetic equation of Ref. 90, in which the emission accompanying such collisions was studied, shows (see Figs. 45–47 and 49–51) that the two models give similar results. However, it should be remembered that in Ref. 90 an adjustable parameter—the number $n_0$ of excitons—was used. Admittedly, the final choice of $n_0$ was based on analysis of not only the $\gamma$-ray reactions but also other reactions; for example, the yield of subthreshold pions was calculated in the same scheme. However, in these reactions too the "bremsstrahlung" mechanism, which was not taken into account, could play an important part, as follows from Ref. 94. The question of the relationship between the contributions of the coherent and incoherent mechanisms to the emission requires further investigation.

Second, the exponential shape of the $\gamma$-ray spectrum observed experimentally does not require for its explanation any "exotic" assumptions, and in the proposed model it is a consequence of purely nuclear circumstances—the exponential behavior of the charge form factors and the optical potential of the colliding nuclei in the region of the nuclear boundary.

Third, using the sensitivity of the computational scheme to the values of the single-nucleon optical potentials, we can independently test these potentials by comparing the theoretical and experimental $\gamma$-ray yields. In our view, investigation of the diffraction structure of the $\gamma$-ray spectrum may also be particularly informative for such purposes. Since in the model the differential cross section of the $\gamma$-ray emission process satisfies

$$d^2\sigma_\gamma/d\mathbf{k}_\gamma\, d\mathbf{P}_f \sim |V_0(\mathbf{q})|^2,$$

the diffraction structure of the Fourier transform of the single-nucleon optical potential $V_0(\mathbf{q})$ [$\mathbf{q}$ is the momentum transfer, and it is assumed that the volume part of $V_0(\mathbf{r})$ is taken in the form of the Fermi distribution] leads to the appearance of diffraction peaks and minima in the shape of the spectrum of the bremsstrahlung $\gamma$ rays as well. However, for their observation it is necessary to determine the momentum $\mathbf{P}_f^{(a)}$ of the scattered ion. In Fig. 52 we show as an example the diffraction pattern for the reactions $^{14}N$(35 MeV/nucleon) + $^{55}Ni$ and $^{12}C$(84 MeV/nucleon) + $^{238}U$ with different optical potentials. Experimental investigation of such spectra could also be interesting from the point of view of obtaining more definite conclusions about the mechanism of the $\gamma$-ray emission process when the predictions of alternative theoretical approaches are compared.

The successful application of the optical-potential theory to the emission of $\gamma$ rays in collisions of ions with energy above 30 MeV/nucleon stimulated its application to the investigation of reactions with ion energy up to 30 MeV/nucleon as well. Of course, in this region of energies the use of the first Born approximation raises certain doubts. How-

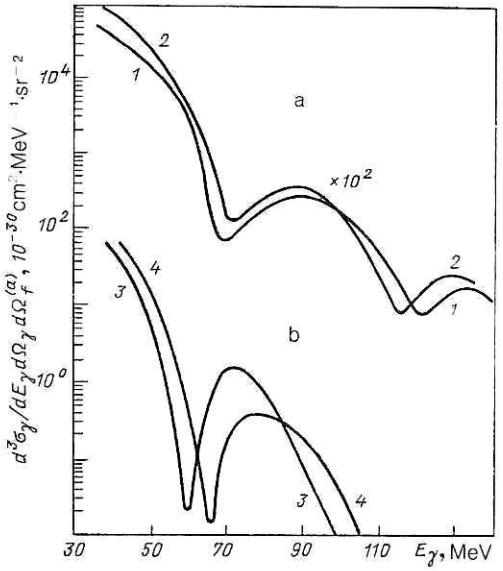


FIG. 52. Values of $d^3\sigma_\gamma/dE_\gamma d\Omega_\gamma d\Omega_f^{(a)}$ for $\theta_\gamma = 30°$ and $\theta_f^{(a)} = 0.5°$ for the following reactions: a) $^{12}C$(84 MeV/nucleon) + $^{238}U$; b) $^{14}N$(35 MeV/nucleon) + $^{58}Ni$. The parameters of the optical potentials are as follows: 1) $V = 40.2$ MeV, $r_0 = 1.9$ F, $a_0 = 0.76$ F; 2) $V = 30.0$ MeV, $r_0 = 1.20$ F, $a = 0.55$ F; 3) $V = 42.2$ MeV, $r_0 = 1.25$ F, $a_0 = 0.65$ F; 4) $V = 61.5$ MeV, $r_0 = 1.04$ F, $a_0 = 0.86$ F.

ever, we hope that our proposed model will make it possible in this region of energies too to identify the main features of the phenomenon, though the quantitative results will now have a large error. A justification for such a conclusion is provided, on the one hand, by the experience in the use of the DWBA, according to which the use of distorted waves to describe the state of motion of nucleons with energy above the separation energy does not, as a rule, radically change the results obtained in the plane-wave approximation, and, on the other, by the fact that the optical-potential method with parameters chosen by analysis of nucleon—nucleus scattering itself already takes into account the effects of the distortion to a certain degree by the energy and mass dependence of these parameters. In addition, the simplicity of the practical realization of the method permits its use, at the least, for preliminary rough estimates of the $\gamma$-ray yields even in cases when the method, strictly speaking, is invalid. We shall now illustrate the possibilities of the model for the description of reactions of ions with energies below 30 MeV/nucleon.

***The reaction $^{40}Ar + {}^{70}Ge$ (15 and 24 MeV/nucleon).***

Results for this reaction were published recently in Ref. 73. The theory and experiment are compared in Fig. 53. Since in the given case the $\gamma$-ray energies were in the range $15 \lesssim E_\gamma \lesssim 50$ MeV, the calculation was made in accordance with the expression (28) with inclusion of the terms $d\sigma_\gamma^{\text{res}}$ to take into account the de-excitation of the giant resonances [see the relations (38)]. We note, however, that in this case their contribution was found to be small compared with the purely "bremsstrahlung" terms. Since the absolute value of the $\gamma$-ray yield was not determined in the experiment, we matched the theoretical curve for $E/A_1 = 24$ MeV/nucleon to the experimental curve at the $\gamma$-ray energy $E_\gamma = 20$ MeV. As can be seen from Fig. 53, good agreement between theory and experiment is observed, and, most important, for the energy 15 MeV/nucleon, where only relative data for both reactions were used, too.

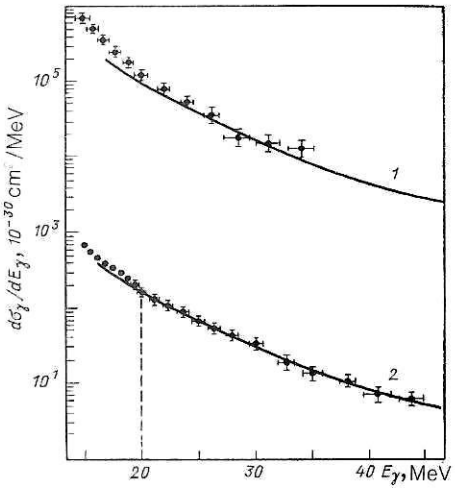


FIG. 53. Values of $d\sigma_\gamma/dE_\gamma$ for the reaction $^{40}Ar + {}^{70}Ge$: 1) $E/A_1 = 15$ MeV/nucleon (all values increased by a factor $10^3$); 2) $E/A_1 = 24$ MeV/nucleon.

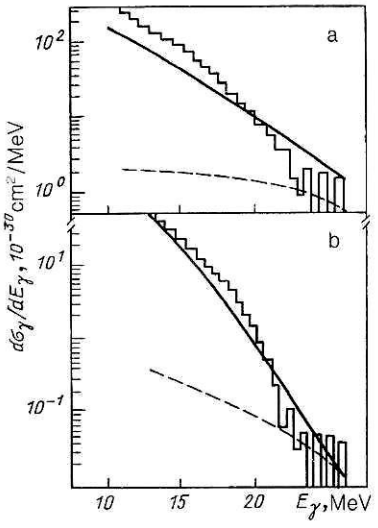


FIG. 54. Values of $d\sigma_\gamma/dE_\gamma$ for the reactions $^3He + {}^{148}Sm$ (a) and $^4He + {}^{154}Sm$ (b) at energy $E = 27$ MeV. The broken curve shows the results of calculations from Ref. 109.

***The reactions $^3He + {}^{148}Sm$, $^4He + {}^{154}Sm$ (energy of ions in beam 27 MeV), and $^{12}C$ (121 MeV) $+ {}^{154}Sm$.***

Data for these reactions, with specification of the absolute $\gamma$-ray yield, were recently given in Ref. 108. A feature of the reactions, in the first place with the He isotopes, was the investigation of the $\gamma$-ray spectra up to the kinematic limit 27 MeV. The theoretical analysis of the reactions made in Ref. 109 using well-known models led the authors of that study to the conclusion that these reactions were particularly "mysterious," since in none of the models that were used could they obtain a sufficient radiation yield, particularly at the high-energy end of the spectrum. Results of calculations in accordance with our model are presented in Figs. 54 and 55. The charge form factors of the He isotopes were taken in the form of Gaussian distributions with parameters from Ref. 110. As follows from Fig. 54, the spectrum of the observed high-energy $\gamma$ rays for the reactions with He ions can be perfectly well interpreted as bremsstrahlung (naturally, un-

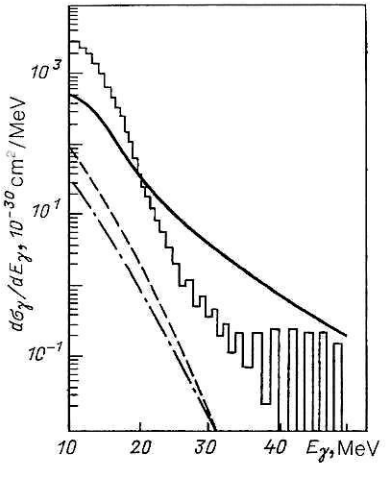


FIG. 55. Values of $d\sigma_\gamma/dE_\gamma$ for the reaction $^{12}C(121\text{ MeV}) + {}^{154}Sm$. The broken curve gives the results of calculations with allowance for interpenetration of the ions, and the chain curve gives the results of calculations from Ref. 109.

derstood in the terminology of our quantum model). With regard to the reaction $^{12}C + {}^{154}Sm$, the calculation without allowance for penetration in accordance with the expression (29) gives a somewhat too large result in the region $E_\gamma > 20$ MeV, though the calculations with and without allowance for the interpenetration of the ions form a corridor of results that have the experimental data within it. Thus, in this case too the observed spectrum can be interpreted as a bremsstrahlung spectrum with allowance for partial interpenetration of the $^{12}C$ and $^{154}Sm$ ions.

The theoretical results that we obtained for the reactions listed above appear to us promising in the light of the previously noted doubts about the validity of the model in the region of relatively low ion energies (below 30 MeV/nucleon).

There have been a considerable number of experimental studies of the emission of $\gamma$-rays in the energy range 5–20 MeV resulting from collisions of ions with energy 8–10 MeV/nucleon (see Sec. 2). Since in these experiments the reaction of fusion of the colliding nuclei was realized and, in addition, $\gamma$ rays of comparatively low energies were detected, the $\gamma$-ray yields were calculated theoretically in accordance with the expressions (35)–(38) with allowance for interpenetration of the ions. Strictly speaking, the calculation of the $\gamma$-ray spectra in the indicated range of $E_\gamma$ should also take into account emission that proceeds through the stage of formation and decay of a compound nucleus. However, attempts at the theoretical description of some of the mentioned reactions in the framework of the equilibrium thermodynamic approach did not make it possible to obtain a yield of $\gamma$ rays with energies above 12 MeV sufficient to explain the results of the experiments. Therefore, from the point of view of establishing the reaction mechanism, an alternative approach in which an additional source of high-energy $\gamma$ rays is considered is of particular interest.

In the framework of our model the $\gamma$-ray spectra were calculated for the reactions $^{40}Ar(300\ MeV) + {}^{159}Tb$ and $^{22}Ne(155\ MeV) + {}^{181}Ta$. The calculations took into account only the giant quadrupole resonances of the colliding nuclei, the energies and widths of which were taken from Ref. 111. Since the calculation used the oscillator sum rule [see the expressions (50) and (51)], the absolute $\gamma$-ray yields were calculated under the condition of a 100% contribution from these sums. The true situation may be different, but in a comparison of the theory and experiment this circumstance does not play a significant role, since the absolute values of the cross sections were not determined in the experiments. The results of calculations are presented in Fig. 56; the experimental and theoretical curves were matched at $E_\gamma = 6$ MeV. It can be seen from Fig. 56 that the theory reproduces entirely satisfactorily the relative behavior of the experimental curve, and the distortion of the shape of the spectrum in these reactions can be fully explained by the strongest (in our model) quadrupole excitations of the heavy nucleus. We emphasize that in the proposed approach the excitation of the giant resonances is due to the internuclear interaction of the colliding ions, for the description of which the standard sets of parameters of the single-nucleon optical potentials found from analysis of nucleon scattering by nuclei were used.

Unfortunately, the experimental studies of Refs. 2, 3, 53, 54, and 65 do not permit more definite conclusions to be

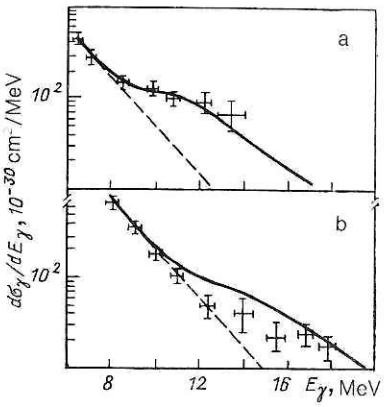


FIG. 56. Values of $d\sigma_\gamma/dE_\gamma$ for the reactions $^{22}Ne(155\ MeV) + {}^{181}Ta$ (a) and $^{40}Ar(300\ MeV) + {}^{159}Tb$ (b). The broken line shows the behavior of $d\sigma_\gamma^{(T)}/dE_\gamma$.

drawn about the validity of the model for investigating the $\gamma$-ray spectra associated with collisions of ions of low energies (8–10 MeV/nucleon), since in them the absolute cross sections for the $\gamma$-ray yields were not measured. Such measurements would undoubtedly be of interest both for study of the reaction mechanism and for comparison of the different theoretical approaches.

## CONCLUSIONS

1. Our analysis of the experimental and theoretical situation in the study of the spectra of high-energy $\gamma$ rays has shown that their emission may be due to several reaction mechanisms—statistical, bremsstrahlung, and through the excitation and subsequent decay of giant multipole resonances both in the colliding nuclei and in the reaction products. It appears that at $E_\gamma < 30$ MeV all three processes are important, while at $E_\gamma > 30$ MeV the bremsstrahlung mechanism makes the most important contribution.

2. To separate the contributions from the various processes, it is necessary when measuring the $\gamma$-ray spectra to separate the reaction channels by using the technique of coincidence of the $\gamma$ rays with the reaction products, the characteristic x rays and $\gamma$ rays, and other reaction products. Because there are experimental indications of correlations between the yields of the high-energy $\gamma$ rays and the reaction parameters in the entrance channel, it is also important to vary the initial parameters of the reaction: the initial energies of the ion beams and the mass and charge numbers of the colliding nuclei. The experimental data hitherto obtained are rather disparate; in the majority of experiments only integrated characteristics have been measured, and, as a consequence, lack of information makes it impossible to choose between one of several competing theoretical models.

3. It appears that high-energy $\gamma$ rays (with $E_\gamma > 30$ MeV) are emitted in an early stage of the collision process. This conclusion follows both from an analysis of spectra obtained in the framework of the Boltzmann equation and from the quantum-mechanical description.

4. In the region $E_\gamma < 30$ MeV the irregularities in the shape of the $\gamma$ ray spectra (bumps) cannot be unambiguously explained in the framework of statistical approaches. The bumps are probably associated with the decay of collective nuclear states, but it is not clear at which stage in the process

they are excited. However, there are indications that these $\gamma$ rays too are emitted in an early stage of the reaction.

5. In the review we have considered only the emission of high-energy $\gamma$ rays. However, experimental information is now available on the subthreshold production of pions in such reactions.[114] The nature of the energy spectra and angular distributions of the pions suggests that the production mechanisms of the high-energy $\gamma$ rays and of the pions could be similar. It would therefore be worth using the already known theoretical approaches to analyze the complete set of experimental data, including the pion production processes.

## APPENDIX TO SEC. 3

We give some auxiliary expressions used in the derivation and calculation of the cross sections $d^2\sigma_\gamma/dE_\gamma d\Omega_\gamma$ in the model of electromagnetic radiation in an optical potential. After separation of the center-of-mass coordinates $\mathbf{R}_a$ and $\mathbf{R}_b$ of the colliding nuclei from the relative coordinates $\boldsymbol{\xi}^{(a)}$ and $\boldsymbol{\xi}^{(b)}$, the operator $H_\lambda^{(\gamma)}$ takes the form

$$H_\lambda^{(\gamma)} = -(2\pi\hbar/\omega)^{1/2}\,\mathbf{u}_k\, e^{-i\mathbf{k}\mathbf{R}_\lambda} \sum_{j=1}^{A_\lambda} e_j e^{i\mathbf{k}\boldsymbol{\xi}_j^{(\lambda)}} (M_\lambda^{-1}\hat{\mathbf{P}}_\lambda + m_j^{-1}\hat{\mathbf{p}}_{\boldsymbol{\xi}_j^{(\lambda)}}), \tag{41}$$

where $\omega$, $\mathbf{k}$, $\mathbf{u}_k$ are the frequency, wave vector, and polarization vector of a $\gamma$ ray; $e_j$ and $m_j$ are the effective charge and mass of nucleon $j$; $\hat{\mathbf{P}}_\lambda = -i\hbar\partial/\partial\mathbf{R}_\lambda$; $\hat{\mathbf{P}}_{\xi^{(\lambda)}} = -i\hbar\partial/\partial\xi^{(\lambda)}$.

Use of the wave functions in the form (18) gives

$$\langle s' \mid H^{(\gamma)} \mid s\rangle = -(2\pi)^3\, e\, (2\pi\hbar/\omega)^{1/2}\,\mathbf{u}_k \times \{M^{-1}\mathbf{P}_s \langle \beta_{s'} \mid Z(\xi, \mathbf{k}) \mid \beta_s\rangle + \langle \beta_{s'} \mid \mathbf{Z}_1(\xi, \mathbf{k}) \mid \beta_s\rangle\}\, \delta(\mathbf{k}_s - \mathbf{k}_{s'} - \mathbf{k}); \tag{42}$$

$$Z(\xi, \mathbf{k}) = \sum_{j=1}^{A} (e_j/e) e^{i\mathbf{k}\xi_j}, \quad \mathbf{Z}_1(\xi, \mathbf{k}) = \sum_{j=1}^{A} (e_j/em_j)\, \hat{\mathbf{p}}_{\xi_j} e^{-i\mathbf{k}\xi_j}.$$

Note that if in the $\gamma$-ray emission process the internal states of the colliding nuclei do not change ($\beta_{s'} = \beta_s$), then the term with $\mathbf{Z}_1(\xi, \mathbf{k})$ in (42) does not contribute. Use of the expressions (42) and (25) in (17) leads to the following form of the matrix element $M^{(\gamma)}$:

$$M^{(\gamma)} = (M_a^{(\gamma)}\delta_{\beta_i^{(b)}, \beta_f^{(b)}} + M_b^{(\gamma)}\delta_{\beta_i^{(a)}, \beta_f^{(a)}})\, \delta(\mathbf{k}_i^{(b)} - \mathbf{k}_f^{(b)} + \mathbf{q}), \tag{43}$$

where

$$M_\lambda^{(\gamma)} = \frac{e}{M_\lambda c}\left(\frac{2\pi\hbar}{\omega}\right)^{1/2} u_0(\mathbf{q}) \langle \beta_f^{(\lambda)} \mid Z(\xi^{(\lambda)}, \mathbf{k}) \mid \beta_i^{(\lambda)}\rangle (\mathbf{u}_k \cdot \mathbf{B}_\lambda). \tag{44}$$

Using (43) and (44), integrating over $\mathbf{P}_f^{(a)}$ and $\mathbf{P}_f^{(b)}$, and summing over the polarizations of the $\gamma$ ray, we obtain for the differential cross section of the process of $\gamma$-ray emission in a nucleus–nucleus collision the result (to be definite we assume that nucleus $b$ is at rest, $\mathbf{k}_i^{(b)} = 0$)

$$\frac{d^2\sigma_\gamma}{dE_\gamma\, d\Omega_\gamma} = \frac{\alpha E_\gamma}{(2\pi\hbar c)^4\, k_i^{(a)}} \int d\Omega_f^{(a)} k_f^{(a)} (|\mathbf{A}|^2 - |\mathbf{k}_0 \cdot \mathbf{A}|^2)\, |U_0(\mathbf{q})|^2. \tag{45}$$

Here

$$\mathbf{A} = \langle \beta_f^{(a)} \mid Z(\xi^{(a)}, \mathbf{k}) \mid \beta_i^{(a)}\rangle \mathbf{B}_a \delta_{\beta_i^{(b)}, \beta_f^{(b)}} + (A_a/A_b) \langle \beta_f^{(b)} \mid Z(\xi^{(b)}, \mathbf{k}) \mid \beta_i^{(\beta)}\rangle \mathbf{B}_b \delta_{\beta_i^{(a)}, \beta_f^{(a)}}. \tag{46}$$

Assuming that after the emission of the $\gamma$ ray the internal states of the colliding nuclei are not determined, and bearing in mind that the energy of the $\gamma$ ray is appreciably greater than the characteristic energies of the nuclear excitations, we obtain the relation (28) after summation over the final states $|\beta_f^{(a)}\rangle$ and $\beta_f^{(b)}\rangle$.

For the calculation of the cross sections of specific reactions, the single-nucleon-optical potentials were chosen in the form[104]

$$V_0(\mathbf{r}) = V_c - Vf(x_0) + (\hbar/\mu c)^2 V_{s0} \times \boldsymbol{\sigma}\cdot\mathbf{l}\,\frac{1}{r}\,\frac{d}{dr} f(x_{s0}) - i\left[Wf(x_W) - 4W_D \frac{d}{dx_D} f(x_D)\right]. \tag{47}$$

Here

$$V_c = \begin{cases} Ze^2/r, & r \geqslant R_c; \\ (Ze^2/2R_c)(3 - r^2/R_c^2), & r \leqslant R_c; \end{cases}$$

$$R_c = r_c A^{1/3};\ f(x_i) = \left(1 + e^{x_i}\right)^{-1};\ x_i = (r - R_i)/a_i;$$
$$R_i = r_i A^{1/3};\ (\hbar/\mu c)^2 = 2\ \mathrm{F}^2,$$

and $Z$ and $A$ are the charge and mass numbers of the considered nucleus. The parameters that are determined from nucleon–nucleus scattering experiments are $r_c$, $r_i$, $a_i$ ($i = s0, 0, W, D$), $V$, $V_{s0}$, $W$, $W_D$. In practice, only the component $Vf(x_0)$ is important in the majority of cases; in individual cases the component $Wf(x_W)$ is important at the high-energy end of the $\gamma$-ray spectrum. The Fourier transforms of the radial functions $f(x_i)$ were calculated on the basis of the expression obtained in Ref. 112:

$$f(\mathbf{q}) = \frac{4\pi^2 R_i a_i}{q\,\mathrm{sh}(\pi a_i q)}\left\{\frac{\pi a_i}{R_i}\sin(R_i q)\,\mathrm{cth}(\pi a_i q) - \cos(R_i q)\right\}. \tag{48}$$

The charge distribution was specified in the form of the two parameter function $\rho^{(p)}(\mathbf{r}) = [1 + \exp((r - R)/a)]^{-1}$, where $R = 1.07A^{1/3}$ F and $a = 0.56$ F (Ref. 106). The form factor $f^{(p)}(\mathbf{k})$ was also calculated on the basis of the expression (48). An exception was made only for the He isotopes, for which we used the distribution (Ref. 110) $f^{(p)}(\mathbf{k}) = \exp(-k^2a^2/6)$, where $a$ is the rms radius of the charge distribution.

For the binary correlation function we chose the expression obtained in the model of a degenerate Fermi gas[113]:

$$G^{(p)}(\mathbf{r}) = 9\pi\,[J_{3/2}(x)]^2/2x^3. \tag{49}$$

Here $x = p_F r/\hbar$; $p_F$ is the limiting Fermi momentum $J_{3/2}(x)$ is a Bessel function. The corresponding terms make a significant contribution to the cross section $d^2\sigma_\gamma/dE_\gamma d\Omega_\gamma$ only for $E_\gamma > 120$ MeV.

The classical oscillator sum rule was used to calculate the reduced probabilities $B_{J_i \to J_f}(EL)$ and $D_{J_i \to J_f}(\mathbf{q}, L)$. In accordance with Ref. 111,

$$B^{(\lambda)}_{J_i^{(\lambda)} \to J_f^{(\lambda)}}(EL) = \begin{cases} \dfrac{9}{8\pi}\,\dfrac{\hbar^2}{m\varepsilon_{1\lambda}^{(\mathrm{res})}} - \dfrac{N_\lambda Z_\lambda}{A_\lambda}, & \text{if } L = 1; \\ \dfrac{15}{4\pi}\,\dfrac{\hbar^2}{m\varepsilon_{2\lambda}^{(\mathrm{res})}}\, Z_\lambda R_{0\lambda}^2, & \text{if } L = 2, \end{cases} \tag{50}$$

where $R_0$ is the nuclear radius. The calculation of the factor $D^{(\lambda)}_{J_i^{(\lambda)}\to J_f^{(\lambda)}}(\mathbf{q},L)$ is somewhat more complicated. If $L=2$, then, for $\lambda=a$, for example, we obtain

$$D^{(a)}_{J_i^{(a)}\to J_f^{(a)}}(\mathbf{q},2)=\frac{5}{4\pi}\frac{\hbar^2 A_a}{2m\varepsilon_{2a}^{(\mathrm{res})}}$$
$$\times|V_0^{(b)}(\mathbf{q})|^2\int_0^\infty\left\{\left[\frac{d}{dr}\,j_2(qr)\right]^2+6\left[j_2(qr)/r\right]^2\right\}\rho_a^{(A)}(r)\,r^2\,dr. \tag{51}$$

However, to treat the dipole excitations it is necessary to separate in (40) the terms that act on the relative coordinates of the neutron and proton subsystems in nucleus $a$ or nucleus $b$. Such a separation is possible only if $q\lesssim R_{0\lambda}^{-1}$. At large values of $q$, the external field begins to oscillate inside the excited nucleus, and the probability of dipole excitation is significantly reduced. In the investigated process, the maximal values of $q$ reach 3 $\mathrm{F}^{-1}$, and it is obvious that the fraction of $q$ values for which the condition $q\leqslant R_{0\lambda}^{-1}$[11] holds is relatively small. This circumstance made it possible to ignore the contribution of the dipole excitations in the studied process.

Finally, ignoring the nucleon–nucleon correlations ($G_\lambda^{(p)}(\mathbf{k})=0$), we give the expression for the differential cross section $d^2\sigma_\gamma/dE_\gamma d\Omega_\gamma$, retaining as independent variables $E_i$ and $E_\gamma$ and the angles $\theta_\gamma$ and $\theta_f^{(a)}$, which determine the directions of the vectors $\mathbf{k}$ and $\mathbf{k}_f^{(a)}$, respectively (it is assumed that $\mathbf{k}_i^{(b)}=0$):

$$\frac{d_2\sigma_\gamma}{dE_\gamma\,d\Omega_\gamma}=\frac{\alpha E_\gamma}{(2\pi\hbar c)^4\,k_i^{(a)}}\int d\Omega_f^{(a)}\,k_f^{(a)}\,|U_0(\mathbf{q})|^2\,(\alpha_1^2k_i^{(a)2}$$
$$+\alpha_2^2k_f^{(a)2}+\alpha_3^2k^2-2\alpha_1\alpha_2k_i^{(a)}k_f^{(a)}\cos\theta_f^{(a)}-2\alpha_1\alpha_3k_i^{(a)}k\cos\theta_\gamma$$
$$+2\alpha_2\alpha_3k_f^{(a)}k\cos\theta-(\alpha_1k_i^{(a)}\cos\theta_\gamma-\alpha_2k_f^{(a)}\cos\theta-\alpha_3k)^2). \tag{52}$$

Here

$$\alpha_1=\varkappa_1-\varkappa_2,\quad \alpha_2=\varkappa_3-\varkappa_2,\quad \alpha_3=\varkappa_3;$$
$$\varkappa_1=\hbar cZ_af_a^{(p)}(\mathbf{k})\left[E_\gamma-\frac{\hbar^2}{2M_a}(2k_i^{(a)}k\cos\theta-k^2)\right]^{-1};$$
$$\varkappa_2=\hbar cZ_bf_b^{(p)}(\mathbf{k})(A_a/A_b)\left[E_\gamma-\frac{\hbar^2}{2M_b}\right.$$
$$\left.\times(2k_i^{(a)}k\cos\theta_\gamma-2k_f^{(a)}k\cos\theta-k^2)\right]^{-1};$$
$$\varkappa_3=\hbar cZ_af_a^{(p)}(\mathbf{k})\left[E_\gamma-\frac{\hbar^2}{2M_a}(2k_f^{(a)}k\cos\theta+k^2)\right]^{-1};$$
$$q=(k_i^{(a)2}+k_f^{(a)2}+k^2-2k_i^{(a)}k\cos\theta_\gamma-$$
$$-2k_i^{(a)}k_f^{(a)}\cos\theta_f^{(a)}+2k_f^{(a)}k\cos\theta)^{1/2};$$
$$\cos\theta=\cos\theta_\gamma\cos\theta_f^{(a)}+\sin\theta_\gamma\sin\theta_\gamma^{(a)}\cos(\varphi_\gamma-\varphi_f^{(a)}).$$

Here $k_i^{(a)}=\hbar^{-1}(2M_aE_i)^{1/2}$, $k=E_\gamma/hc$, and to find $k_f^{(a)}$ it is necessary to solve the equation

$$k_f^{(a)2}=k_i^{(a)2}-2M_aE_\gamma/\hbar_2-q^2A_a/A_b.$$


[1]M. Lebrun, J. Deutsch, D. Fevart, *et al.*, Nucl. Instrum. Methods **166**, 151 (1979).
[2]V. V. Kamanin, A. Kugler, Yu. É. Penionzhkevich, and Yu. G. Sobolev, Izv. Akad. Nauk SSSR **50**, 1929 (1986).
[3]V. V. Kamanin, A. Kugler, Yu. E. Penionzhkevich, Z. Phys. A **327**, 109 (1987); Preprint E7-86-457, JINR, Dubna (1986).
[4]R. Hingmann, W. Kuhn, V. Metag, *et al*, Phys. Rev. Lett. **58**, 759 (1987).
[5]R. Novotny, R. Riess, R. Hingmann, *et al.*, Nucl. Instrum. Methods **262**, 340 (1987).
[6]F. A. Agaronyan, A. G. Akhperdzhanyan, M. Gonusek, *et al.*, Communication R13-87-15 [in Russian], JINR, Dubna (1987).
[7]V. Metag and R. S. Simon, Report GSI 87-19, Darmstadt (1987).
[8]H. Grassmann, E. Lorenz, and H. G. Moser, Nucl. Instrum. Methods **228**, 323 (1985).
[9]J. Alarja, A. Dauchy, A. Giorni, C. Morand, E. Pollaco, *et al.*, Nucl. Instrum. Methods **A242**, 352 (1986).
[10]N. Herrmann, R. Bock, H. Emling, *et al.*, Report GSI 87-65, Darmstadt (1987).
[11]T. Kishimoto, T. Shibata, M. Sasao, *et al.*, Nucl. Instrum. Methods **198**, 269 (1982).
[12]A. M. Sandorfi and M. T. Collins, Nucl. Instrum. Methods **222**, 479 (1984).
[13]N. Alamanos, P. Braun-Munzinger, R. F. Freifelder, *et al.*, Phys. Lett. **173B**, 392 (1986).
[14]E. Grosse, P. Grimm, H. Heckwolf, *et al.*, Europhys. Lett. **2**, 9 (1986); P. Grimm and E. Grosse, *Proc. of the Intern. School of Nuclear Physics, Erice, 10–22 April 1985* (Oxford, 1985), p. 339.
[15]R. Brun, Report CERN/DD/EE/84-1, Geneva (1986).
[16]D. W. O. Rogers, Nucl. Instrum. Methods **199**, 531 (1982).
[17]N. Herrmann, Report GSI 87-16, Darmstadt (1987).
[18]V. V. Kamanin, A. Kugler, Yu. G. Sobolev, *et al.*, Preprint 13-86-875 [in Russian], JINR, Dubna (1986).
[19]M. Yoshimori, H. Watanabe, and F. Shiraishi, Nucl. Instrum. Methods **245**, 191 (1986).
[20]C. Bourgeois and N. Perrin, Report IPNO D.RE. 85-17, Orsay (1985).
[21]N. Perrin and H. Tricoire, Report IPNO D.RE. 82-05, Orsay (1982).
[22]R. M. Diamond and F. S. Stephens, Report LBL-10325, Berkeley (1980).
[23]J. O. Newton, B. Herskind, R. M. Diamond, *et al.*, Phys. Rev. Lett. **46**, 1383 (1981).
[24]A. V. Ignatyuk and I. N. Mikhailov, Yad. Fiz. **33**, 919 (1981) [Sov. J. Nucl. Phys. **33**, 483 (1981)].
[25]K. Neergard, Phys. Lett. **110B**, 7 (1982).
[26]J. L. Egido and P. Ring, Phys. Rev. C **25**, 3239 (1982).
[27]R. R. Hilton, Z. Phys. A **309**, 233 (1983).
[28]S. N. Fedotkin, I. N. Mikhaylov, and R. G. Nazmitdinov, Phys. Lett. **121B**, 15 (1983).
[29]M. Faber, J. L. Egido, and P. Ring, Phys. Lett. **127B**, 5 (1983).
[30]J. Meyer, P. Quentin, and M. Brack, Phys. Lett. **133B**, 279 (1983).
[31]H. M. Sommermann, Ann. Phys. (N.Y.) **151**, 163 (1983).
[32]M. Di Nargo, M. Di Toro, G. Giansiracusa, *et al.*, Phys. Lett. **125B**, 240 (1983).
[33]O. Civitarese, S. Furui, M. Ploszajczak, and A. Fassler, Nucl. Phys. **A408**, 61 (1983).
[34]V. V. Volkov, *Deep Inelastic Nuclear Transfer Reactions* [in Russian] (Énergoizdat, Moscow, 1982).
[35]J. E. Draper, J. O. Newton, L. G. Sobotka, *et al.*, Phys. Rev. Lett. **49**, 434 (1982).
[36]F. E. Bertrand, Nucl. Phys. **A354**, c129 (1981).
[37]D. M. Brink, Doctoral Thesis, University of Oxford (1955).
[38]A. M. Sandorfi, J. Barrette, M. T. Collins, *et al.*, Phys. Lett. **130B**, 19 (1983).
[39]E. F. Garman, K. A. Snover, S. H. Chew, *et al.*, Phys. Rev. C **28**, 2554 (1983).
[40]B. Haas, D. C. Radford, F. A. Beck, *et al.*, Phys. Lett. **120B**, 79 (1983).
[41]C. A. Gosset, K. A. Snover, J. A. Behr, *et al.*, Phys. Rev. Lett. **54**, 1486 (1985).
[42]P. Carlos, H. Beil, R. Bergere, *et al.*, Nucl. Phys. **A225**, 171 (1974).
[43]R. Begere, H. Beil, P. Carlos, and A. Veyssiere, Nucl. Phys. **A133**, 417 (1969).
[44]B. L. Berman and S. C. Fultz, Rev. Mod. Phys. **47**, 713 (1975).
[45]M. Danos, Nucl. Phys. **5**, 23 (1958).
[46]K. E. G. Lobner, M. Vetter, and V. Honig, Nucl. Data Tables **7**, 495 (1970).
[47]S. Bjornholm, A. Bohr, and B. R. Mottelson, *Proc. of the Third IAEA Symposium on the Physics and Chemistry of Fission in Rochester, 1973*, Vol. 1 (IAEA, Vienna, 1974), p. 367.
[48]W. Hennerici, V. Metag, H. J. Hennrich, *et al.*, Nucl. Phys. **A396**, 329c (1983).
[49]J. J. Gaardhoje, O. A. Andersen, R. M. Diamond, *et al.*, Phys. Lett. **139B**, 273 (1984).
[50]K. A. Snover, J. Phys. (Paris) **C4**, 337 (1984).

[51]Ch. Bargholtz, J. Becker, B. Ritzen, and P.-E. Tegner, J. Phys. G **10**, L275 (1984).
[52]K. A. Snover, *Proc. of the Fifth Intern. Symposium on Capture Gamma-Rays Spectroscopy and Related Topics, Knoxville, Tenn., Sept. 10–14, 1984* (New York, 1985), p. 660.
[53]V. V. Kamanin, A. Kugler, T. I. Mikhailova, *et al.*, *Proc. of the Fourth Intern. Conf. on Nuclear Reaction Mechanism at Varrena, June 10-15, 1985* (Universitá degli Studi di Milano, Milan, 1985), p. 413.
[54]V. V. Kamanin, A. Kugler, Yu. É. Penionzhkevich, *et al.*, Communication D7-86-434 [in Russian], JINR, Dubna (1986), p. 87; Communication D7-87-65 [in Russian], JINR, Dubna (1987), p. 489.
[55]F. Puhlhofer, Nucl. Phys. **A280**, 267 (1977).
[56]A. S. Il'inov and E. A. Cherepanov, Communication R7-84-68 [in Russian], JINR,-Dubna (1984).
[57]V. V. Kamanin, A. Kugler, Yu. G. Sobolev, and A. S. Fomichev, Communication R15-87-783 [in Russian], JINR, Dubna (1987).
[58]V. V. Kamanin, A. Kugler, Yu. É. Penionzhkevich, *et al.*, in: *Abstracts of Papers at 38th Symposium on Nuclear Spectroscopy and Nuclear Structure* [in Russian] (Baku, 1988), p. 372.
[59]A. Lazzarini, D. Habs, W. Hennerici, *et al.*, Phys. Rev. Lett. **53**, 1045 (1984).
[60]Th. Arctaedius, Chr. Bargholtz, R. E. Ekström, *et al.*, Phys. Lett. **158B**, 205 (1985).
[61]D. R. Chakrabarty, S. Sen, M. Thoennessen, *et al.*, Phys. Rev. C **36**, 1886 (1987).
[62]P. Oblozinsky and S. Hlavac, *Proc. of the Europhysics Topical Conference on Neutron Induced Reactions* (Smolenice, 1982), p. 397.
[63]C. Cabot, H. Gauvin, H. Sergolle, and P. Auger, Z. Phys. A **322**, 393 (1985).
[64]S. D. Beĭzin, M. G. Itkis, Yu. A. Muzychka, *et al.*, Yad. Fiz. **37**, 809 (1983) [Sov. J. Nucl. Phys. **37**, 482 (1983)].
[65]V. V. Kamanin, A. Kugler, T. I. Mikhailova, *et al.*, R7-86-322 [in Russian], JINR, Dubna (1986), p. 41.
[66]R. A. Broglia, C. H. Dasso, A. Winther, *et al.*, Phys. Lett. **61B**, 113 (1976).
[67]R. V. Jolos, R. Schmidt, and J. Teichert, Preprint R4-84-245 [in Russian], JINR, Dubna (1984).
[68]A. Lukasiak and W. Norenberg, Report GSI 85-1, Darmstadt (1985).
[69]I. S. Batkin, V. V. Kamanin, I. V. Kopytin, and Yu. É. Penionzhkevich, Izv. Akad. Nauk SSSR, Ser. Fiz. **52**, 67 (1986).
[70]Yu. É. Penionzhkevich, E. Gierlik, V. V. Kamanin, and C. Borcea, Fiz. Elem. Chastits At. Yadra **17**, 165 (1986) [Sov. J. Part. Nucl. **17**, 65 (1986)].
[71]E. Betak, *Proc. of the Adriatic Intern. Conf. on Nuclear Physics, Frontiers of Heavy Ion Physics* (Dubrovnik, 1987), p. 49.
[72]V. A. Ilyuĭko, in: *Abstracts of Papers at the 38th Symposium on Nuclear Spectroscopy and Nuclear Structure* [in Russian] (Baku, 1988), p. 468.
[73]J. J. Gaardhoje, A. M. Bruce, J. D. Garrett, and B. Herskind, Phys. Rev. Lett. **59**, 1409 (1987).
[74]J. Stevenson, K. B. Beard, W. Benennson, *et al.*, Phys. Rev. Lett. **57**, 555 (1986).
[75]M. Kwato Njock, M. Maurel, E. Monnand, *et al.*, Phys. Lett. **175B**, 125 (1986).
[76]K. B. Beard, W. Bennenson, C. Bloch, *et al.*, Phys. Rev. C **32**, 1111 (1985).
[77]R. M. Bertholet, M. Kwato Njock, and M. Maurel, *et al.*, Nucl. Phys. **A474**, 541 (1987).
[78]B. A. Remington, M. Blann, and G. F. Bertsch, Phys. Rev. C **35**, 1720 (1987).
[79]H. Nifenecker and J. P. Bondorf, Nucl. Phys. **A442**, 478 (1985).
[80]D. Neuhaser and S. E. Koonin, Nucl. Phys. **A462**, 163 (1987).
[81]D. Vasak, W. Greiner, B. Muller, *et al.*, Nucl. Phys. **A428**, 291c (1984).
[82]D. Vasak, B. Miller, and W. Greiner, J. Phys. G **11**, 1309 (1985).
[83]T. Stahl, M. Uhlig, B. Muller, *et al.* Z. Phys. A **327**, 311 (1987).
[84]D. Vasak, Phys. Lett. **176B**, 276 (1986).
[85]W. Cassing, T. Biro, U. Mosel, *et al.*, Phys. Lett. **181B**, 217 (1986).
[86]W. Bauer, W. Cassing, U. Mosel, *et al.*, Nucl. Phys. **A456**, 159 (1986).
[87]K. Nakayama and B. Bertsch, Phys. Rev. C **34**, 2190 (1986).
[88]W. Bauer, G. Bertsch, W. Cassing, and U. Mosel, Phys. Rev. C **34**, 2127 (1986).
[89]B. A. Remington, M. Blann, and G. Bertsch, Phys. Rev. Lett. **57**, 2909 (1986).
[90]B. A. Remington, M. Blann, and G. Bertsch, Phys. Rev. C **35**, 1720 (1987).
[91]B. A. Remington and M. Blann, Phys. Rev. C **36**, 1387 (1987).
[92]Ko Che Ming, G. Bertsch, and J. Aichelin, Phys. Rev. C **31**, 2324 (1985).
[93]R. Shyam and J. Knoll, Nucl. Phys. **A448**, 322 (1986).
[94]I. S. Batkin and I. V. Kopytin, Izv. Akad. Nauk SSSR, Ser. Fiz. **50**, 2038 (1986).
[95]I. S. Batkin and I. V. Kopytin, Yad. Fiz. **45**, 396 (1987) [Sov. J. Nucl. Phys. **45**, 249 (1987)].
[96]I. S. Batkin, I. V. Kopytin, and M. N. Berkman, Yad. Fiz. **47**, 1602 (1988) [Sov. J. Nucl. Phys. **47**, 1015 (1985)].
[97]V. A. Plyuĭko and V. A. Poyarkov, Fiz. Elem. Chastits At. Yadra **18**, 374 (1987) [Sov. J. Part. Nucl. **18**, 159 (1987)].
[98]B. Bertsch, H. Kruse, and S. das Gupta, Phys. Rev. C **29**, 673 (1984).
[99]J. Aichelin and G. Bertsch, Phys. Rev. C **31**, 1730 (1985).
[100]M. Blann, Phys. Rev. C **31**, 1245 (1985).
[101]M. Blann, Phys. Rev. C **32**, 1231 (1985).
[102]C. Michel, E. Grosse, and H. Noll, Nucl. Instrum. Methods **A243**, 395 (1986).
[103]R. Shyam and J. Knoll, Nucl. Phys. **A426**, 606 (1984).
[104]C. M. Perey and F. G. Perey, At. Data Nucl. Data Tables **17**, 1 (1976).
[105]V. N. Bragin and M. V. Zhukov, Fiz. Elem. Chastits At. Yadra **15**, 725 (1984) [Sov. J. Part. Nucl. **15**, 325 (1984)].
[106]I. S. Gul'karov, *Investigation of Nuclei by Electrons* [in Russian] (Atomizdat, Moscow, 1977).
[107]N. G. Afanas'ev, V. A. Gol'dshteĭn, S. V. Dementiĭ, *et al.*, Yad. Fiz. **5**, 1134 (1967) [Sov. J. Nucl. Phys. **5**, 808 (1967)].
[108]K. Snover, Ann. Rev. Nucl. Part. Sci. **36**, 545 (1986).
[109]K. Nakayama and G. Bertsch, Phys. Rev. C **36**, 1848 (1987).
[110]R. Hofstadter, Rev. Mod. Phys. **28**, 214 (1956).
[111]A. Bohr and B. R. Mottelson, *Nuclear Structure*, Vol. 2, (Benjamin, Reading, Mass., 1975) [Russ. transl., Mir, Moscow, 1987].
[112]V. K. Luk'yanov and Yu. S. Pol', Fiz. Elem. Chastits At. Yadra **5**, 955 (1974) [Sov. J. Part. Nucl. **5**, 385 (1975)].
[113]M. L. Goldberger and K. M. Watson, *Collision Theory* (Wiley, New York, 1964) [Russ. transl., Mir, Moscow, 1967].
[114]W. Benennson, Nucl. Phys. **A482**, 503 (1988).

Translated by Julian B. Barbour